LOCKHEED MARTIN ENERGY RESEARCH LIBRARIES
3 4456 0509834 6

0-4

ORNL/TM-5993

Cy. 112

Advanced Fuel Recycle Program Progress Report for Period April 1 to June 30, 1977

[redacted]

OAK RIDGE NATIONAL LABORATORY
CENTRAL RESEARCH LIBRARY
CIRCULATION SECTION
4500N ROOM 175
LIBRARY LOAN COPY
DO NOT TRANSFER TO ANOTHER PERSON.
If you wish someone else to see this report, send in name with report and the library will arrange a loan.
ORNL-118 (6-97)

OAK RIDGE NATIONAL LABORATORY
OPERATED BY UNION CARBIDE CORPORATION FOR THE ENERGY RESEARCH AND DEVELOPMENT ADMINISTRATION

Printed in the United States of America. Available from
the Energy Research and Development Administration,
Technical Information Center
P. O. Box 62, Oak Ridge, Tennessee 37830
Price: Printed Copy $5.50; Microfiche $3.00

This report was prepared as an account of work sponsored by the United States Government. Neither the United States nor the Energy Research and Development Administration/United States Nuclear Regulatory Commission, nor any of their employees, nor any of their contractors, subcontractors, or their employees, makes any warranty, express or implied, or assumes any legal liability or responsibility for the accuracy, completeness or usefulness of any information, apparatus, product or process disclosed, or represents that its use would not infringe privately owned rights.

ORNL/TM-5993
Dist. Category UC-79c

Contract No. W-7405-eng-26

ADVANCED FUEL RECYCLE PROGRAM PROGRESS REPORT FOR PERIOD APRIL 1 TO JUNE 30, 1977

W. D. Burch, Program Director

M. J. Feldman
Manager, Engineering Systems

W. S. Groenier
Manager, Engineering Research

B. L. Vondra
Manager, Process Research and Development

Report compiled by
W. E. Unger
Technical Assistant to the Program Director

Date Published: September 1977

NOTICE: This document contains information of a preliminary nature. It is subject to revision or correction and therefore does not represent a final report.

OAK RIDGE NATIONAL LABORATORY
Oak Ridge, Tennessee 37830
operated by
UNION CARBIDE CORPORATION
for the
ENERGY RESEARCH AND DEVELOPMENT ADMINISTRATION

LOCKHEED MARTIN ENERGY RESEARCH LIBRARIES

3 4456 0509834 6

CONTENTS

ABSTRACT v

1. HIGHLIGHTS 1-1
   1.1 PROCESS RESEARCH AND DEVELOPMENT 1-1
   1.2 ENGINEERING RESEARCH 1-1
   1.3 ENGINEERING SYSTEMS 1-2
   REFERENCES FOR SECTION 1 1-3

2. PROCESS RESEARCH AND DEVELOPMENT 2-1
   2.1 HOT-CELL OPERATIONS 2-1
      2.1.1 Development of in-cell equipment 2-1
      2.1.2 Flowsheet studies 2-1
   2.2 LABORATORY STUDIES 2-14
      2.2.1 Plutonium dioxide dissolution studies 2-14
      2.2.2 Hydroxylamine and hydrazine chemistry in Purex processing 2-17
      2.2.3 Solvent chemistry studies 2-29
      2.2.4 Reduction of Pu(VI) with NO_2 and NO gases 2-33
      2.2.5. Pu(IV) polymer reaction in aqueous solutions 2-35
      2.2.6. Materials compatibility studies 2-35
   2.3 PRODUCT CONVERSION 2-35
   REFERENCES FOR SECTION 2 2-36

3. ENGINEERING RESEARCH 3-1
   3.1 VOLOXIDATION 3-1
   3.2 DISSOLUTION 3-2
      3.2.1 Four-foot-diameter dissolver prototype 3-2
      3.2.2 Operational testing of ferrofluidic seals 3-4
      3.2.3 Nitrogen oxide scrubbing 3-4
   3.3 FEED PREPARATION 3-8
      3.3.1 Iodine evolution 3-8
   3.4 FLUOROCARBON ABSORPTION STUDIES 3-8
      3.4.1 Pilot-plant operation 3-8
      3.4.2 Process application 3-11
      3.4.3 Chemical studies of contaminants in LWR off-gas processing 3-12
   3.5 IODOX PROCESS 3-16
   3.6 INSTRUMENTATION AND CONTROL SYSTEMS 3-18
      3.6.1 Nondestructive assay of spent fuels 3-18
      3.6.2 Process sensors and control 3-19
   3.7 SOLVENT EXTRACTION 3-24
   REFERENCES FOR SECTION 3 3-25

4. ENGINEERING SYSTEMS 4-1
   4.1 ENGINEERING ANALYSIS 4-2

4.2 COMPONENT DEVELOPMENT 4-2
4.2.1 Disassembly and fuel cutting–contracted work 4-2
4.2.2 Disassembly and cutting–ORNL program 4-6
4.2.3 Dissolution 4-12
4.3 SYSTEMS DEVELOPMENT 4-19
4.3.1 Integrated Equipment Test (IET) Facility 4-20
4.3.2 Receiving and storage 4-21
4.3.3 Remote maintenance task 4-29
4.3.4 Waste handling 4-32
4.3.5 Uranium for tests 4-33
4.4 HOT EXPERIMENTAL FACILITY (HEF) CONCEPTUAL DESIGN 4-33
4.4.1 HEF process design 4-34
4.4.2 HEF design 4-34
REFERENCE FOR SECTION 4 4-36
5. NUCLEAR SAFETY 5-1
REFERENCES FOR SECTION 5 5-2

ABSTRACT

This quarterly progress report on the Fuel Recycle Program covers the ongoing development program aimed at providing the technology for production-scale advanced fuels recycle. The continuing basic laboratory and hot-cell studies, engineering research, and component equipment development activities are in support of a cold integrated equipment test scheduled for 1981 and a current conceptual design of a hot experimental facility scheduled for operation in 1988.

1. HIGHLIGHTS

1.1 PROCESS RESEARCH AND DEVELOPMENT

B. L. Vondra

Process research and development studies were continued in the laboratory and hot cells to define process parameters and conditions for an LMFBR reprocessing flowsheet. Work is in progress on the following: (1) the dissolution of PuO_2 in hydriodic acid (HI), (2) the removal of impurities in aqueous recycle streams, (3) head-end parametric studies with irradiated fuel, (4) the recycle of nitrogen oxides for gaseous reagent usage, (5) solvent chemistry, and (6) iodine behavioral studies (Iodox).

Results of the first set of three base-line experiments with highly irradiated mechanically blended $(U,Pu)O_2$ are presented. These experiments include two tests with voloxidation and one in the absence of voloxidation.

A new task has been initiated to develop the technology for product conversion.

Alternate holding reductants for Pu^{3+} are being screened; urea, based on its rapid reaction with nitrous acid, shows promise.

Butylauryl phosphate (a known secondary degradation product) forms a sodium salt that can be removed from the organic phase by water scrubbing.

The more rapid reduction of Pu(VI) to Pu(IV) by nitric oxide (NO), as compared with NO_2, is probably due to the higher rate of formation of nitrous acid from NO.

Results of initial voloxidation–dissolution tests with highly irradiated, mechanically blended LMFBR fuels are presented.

1.2 ENGINEERING RESEARCH

Particle-rinsing tests recently conducted in the 4-ft-diam rotary dissolver indicated a single-stage rinse efficiency of 65 to 70%. Candidate test materials have been selected for planned erosion–corrosion tests in the rotary dissolver. Radiation test results of a fluorocarbon-based ferrofluid (using ^{60}Co) showed stability up to 10^7 R. This material will be used to evaluate a backup dissolver seal concept. Engineering studies of NO_x scrubbing from off-gases in packed and plate columns have demonstrated efficiencies as high as 97% and have met flowsheet criteria of <2% (vol.) NO_x in the effluent.

Pilot-plant tests and applications studies of the krypton absorption system have identified a possible practical application of the fractionator pinch-point phenomenon to enable the three operations of absorption, fractionation, and stripping to occur in a single unit. The success of such a process simplification will depend upon effective process instrumentation and control; one possible control method has been identified.

Iodox experiment IXD-10, a 43-hr run with CH_3I, indicated an overall column decontamination factor of 2.7×10^4, a value comparable to that measured earlier in a short run. This extended-length run proceeded smoothly.

The storage shield facility for the nondestructive assay experiment has been fabricated and installed in Building 7930. Test samples of enriched uranium subassemblies have been procured for the assay investigations.

Vibration signatures on the rotary dissolver have been analyzed to the extent that reference signatures for each mode of operation can be identified, even in the presence of vibration noise from mechanical anomalies.

Sensor development for process analysis has been initiated with the use of cold-uranium and rare-earth solutions to characterize spectral properties of dissolver solutions. This work will lead to a spectrophotometry system for hot-cell evaluation.

An existing annular centrifugal solvent extraction contactor has been modified and tested at Argonne National Laboratory to explore one means for providing increased residence time for contacting solutions that exhibit relatively slow chemical kinetics. The design of a 0.5-metric ton/day, single-stage contactor is essentially complete.

1.3 ENGINEERING SYSTEMS

In this issue of the Quarterly Report, the areas of Hot Experimental Facility (HEF, formerly HPP) conceptual design, Engineering Analysis, Component Development, and Systems Development [including the Integrated Equipment Test (IET) (formerly IPET)] are reported under the Engineering Systems Section.

A report dealing with the solubility of plutonium-bearing mixed-oxide fuels[1] was completed and is in publication. Initial outlining of the program effects of the Administration's nonproliferation policy has begun in the Engineering Analysis group. The large area formerly called Component Development has been divided into two groups—Component Development and Systems Development.

In the disassembly and cutting task, the detail design of the disassembly machine has continued and orders have been placed for a few long-lead items. Modifications in the ORNL shear have been completed, and instrumentation and controls are being installed. One additional test was performed on the machining equipment, but this method has now been discontinued as a viable alternative to conventional shearing.

In the dissolution task, fabrication of the dissolver has continued on schedule. Several auxiliary components have been received from vendors, and the balance of these components are on order. The installation package for the entire system has been completed, and the cost and schedule is being estimated by the subcontractor. Work should start in July.

The functional area, Systems Development, is newly incorporated and encompasses the tasks that involve major systems rather than individual components, namely, IET, receiving and storage, remote maintenance, waste handling, and decontamination. One other task has been added to Systems Development, although this task does not meet a basic requirement, that being the procurement of depleted uranium fuel for testing in prototype equipment. All of these tasks except decontamination are functioning in Systems Development, and the progress of each is reported.

Title I engineering for IET has continued during this quarter using Construction Planning and Design funds. The IET Project Management Plan has been completed and published.[2] The

preparation of process flowsheets is well under way, and the draft of the environmental impact assessment has been completed. In addition, the draft of the criteria document has been completed and approved and is being used as a working document. The design document master inventory listing all necessary IET drawings, documents, and schedules has been issued.

The first phase of the corrosion work in the receiving and storage task has been completed. No failure of type 316 stainless steel coupons was encountered during the three-month exposure to the four water baths tested. The recommendation that water storage be used for the storage of fuel and blanket subassemblies has been submitted to the HEF conceptual design group. The second phase of the corrosion test program that will provide statistical verification of the preliminary results for type 316 stainless steel is under way.

A program has been initiated in the remote maintenance task to either improve the basic Hanford-Purex line connector or replace it with a smaller and lighter substitute. Bids are being solicited to replace the organic seal in the existing connector with a metallic seal and to provide the program with designs for a different connector that will be remotely operable. This task is also investigating the use of Nitinol (memory alloy) pipe couplings as a method of remotely repairing or replacing damaged or cut sections of pipe.

The waste-handling task has been established to investigate five major areas: (1) the preparation and packaging of stainless steel wastes from subassembly hardware and scrap equipment; (2) the conversion of in-cell organic waste streams to a stable solid; (3) the conversion of high-level liquid waste to a stable solid; (4) the disposal method for other radioactive waste, including gases and low-level solids; and (5) the nondestructive assay of waste streams.

The task for the procurement of fuel for testing is divided into three areas: (1) depleted uranium oxide powder to feed the voloxidizer and/or the dissolver, (2) dummy subassemblies containing depleted uranium oxide or aluminum oxide, and (3) disposal and/or recycle of uranyl nitrate. For the first item, an order for 10,000 kg of U_3O_8 powder from the Y-12 Plant has been initiated. No orders have been prepared for obtaining subassemblies; however, a specification package to obtain bids will be completed in July.

The conceptual design of the HEF has continued on schedule. The change in U.S. policy toward reprocessing is being studied and will be reflected in the design. Capital funding for Title I design, originally planned for FY 1979, will be delayed for one year to FY 1980. The conceptual design phase will be extended from the previously scheduled two years to three years.

REFERENCES FOR SECTION 1

1. E. L. Nicholson, *The PuO_2 Dissolution Problem for LWR Plutonium Recycle and LMFBR Fuels: Fabrication and Reprocessing Problems and Their Resolution,* ORNL/TM-5903 (July 1977).

2. *Project Management Plan for Integrated Prototype Equipment Test Facility* (X-OE-39), May 15, 1977.

2. PROCESS RESEARCH AND DEVELOPMENT

B. L. Vondra

2.1 HOT-CELL OPERATIONS

V. C. A. Vaughen

2.1.1 Development of in-cell equipment

J. H. Goode, R. G. Stacy, G. K. Ford, E. C. Hendren, J. R. Travis, and C. S. Webster

The equipment-removal glove box for the tops of cells 3 and 4 was designed, and construction was initiated.

2.1.2 Flowsheet studies

J. H. Goode, R. G. Stacy, E. C. Hendren, J. R. Travis, and C. S. Webster

Fuel from NUMEC was dissolved, voloxidized, and dissolved. The results are presented below.

Irradiation history and post-irradiation examination results. NUMEC rod No. B-7 was inserted into EBR-2 in S/A X015 on November 15, 1966, for irradiation to a nominal 60,000 MWd/ton. The rod contained two types of 20% PuO_2–80% UO_2 as flat end-pellets:

Type of fuel	Upper fuel, mechanically blended	Lower fuel, coprecipitated
Weight, g	39.43	41.23
Length, in.	6.95	7.37
Density, % theoretical	85.44	82.80
Smear density, %	83.04	81.90
O:M ratio	1.992	2.003

An approximately 6-in.-tall stack of UO_2 pellets was positioned above the mechanically blended fuel, and a 0.25-in. UO_2 pellet was positioned below the lower fuel adjacent to the bottom end plug of the rod. The sodium-encapsulated rod was actually irradiated at about 14 kW/ft in S/A X015, X080, X148, and X167 to a nominal burnup of 16.5% and was discharged in July 1973. The capsule and others were then shipped to ORNL by Argonne National Laboratory in 1975.

The EBR-2 core flux shape is given in Fig. 2.1, which shows the positions of the fuel used in these experiments. The experiments with NUMEC rod B-7 top (FBR-1A, -B, -1C) are described below.

Fig. 2.2 shows the fuel and blanket locations and a differential gamma scan (0.55 to 0.75 MeV) of the rod that was made at ORNL in December 1976. The scan showed redistribution of cesium; in addition to the usual peaks at the ends of the fuel column at the UO_2 blanket pellets, other peaks along the column were also caused by ^{137}Cs (Similar appearing cesium peaks were noted at LASL

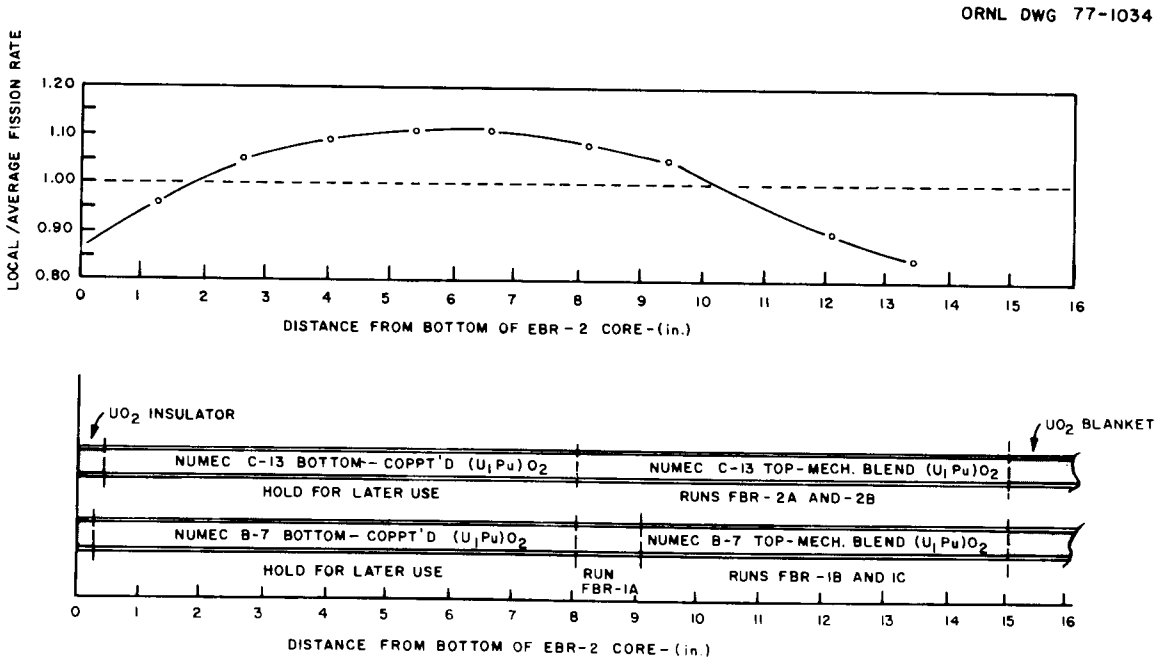

Fig. 2.1. Variations in fission rate as function of location and sectioning diagram for NUMEC fuel rods.

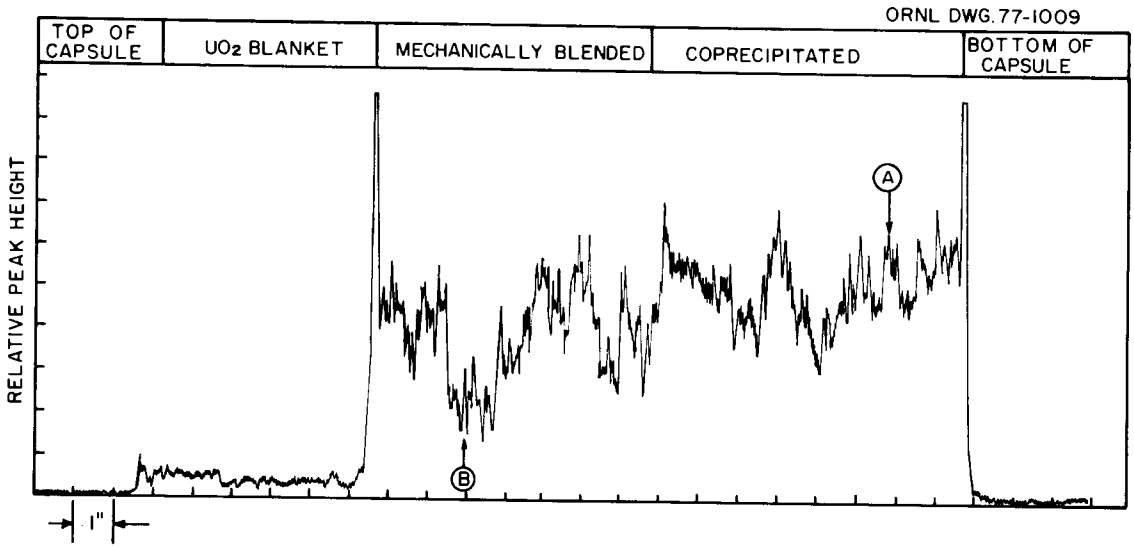

Fig. 2.2. Differential (0.55 to 0.75 MeV) gamma scan of NUMEC rod B-7, showing fuel types in rod.

for other NUMEC rods from the A-series of irradiations.)[1] A qualitative scan at the peak at point A showed $^{137}Cs >>> ^{106}Ru$, and a scan at valley point B showed $^{137}Cs >> ^{106}Ru > ^{144}Ce, ^{134}Cs, ^{60}Co$ (i.e., more "normal" fuel and cladding).

The rod plenum was punctured and released 204.337 cm^3 (STP) of gas from a void volume of 16.726 cm^3. Analysis of the puncture gas showed:

Gas released	Amount (% of total)	Gas released	Amount (% of total)
H_2	<0.01	A	<0.01
He	8.8	CO_2	0.01
H_2O	0.05	Kr	12.0
N_2+CO	0.02	Xe	79.2
O_2	<0.01		

Analyses of the xenon and krypton isotopes in the puncture gas were:

Krypton isotope	Amount (%)	Xenon isotope	Amount (%)
^{82}Kr	0.03%	^{128}Xe	0.01%
^{83}Kr	15.91	^{130}Xe	0.05
^{84}Kr	28.61	^{131}Xe	14.57
^{85}Kr	4.95	^{132}Xe	22.70
^{86}Kr	50.50	^{134}Xe	34.04
		^{136}Xe	28.63

A total of 7.683×10^{10} dis/sec of ^{85}Kr was released when the plenum was punctured; this is equivalent to about 95% of the total amount of ^{85}Kr recovered (about 4.50×10^9 dis/sec of ^{85}Kr was recovered from the dissolution).

Shearing. The single-pin fuel shear was used to cut NUMEC rod B-7 into 0.5-in.-long segments for the base-line voloxidation and dissolution studies. The following cutting pressures were noted for each section of the rod:

Type of fuel	Average pressure per cut (psig)
Coprecipitated	151
Mechanically blended	117
UO_2 blanket	266

The value of the blanket region is approximately one-third of the force required to shear 31,000 MWd/ton of Zircaloy-clad UO_2 discharged from the H. B. Robinson-2 reactor. Deformation to the ends of the cut pieces was moderate, with a large number having jagged, uneven edges; but there was no evidence of significant pillowing (closure) on the ends.

The mechanically blended fuel from NUMEC rod B-7 was further characterized before its use in the FBR-1 series of base-line experiments. The total weight of $(U,Pu)O_2$ and fission products

from that section was 36.1 g, with 10% being dislodged from the hulls during the shearing operation. Screen-mesh analysis of the as-sheared fines was as follows:

Mesh	Weight (g)	Percent total
+35	1.96	54
+100	0.92	26
−100	0.72	20
Total	3.60	

Two 0.5-in.-long segments of the stainless steel clad mechanically blended $(U,Pu)O_2$ were selected at random for dissolution in nitric acid to provide base-line information for comparison with voloxidized fuel and other experiments (see Dissolution below). The remaining mechanically blended fuel was charged to the rotary burner for voloxidation (run FBR-1). The sheared segments of coprecipitated and blanket materials were stored for subsequent studies.

Voloxidation. The voloxidation apparatus, the gas flow system, and the operating and sampling procedures employed for fast reactor fuel studies are essentially the same as those used for LWR fuel studies and are described in quarterly project progress reports. The entire system is diagrammed in Fig. 2.3. Voloxidation off-gases are sent to the penthouse area above the cell where they are sequentially trapped for ^3H_2O content, continuously analyzed for ^{85}Kr and O_2 content, and finally collected for cumulative measurements on ^{85}Kr and ^{14}C release. The system is sampled for particulates and semivolatile species in the following sequence:

1. Sheet specimens and coupons are located inside the voloxidizer to check for fission product deposition and scouring by hulls.

2. A 35-μ pore size sintered metal frit in the exit end of the burner is followed by stainless steel deposition tubing inserts and steel wool packing.

3. A heated filter pack containing metal frits, graded filter papers, and charcoal granules is positioned after the deposition inserts.

4. A HEPA filter is located immediately outside the cell for secondary particulate removal.

During the FBR-1 voloxidation, the HEPA filter was not used because of earlier difficulties in keeping it adequately heated. In later experiments, another model HEPA filter was inserted and used successfully. Not shown in Fig. 2.3 is a newly-installed gas sampling port adjacent to the flow-through sensor for the multichannel analyzer. It was used for the first time during the FBR-1 run to extract flowing-stream gas samples directly from the off-gas stream while the gas was being counted for ^{85}Kr content. A mass flow metering system, including a flow totalizer and a calibrated flow splitter in the line, permitted measurement of accumulated off-gas volumes without using the wet test meter.

The rotary voloxidizer was charged with 40.4 g of sheared mechanically blended $(U,Pu)O_2$ from NUMEC rod B-7 (11 clad pieces containing 28.1 g of fuel and 3.6 g of loose oxide fines). Treatment conditions for the run were as follows: time, 3.2 hr; temperature, 650°C; atmosphere, air fed at 300 cm^3/min; agitation, rotation at 12 rpm. To assure completeness of reaction, the experiment was continued beyond the point at which there was evidence of oxygen consumption and the ^{85}Kr content in the off-gas had returned to near background levels.

ORNL DWG. 77-616

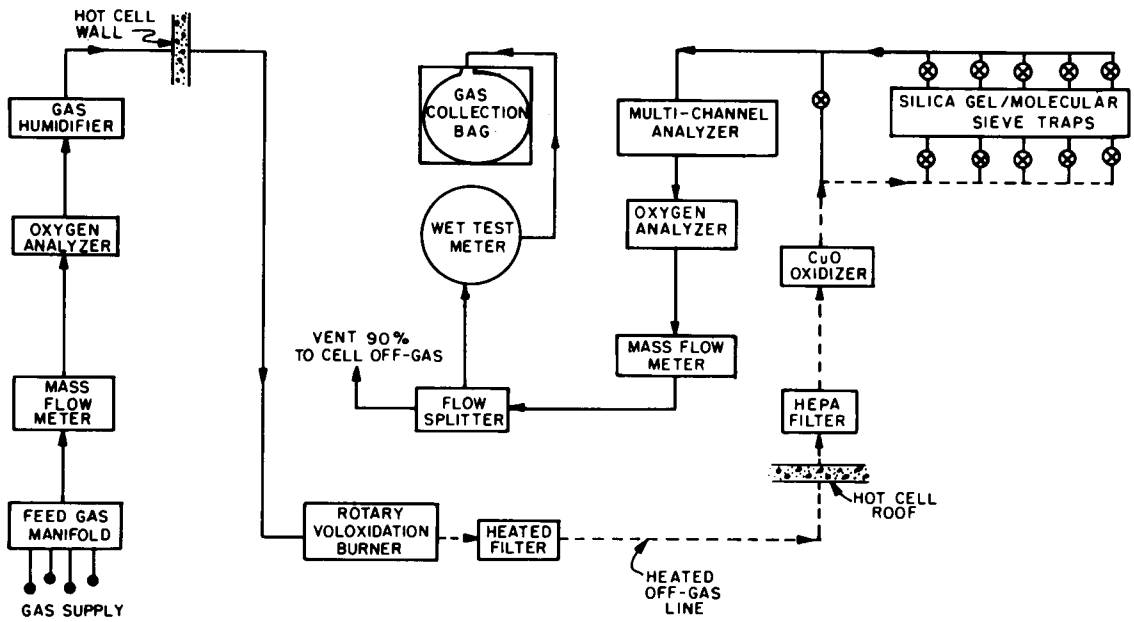

Fig. 2.3. Voloxidation gas-flow system at Building 4507.

Oxide conversion and gas evolution. Evolution rate curves for krypton and tritium are related to the corresponding oxygen content in the voloxidizer off-gas as a function of run time (Fig. 2.4). The evolution information is derived from a measured amount of radionuclide activity present in a known volume of off-gas collected over a specific time interval. Tritium was collected as ^3H_2O on silica gel and molecular sieve traps, and the krypton (^{85}Kr) content was determined by gamma scanning the flowing-stream gas samples. Release profiles (percentages of amounts initially in the fuel) are shown for the FBR-1 voloxidation (Fig. 2.5). A profile for the conversion of the UO_2 in the $(U,Pu)O_2$ to U_3O_8 is shown in Fig. 2.6. In all the displays (Figs. 2.3–2.6), the graph time of 0.0 hr represents the point of first signs of ^{85}Kr evolution (temperature = 300°C). The tritium traps were not replaced soon enough in this run to describe adequately the early tritium release curve. About 28% of the total was evolved during the heat-up to 650°C (as compared with about 5% of the total ^{85}Kr released in the same period). Most of the evolved ^3H and ^{85}Kr was measured in the first hour at temperature, with the evolution rates diminishing rapidly thereafter. After slightly more than 3.0 hr of voloxidation at 650°C, nearly 38% of the original ^{85}Kr had evolved, and the measured ^3H release was about 93%. Another 3% of the ^3H was released during the cooling period, bringing the total ^3H release during voloxidation up to 96% of the total found in all steps.

During the preheat period, oxygen consumption began as the temperature of that charge reached 400°C; approximately 6% of the UO_2 was converted to U_3O_8 by that time. Oxygen consumption peaked within 10 min of the time at 650° and was nearly finished at 0.5 hr. A final conversion level of 51.5% was attained after 1.0 hr. This corresponds to the measured 0.5-g weight gain for the charged fuel and verifies that all the converted oxide was released from the hulls as fines (Table 2.1). Screen mesh analysis on the 19.0 g of powdered fuel showed that 44% was +100 mesh,

ORNL DWG 77-1036

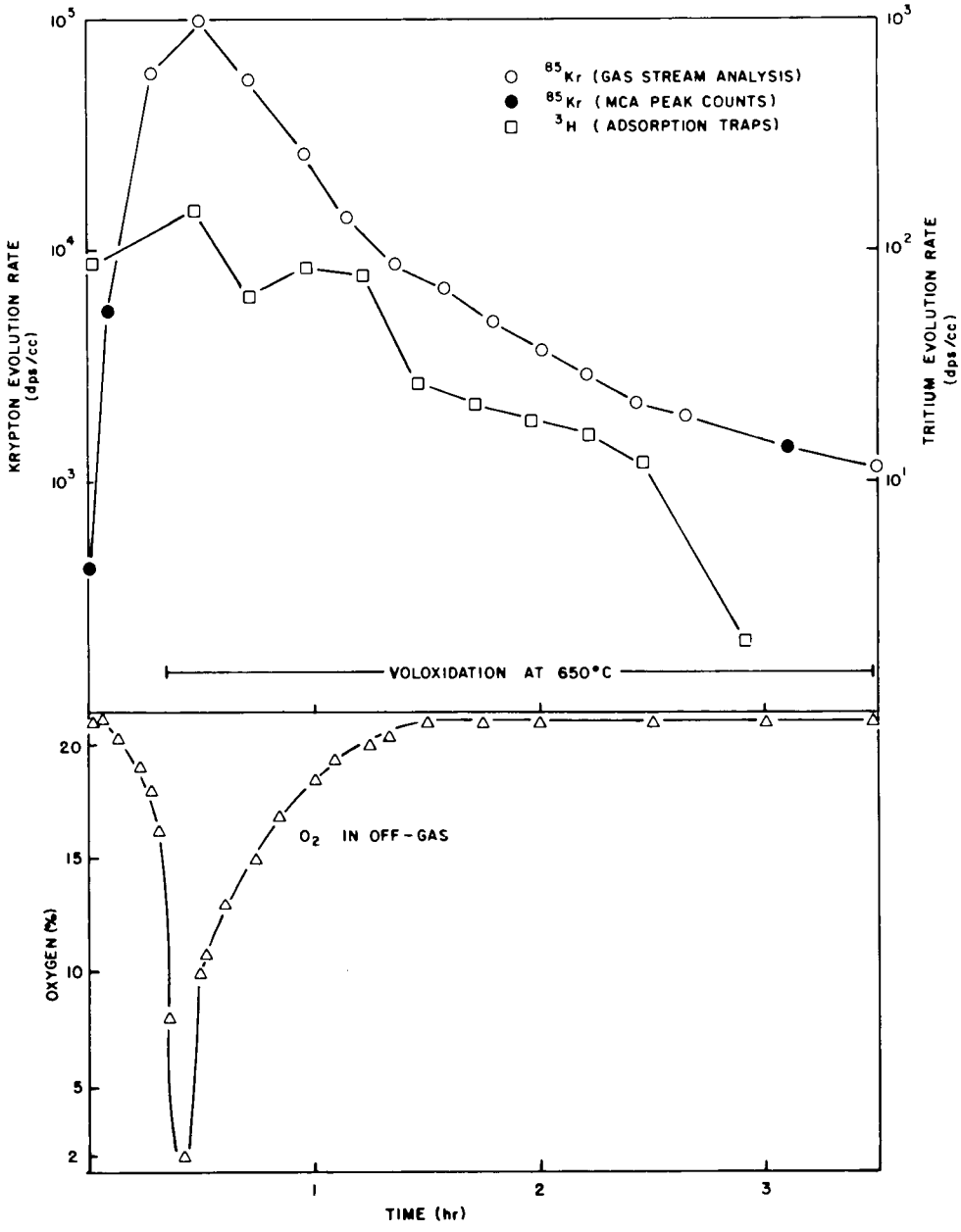

Fig. 2.4. Tritium and krypton evolution and oxygen consumption during voloxidation of NUMEC B-7 (20% PuO_2–80% UO_2) in air at 650°C (run FBR-1).

ORNL DWG 77-1037

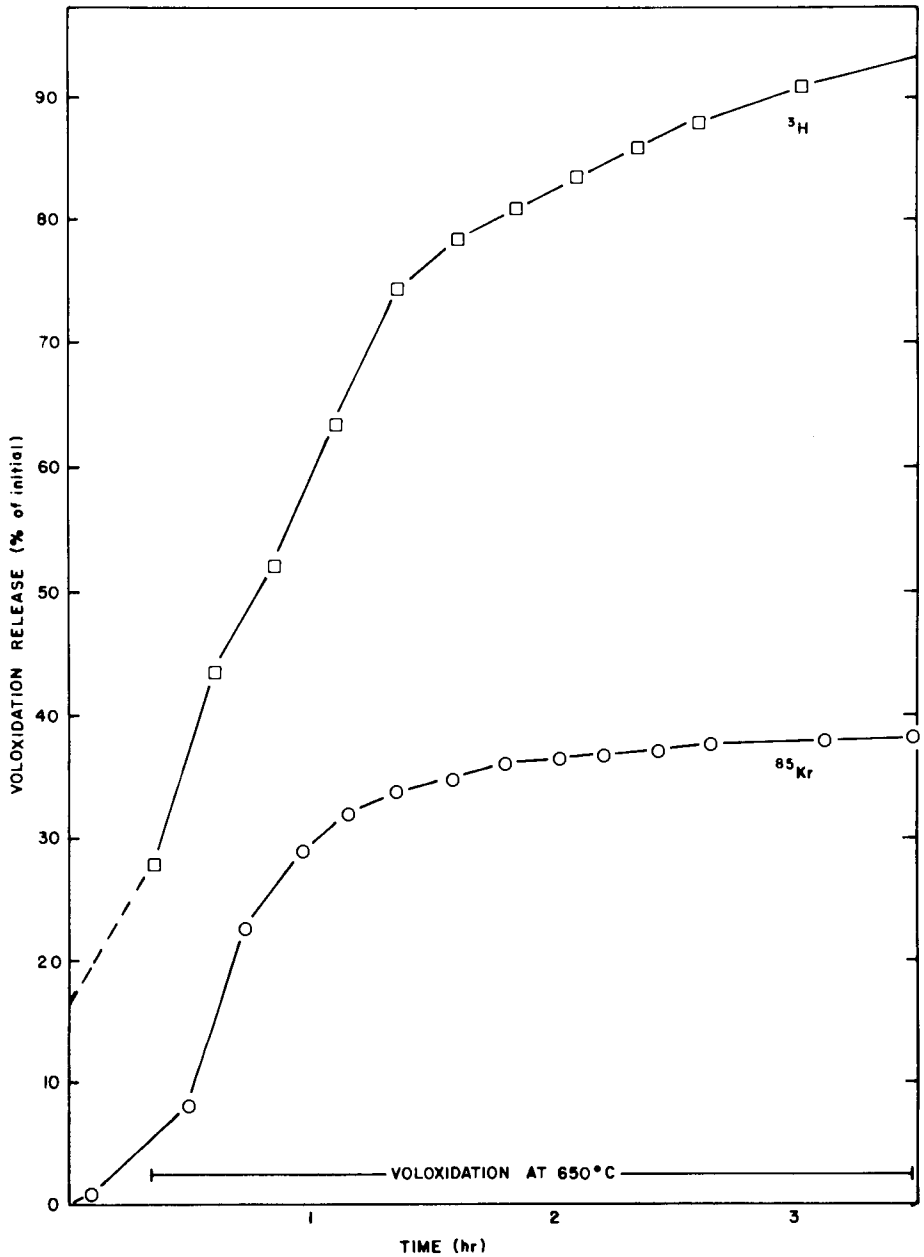

Fig. 2.5. Release of tritium and krypton during voloxidation of NUMEC B-7 (20% PuO_2–80%UO_2) in air at 650°C (run FBR-1).

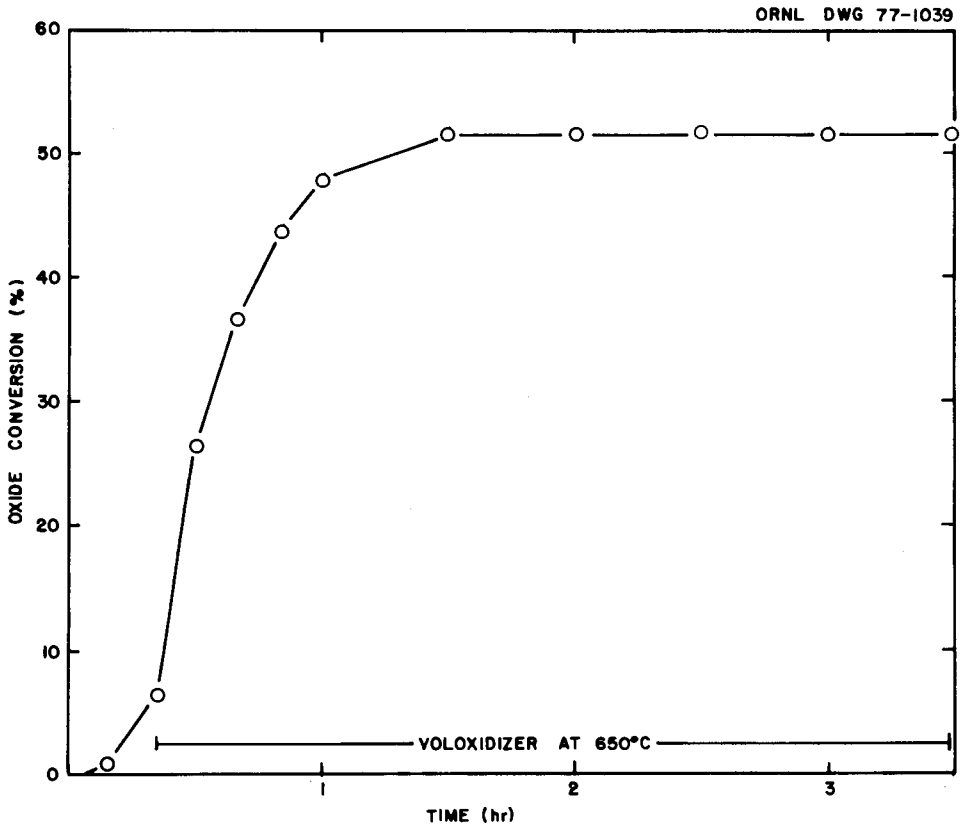

Fig. 2.6. Conversion of UO_2 to U_3O_8 during voloxidation of NUMEC B-7 (20% PuO_2–80% UO_2) in air at 650°C (run FBR-1).

Table 2.1 Material balance on voloxidation of NUMEC B-7 mechanically blended $(U,Pu)O_2$ in air at 650°C (run FBR-1)

Material balance	Weight (g)
Input[a]	
$(U,Pu)O_2$ (clad)	28.1
$(U,Pu)O_2$ (fines)	3.6
Cladding	8.7
Total	40.4
Output[a]	
Oxidized $(U,Pu)O_2$ (clad)[b]	13.2
Oxidized $(U,Pu)O_2$ (fines)	19.0
Cladding	8.7
Total	40.9
Weight gain, g	0.5
UO_2 conversion, %[c]	51.5

[a]$(U,Pu)O_2$ totals include weight of fission products.
[b]Includes weight of unconverted oxide.
[c]Assuming minimal oxidation of 316 stainless steel.

21% was +325 mesh, and 35% was −325 mesh. Voloxidation of the mechanically blended $(U,Pu)O_2$ air at 650°C increased the amount of loose fuel to about 59% of the total, nearly a five-fold increase in the amount initially dislodged on shearing.

The close correspondence between ^{85}Kr evolution and O_2 consumption that was seen in voloxidation of Zircaloy-clad UO_2 (H. B. Robinson) was also present during the voloxidation of the NUMEC mechanically blended mixed oxides. The major apparent difference was the absence of a double peak for ^{85}Kr evolution and O_2 consumption (noticed in the H. B. Robinson fuel voloxidations at 480°C).

Dissolution. In this experiment, two pieces of clad fuel were removed from the batch of sheared fuel from NUMEC rod B-7 to provide baseline data for other experiments with this fuel. There is now some doubt that these samples were truly representative (or random) in that the fission product inventories (described later) were more typical of the high burnup end of the rod.

The leaching procedure was chosen to simulate plant practice. In this experiment, the 5.9 g of clad fuel segments was leached in 8 *M* HNO_3. The cladding was then separated from the insoluble fuel residue and washed. The residue and cladding were then treated in separate vessels for the rest of the experiment.

The complete leaching sequence was:

1. 1st leach: 8 *M* HNO_3, 2 hr, 92–95°C (fuel plus cladding),
2. 2nd leach: 3 *M* HNO_3, 2 hr, 92–95°C (fuel residue and cladding separated),
3. 3rd leach: 8 *M* HNO_3, 2 hr, 92–95°C (fuel residue and cladding separated),
4. 4th leach: 8 *M* HNO_3–0.05 *M* KF, 2 hr, 92–95°C (residue only), 5 *M* HNO_3–2 *M* HCl–0.05 *M* KF, 2 hr, 92–95°C (cladding only).

The final leaches with fluoride were for material balance purposes.

The off-gases from the first nitric acid leach were passed through a reflux condenser and an empty condensate trap and bubbled through a fritted glass dispersion tube into a gas washing bottle filled with 3 *M* NaOH. Each vessel was rinsed and sampled for fission product activity.

Material balances. The overall weight material balance was about 102%; the input weight was 5.9 g. We recovered: 3.56 g of UO_2, 0.77 g of PuO_2, 0.05 g of insoluble fuel residue, 1.38 g of stainless steel (calculated from iron concentrations), 0.03 g of cladding residue and 0.21 g of soluble fission products for a total of 6.00 g. The uranium and plutonium isotopic analysis for the first leach solution showed:

Isotope	Amount (%)	Isotope	Amount (%)
^{233}U	0.001	^{238}Pu	0.042
^{234}U	0.672	^{239}Pu	91.13
^{235}U	89.23	^{240}Pu	8.41
^{236}U	3.02	^{241}Pu	0.38
^{238}U	7.08	^{242}Pu	0.031

Plutonium material balances were calculated from the mass spectroscopic (isotopic) analysis of the plutonium in the first leach solution and the specific activity of each plutonium isotope as follows:

Isotope	Fraction	Specific activity (counts min^{-1} mg^{-1})	Plutonium (counts min^{-1} mg^{-1})
^{238}Pu	0.00042	1.97×10^{10}	8.27×10^{6}
^{239}Pu	0.9113	6.95×10^{7}	6.33×10^{7}
^{240}Pu	0.0841	2.70×10^{8}	2.27×10^{7}
^{242}Pu	0.00031	4.41×10^{6}	1.37×10^{3}
Total			9.43×10^{7}

Table 2.2 shows that 99.99% of the plutonium and 99.98% of the uranium were soluble in nitric acid. This may be compared with 0.18% insoluble plutonium after 6 hr in 6 *M* HNO_3 in a 1974 experiment with NUMEC A-series rods containing fuels from the same fabrication batches at 33,000 MWd/ton burnup.[2]

Table 2.2 Leaching of irradiated, stainless-steel-clad, mechanically blended 20% PuO_2–80% UO_2 from NUMEC rod B-7 (2 hr each, 92–95°C)

Leach	Dissolvent	Fuel fraction				Cladding fraction			
		Uranium		Plutonium		Uranium		Plutonium	
		(mg)	(%Σ)	(mg)	(%Σ)	(mg)	(%Σ)	(mg)	(%Σ)
1	8 *M* HNO_3	3123.7	99.72	672.50	99.78				
2	3 *M* HNO_3	3.48	0.11	0.59	0.09	0.02	<0.001	0.002	<0.01
3	8 *M* HNO_3	4.08	0.13	0.78	0.12	0.18	0.01	0.04	<0.01
4	8 *M* HNO_3–0.05 *M* KF	0.60	0.02	0.01	<0.01	0.29	<0.01	0.07	0.01
Residue	5 *M* HNO_3–2 *M* HCl	0.04	<0.01	<0.01	<0.01	0.07	<0.01	0.01	<0.01
Total[a]		3132	99.98	677	99.99	0.56	0.02	0.13	0.01

[a]Total heavy metal oxide: UO_2, 3.556 g; PuO_2, 0.768 g; total, 4.324 g.

Dissolution of fission products. Analyses of the clarified first leach solution gave the following composition:

Material	Concentration	Material	Concentration
Total U	64.55 mg ml^{-1}	^{99}Tc	10.3 μg ml^{-1}
Total Pu	14.21 mg ml^{-1}	^{106}Ru	$\leq 8.7 \times 10^{6}$ dis sec^{-1} ml^{-1}
^{241}Am	0.044 mg ml^{-1}	^{125}Sb	3.07×10^{7} dis sec^{-1} ml^{-1}
^{242}Cm	1.6×10^{-6} counts min^{-1} ml^{-1}	^{129}I	0.507 μg ml^{-1}
Gross alpha	1.41×10^{9} counts min^{-1} ml^{-1}	^{134}Cs	2.30×10^{7} dis sec^{-1} ml^{-1}
Gross gamma	1.92×10^{8} counts sec^{-1} ml^{-1}	^{137}Cs	9.98×10^{8} dis sec^{-1} ml^{-1}
$^{3}H_2O$	4.44×10^{2} dis sec^{-1} ml^{-1}	^{144}Ce	2.51×10^{8} dis sec^{-1} ml^{-1}
^{14}C	1.76×10^{2} dis sec^{-1} ml^{-1}	^{154}Eu	$\leq 3.5 \times 10^{6}$ dis sec^{-1} ml^{-1}
HNO_3	7.93M		

Spark source mass spectrometry (SSMS) indicated that this solution also contained (in μg/ml): 900 Nd, 900 Cs, 400 Mo, 350 Sm, 300 Ba, 300 Pd, 250 Ce, 200 Te, 150 Pr, 150 La, 150 Rb, 120 Sr, 80 Y, 50 Eu, 40 Pm, and 40 Ag, along with smaller quantities of tin, technetium (10 μg/ml), ruthenium, rhodium, and other elements. The dissolved fission products totaled 0.206 g.

Insoluble residues. The 49-mg residue remaining from the four leaches was about 1.1 wt % of the oxide charged into the dissolver. Emission spectroscopy analysis showed the following (in wt %): 45 Ru, 20 Tc, 10 Rh, 10 Fe, 7.5 Pd, 5 Cr, 5 Mo, 3 Ni, 2 Zr, and 0.3 Si.

The residue contained ^{106}Ru (2.47×10^6 Ci/g of residue), ^{90}Sr (1.11×10^4 Ci/g), ^{137}Cs (4.65×10^3 Ci/g), and smaller quantities of ^{125}Sb and ^{99}Tc.

Volatilization of fission products on dissolution. Dissolution of the fuel in nitric acid released the contained ^{85}Kr in essentially one "burst," as measured on a multichannel analyzer in the off-gas system. We collected 5.58×10^7 dis/sec of ^{85}Kr/g (U+Pu). The quantities of other fission products found in the dissolver and residue, the reflux condenser and condensate trap, and the sodium hydroxide scrubber are summarized in Table 2.3. All but the ^{14}C and ^{129}I remained in the dissolver solution or residue.

Table 2.3. Volatilization of fission products during dissolution of $(U,Pu)O_2$ in 8 *M* HNO_3

Nuclide	Total found (U+Pu)+cr (dis sec^{-1} g^{-1})	Amount found (percent of total)		
		Dissolver solution and residue	Condenser and condensate traps	NaOH Scrubber
Gross γ	2.47×10^{9a}	99.99	0.004	<0.001
^3H_2O	5.93×10^3	92.58	6.59	<0.001
^{14}C	5.88×10^4	3.06	<0.01	96.94
^{106}Ru	1.34×10^9	99.99	0.003	0.001
^{125}Sb	4.06×10^8	99.99	0.004	0.001
^{129}I	220.4^b	2.87	0.03	93.97
^{137}Cs	1.19×10^{10}	99.99	0.004	<0.001
^{144}Ce	3.13×10^9	99.99	0.003	<0.001

[a]Counts sec^{-1} g^{-1}.
[b]μg g^{-1}.

Effects of voloxidation on dissolution. The 40.4 g of stainless-clad $(U,Pu)O_2$ produced 40.9 g of voloxidizer product (above), which was divided into a fraction of loose oxide (19.0 g) and a fraction of loose and partially clad oxide (21.9 g). The fractions were dissolved in two separate experiments (FBR-1B and -1C). The results have been combined and are reported here as one experiment (FBR-1BC).

Material balance. The input weights were calculated from the results of FBR-1A (reported above). The results after the standard leaching procedure (above) are given for comparison:

Material	Input, calculated (g)	Output, measured (g)
Cladding	8.65	8.50
(U+Pu)	26.61	26.54
Insoluble residue	0.35	0.50
Soluble fission products (estimated)	1.44	1.44
Oxygen [calculated as $(U,Pu)O_2$]	3.85	3.58
Total	40.90	40.56

The first effect of voloxidation was an increase in the weight of the insoluble residue after the four leaches, that is, from 1.1 wt % of the $(U,Pu)O_2$ to 1.67 wt % after voloxidation. Table 2.4 summarizes the dissolution results for uranium and pluonium. The voloxidation treatment apparently decreased the solubility of the heavy metals from that of the nonvoloxidized fuel in the following manner:

	Solubility in nitric acid	
	Uranium (%)	Plutonium (%)
Nonvoloxidized	99.98	99.99
Voloxidized	99.80	98.35

Further experiments must confirm whether the lower solubility was caused by voloxidation or by some other effect (see burnup description), because most of the earlier work did not show such a pronounced effect.

Table 2.4. Leaching of voloxidized, irradiated stainless-steel-clad, mechanically blended $(U,Pu)O_2$ from NUMEC rod B-7 (2 hr each, 92–95°C)

Leach	Dissolvent	Uranium (mg)	Dissolved (%)	Plutonium (mg)	Dissolved (%)
1	8 *M* HNO_3	21,453.32	99.27	4785.00	97.32
2	3 *M* HNO_3	78.48	0.36	21.99	0.45
3	8 *M* HNO_3	35.31	0.16	28.41	0.58
4	8 *M* HNO_3–0.05 *M* KF	31.43	0.15	77.29	1.57
Leached cladding	–	1.00	<0.01	0.90	0.02
Insoluble residues	–	11.13	0.05	3.11	0.06
Total		21,612[a]		4917[b]	

[a]≅ 24.53 g of UO_2.
[b]≅ 5.57 g of PuO_2.

Fission product recoveries. Considerable variation was found in the amounts of fission products found (per gram of (U+Pu) in the oxidized and nonoxidized fuel (Table 2.5.) The randomly selected segments used in run FBR-1A showed generally higher values for many of the nuclides, except for tritium. The ratio of the amounts found (FBR-1A:FBR-1BC) were generally between about 0.8 and 1.3 except for ^{3}H, ^{14}C, and ^{125}Sb. This range represents our current analytical uncertainties.

Insoluble residues. The 503 mg of insoluble residue remaining after four leaches of the voloxidized fuel represented 1.67 wt % of the dissolved mixed oxide. The residue was similar in composition to the residue obtained with nonvoloxidized fuel; it contained (per gram of residue): 1.7×10^6 Ci of ^{106}Ru, 2.1×10^5 Ci of ^{125}Sb, and 1.5×10^4 Ci of ^{137}Cs.

Release of fission products during dissolution of voloxidized fuel. The quantities of fission products volatilized during the dissolution of voloxidized fuel is presented in Table 2.6. The results are similar to those with nonvoloxidized fuel (Table 2.3); most nuclides remained in the dissolver solution.

Cladding solubility. The various leach solutions were analyzed for iron to determine the amount of type 316 stainless steel that dissolved in the various reagents. The successive 2-hr leaches at

Table 2.5. Overall fission product recoveries from FBR-1 series (NUMEC B-7) $(U,Pu)O_2$

Nuclide	Recovered in dissolution (dis sec^{-1} g^{-1})(U+Pu)		Total recovered (FBR-1BC)[b]	Ratio run BC:run A
	Nonoxidized (FBR-1A)	Oxidized (FBR-1BC)[a]		
(U+Pu)[c]	3.81	26.54	26.54	
$^{3}H_2$	5.93×10^{3}	3.99×10^{3}	1.01×10^{5}	17.0
^{14}C	5.88×10^{4}	5.76×10^{3}	3.31×10^{4}	0.56
^{85}Kr	5.58×10^{7}	2.28×10^{7}	4.41×10^{7}	0.79
^{106}Ru	1.34×10^{9}	1.71×10^{9}	1.71×10^{9}	1.28
^{125}Sb	4.06×10^{8}	7.01×10^{8}	7.01×10^{8}	1.73
^{129}I[d]	220	8	186	0.85
^{137}Cs	1.19×10^{10}	1.03×10^{10}	1.05×10^{10}	0.88
^{144}Ce	3.13×10^{9}	2.92×10^{9}	2.92×10^{9}	0.93

[a]Total for runs 1B and 1C.
[b]Includes amount volatilized in the voloxidation step.
[c]Grams.
[d]Mg g^{-1} (U+Pu).

Table 2.6. Volatility of fission products during dissolution of voloxidized $(U,Pu)O_2$ in 8 *M* HNO_3 (run FBR-1BC)

Nuclide	Total found (U+Pu) (dis sec^{-1} g^{-1})	Amount found (percent of total)		
		Dissolver and residue	Condenser and trap	NaOH scrubber
Gross γ	2.25×10^{9}[a]	~99.99	0.005	<0.001
$^{3}H_2O$	4.11×10^{3}	70.01	3.70	23.11
^{14}C	5.77×10^{3}	22.90	<0.01	77.19
^{85}Kr	4.41×10^{7}			
^{106}Ru	2.91×10^{9}	>99.99	<0.001	<0.001
^{125}Sb	7.01×10^{8}	>99.99	<0.001	<0.001
^{129}I	167.5[b]	5.4	3.6	90.8
^{137}Cs	1.04×10^{10}	>99.99	0.006	<0.001
^{144}Ce	2.92×10^{9}	>99.99	0.006	<0.001

[a]Counts sec^{-1} g^{-1}.
[b]μg g^{-1}.

92–95°C with 8 *M* HNO_3, 3 *M* HNO_3, and 8 *M* HNO_3 dissolved 0.47, 0.12, and 0.18%, respectively, of the stainless steel. In the last leach with 8 *M* HNO_3–0.05 *M* KF, 3.58% was dissolved.

Discussion. Although two pieces of clad fuel were taken at random from the batch of sheared fuel for the control (the nonvoloxidized baseline case), fission product and heavy metal analyses indicate that these two pieces had experienced higher burnup and perhaps higher temperatures than the bulk of the fuel.

This result could be explained by axial variations in fission rate and subsequent different local burnups in EBR-2 (Fig. 2.2). Assume the two 0.5-in. segments used in FBR-1A came from the lower 1-in. of the mechanically blended fuel (nearer the center of the EBR-2 core) where the local-to-average fission rate was about 1.08; assume the rest of the mechanically blended fuel used in FBR-1B and -1C had a local to average fission rate of about 0.91. An indicated burnup ratio

between the two samples of 0.84 is obtained between -1A and -1BC. The ratios of various fission products in each run of krypton, iodine, cesium, and cerium were found to have similar values (Table 2.5). In addition, tritium differences may be caused by the higher temperature at the center location. Finally, the fuel segments used in -1A also had less plutonium (1.04X) than did the fuel used in -1BC.

We conclude that the samples were not "random" with respect to the average flux.

2.2 LABORATORY STUDIES

J. C. Mailen

2.2.1 Plutonium dioxide dissolution studies

O. K. Tallent and Karen Williams

Introduction. We are examining methods for dissolving residues after nitric acid dissolution of mixed UO_2–PuO_2 fuels.[3] These residues contain various fission and corrosion products along with highly refractory undissolved PuO_2 and UO_2. The HI dissolution method under consideration[4] includes process steps in which the residues are refluxed in 6.0 *M* HI solution; the HI solution is distilled to dryness, and the dried cake containing metal iodides and oxides is dissolved in 8.0 *M* HNO_3. The dissolution reaction for the PuO_2 component[5] in the residues has been shown to be

$$PuO_2 + 2\ Hi \rightarrow PuOI + H_2O + {}^1/_2 I_2\ . \tag{2.1}$$

The dissolution of UO_2 in HI solutions is more complex and involved and is less well understood than the PuO_2 dissolution. It has been reported that UO_2 dissolves at a slower rate than PuO_2 in HI solutions.[4] This low dissolution rate does not present a serious problem because UO_2 can be dissolved readily in HNO_3 solutions after the PuO_2 from the residue has been converted to PuOI. The dissolution of UO_2 in HI solution is, nevertheless, of interest because it represents a part of the chemistry occurring in the UO_2–PuO_2 residue dissolution process.

There is little information in the open literature on the chemistry of uranium iodides. Mellor's treatise[6] refers to a report dating to 1842, which states that hydrated uranium dioxide dissolves in aqueous HI solution to produce a green solution containing UI_4 and that this solution when heated turns brown and precipitates. Since this early report, there have been other reports[7–12] on the physical and chemical properties of UI_4, UI_3, and UO_2I_2; but there has been no substantiative new information on the aqueous chemistry of these substances.

We have completed a number of experiments in which UO_2 microspheres were partially dissolved in aqueous HI solutions. The results from these experiments are not particularly definitive, as is discussed further on in the report. The experiments along with representative examples of the results obtained are described below.

Experimental methods. The dissolution tests were conducted by digesting either 0.5 or 1.0 g of UO_2 microspheres having a density of 10.44 g/cm^3, a surface area of 0.01 m^2/g, and a diameter of 350 to 420 μ in 6 or 25 ml of aqueous HI solution. The dissolution time was varied from 7 to 24 hr, the HI concentration from 1.0 to 6.0 *M*, and the dissolution temperature from 42 to 100°C. Samples

of the dissolver solutions were taken in small volumes at temperature, cooled, filtered, and analyzed for uranium.

Experimental results. The concentrations of uranium dissolved (from 0.5 g of microspheres) in 6.0 ml of 2.5, 3.3, and 5.5 *M* HI solution at 100°C are plotted in Fig. 2.7 as a function of dissolution time. The data plotted in the figure are in many respects typical of a large body of data that we have obtained in this work. No clear systematic relationship between uranium dissolution rate and HI concentration is indicated. The amount of uranium dissolved in 2.5 *M* HI is shown in the figure to be greater at times than that dissolved in 5.5 *M* HI, but at other times it is less than that dissolved in 3.3 *M* HI. The data in the figure also show that the concentration of uranium in soluton first increases and then decreases with dissolution or digestion time. A similar decrease in uranium concentration with time is illustrated by the data plotted in Fig. 2.8, where the concentration of uranium dissolved (from 1.0 g of microspheres) in 25 ml of 6.0 *M* HI solution at 42°C is plotted as a function of dissolution time. It can be seen in the figure that the concentration of uranium in solution increased to 107 μg/ml in the first hour and then decreased to 32 μg/ml during the next 9 hr. Decreases in uranium concentration in solution such as those shown in Figs. 2.7 and 2.8 have been typically obtained in a number of experiments under a variety of conditions.

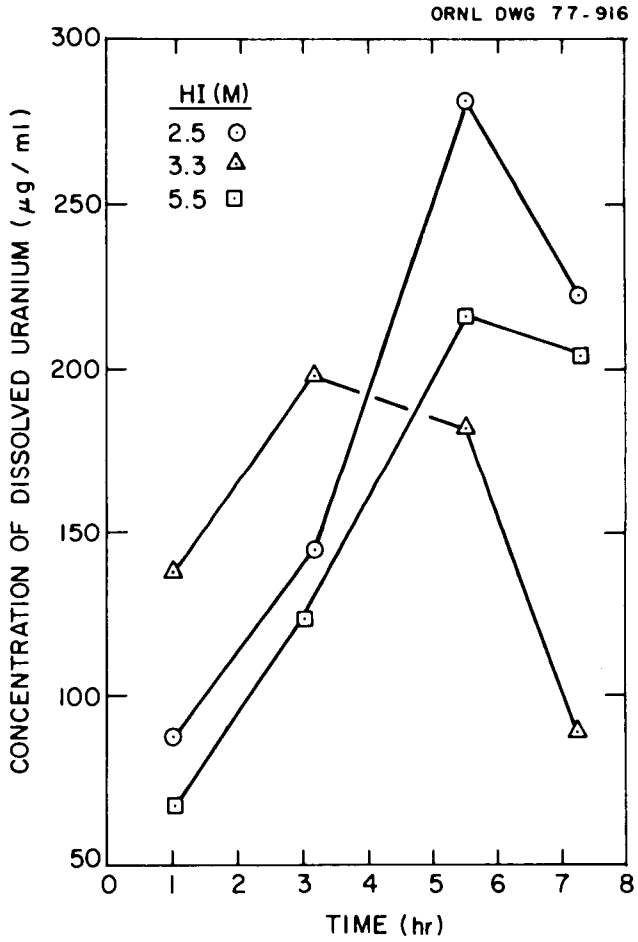

Fig. 2.7. Dissolution of UO_2 in HI solutions at 100°C.

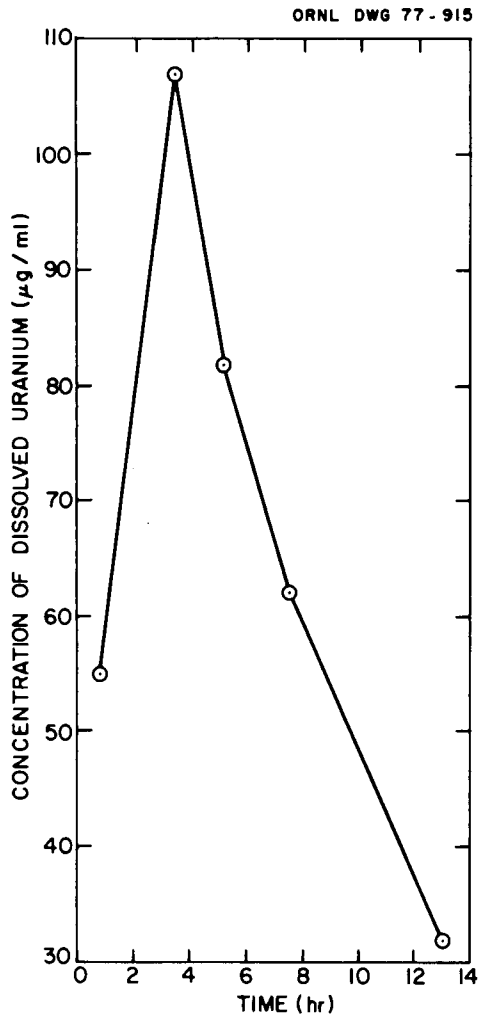

Fig. 2.8. Dissolution of UO_2 in 6.0 *M* HI solution at 42°C.

The concentration of ruthenium in solution in 6.0 *M* HI has also been found to decrease with increasing dissolution or digestion time.[13] The data showing this effect were obtained from an experiment in which 1.0 g of RuO_2 was digested in 60 ml of 5.5 *M* HI at 122°C. The concentration of ruthenium in solution as a function of digestion (or dissolution) time is plotted in Fig. 2.9. The concentration in solution decreased from 620 to 270 μg/ml over a period of 5 hr of digestion time.

Discussion. It is apparent from the data obtained that the dissolution of UO_2 in HI solutions involves two or more competing or consecutive reactions. It can be speculated that reactions such as

$$UO_2 + 4HI \rightleftarrows UI_4 + 2H_2O \tag{2.2}$$

and

$$UO_2 + 4HI \rightleftarrows UI_3 + 2H_2O + {}^1/_2I_2 \tag{2.3}$$

occur to increase the concentration of uranium in solution and that other reactions occur to form uranium oxides or oxyiodides that precipitate and decrease the uranium concentration in solution.

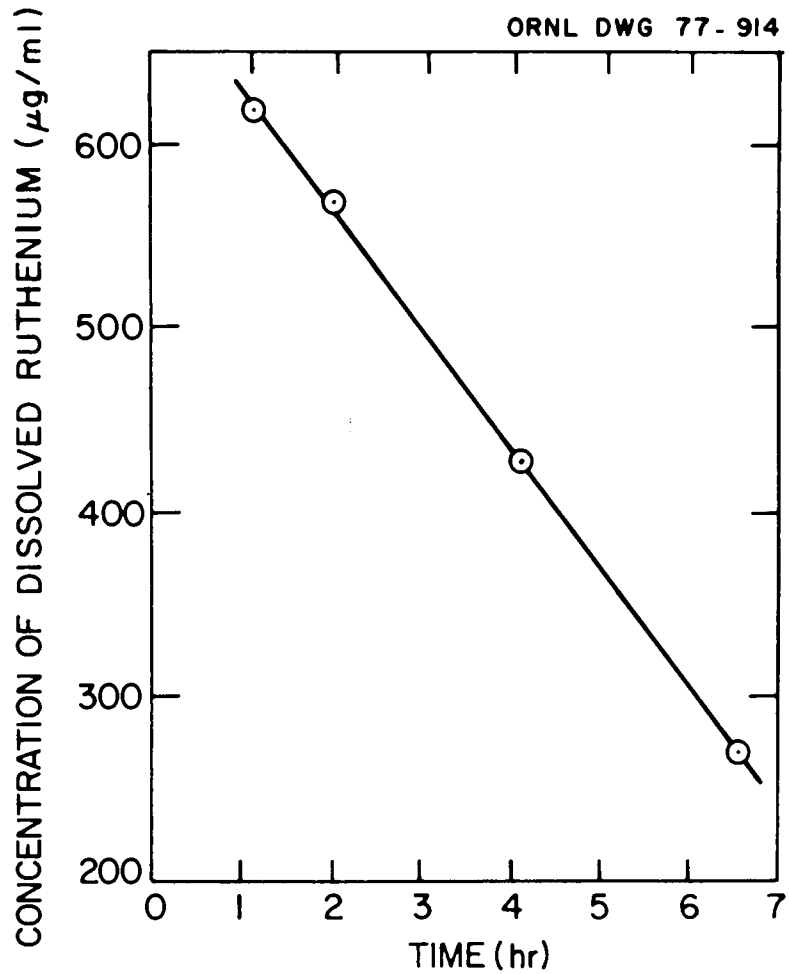

Fig. 2.9. Ruthenium dissolved in 6 *M* HI solution at 122°C.

2.2.2 Hydroxylamine and hydrazine chemistry in Purex processing

Search for alternate holding reductants (D. Y. Valentine and A. D. Kelmers, ORNL Chemistry Division). During certain steps in Purex processing, plutonium is held in the 3+ oxidation state, which either prevents plutonium(III) extraction by TBP-diluent solutions or results in stripping of previously extracted plutonium(IV) as plutonium(III) from TBP-diluent solutions. It is difficult, however, to maintain plutonium in the 3+ oxidation state in nitric acid solutions because of an autocatalytic reaction between plutonium(III) and nitric acid,

$$2Pu(NO_3)_3 + 3HNO_3 \xrightarrow{HNO_2} 2Pu(NO_3)_4 + HNO_2 + H_2O \ , \tag{2.4}$$

where nitrous acid is both a reaction product and a catalyst. Once this reaction is initiated by small quantities of nitrous acid, it will cascade and result in rapid oxidation of the plutonium(III). Experience has shown that plutonium(III) in process solutions can rapidly and unpredictably reoxidize, either in the presence of hydroxylamine nitrate or uranium(IV) nitrate (the conventional

plutonium reductants) or in electrolytic cells. This reoxidation has been assumed to result from a difference in reaction rates, the autocatalytic reoxidation reaction being more rapid than the conventional plutonium reduction reactions. As a result, plutonium reoxidation and concomitant process upsets can occur. To prevent this, holding reductants are added to destroy the nitrous acid. These reductants are compounds that react even more rapidly with nitrous acid than does plutonium(III). Only two compounds have been used as holding reductants: hydrazine and sulfamic acid. For many years, ferrous sulfamate was used as the plutonium reductant. In acid solutions, sulfamic acid is not dissociated; thus, the solutions employed were actually mixtures of ferrous nitrate (which functioned as the plutonium reductant) and sulfamic acid (which acted as the holding reductant). Sulfamic acid might not be a suitable holding reductant in Purex processing of LMFBR fuel because the reaction of sulfamic acid and nitrous acid,

$$NH_2SO_3H + HNO_2 \rightarrow N_2 + H_2SO_4 + H_2O \ , \tag{2.5}$$

produces sulfuric acid. Sulfuric acid increases the corrosion of stainless-steel equipment and can form plutonium(IV) sulfate complexes that do not extract well into TBP-diluent solutions. Hydrazine is being considered for use as the holding reductant in future applications both in the United States and in Europe. It would be desirable, however, to have additional holding reductants available; therefore, a screening program has been initiated to search for other compounds that could function as holding reductants. Compounds which give reaction rates equivalent to or faster than the reaction rate of nitrous acid with hydrazine or sulfamic acid might be potential alternate holding reductants.

Experimental methods. The kinetics of the reaction of nitrous acid with various reductants in nitric acid media are being investigated by using the Centrifugal Fast Analyzer.[14] The analyzer has two modes of data acquisition: time-based and counts-based. The time-based mode allows the rotor to be accelerated, stopped, and reaccelerated to the run speed, after which data acquisition begins as a function of time. This mode of operation ensures thorough mixing of viscous samples. In the counts-based mode, the rotor is accelerated to the preset run speed and measurements commence at much shorter times. When used in this mode with a parallel-channel rotor, adequate mixing of low-viscosity samples occurs as the samples enter the cuvet. In the following experiments, the analyzer was used in the counts-based acquisition mode with a 17-cuvet parallel-channel rotor to study the reactions at the earliest possible times.

A solution of nitrous acid (60 μl, 0.002 to 0.08 *M* $NaNO_2$ in 2 *M* HNO_3) was placed in one channel, and an equal volume of a solution of the reductant (0.05 to 0.50 *M*) was placed in the corresponding parallel channel. Basic reductants had been neutralized with 1 equiv of nitric acid. Excess reductant over that required for the reaction with nitrous acid was added to simulate Purex process conditions, where an excess of holding reductant would be used to destroy nitrous acid. To mix the solution and thereby initiate the reaction, the rotor was accelerated to 4000 rpm. The sample cuvets, each containing 120 μl of the final mixture of reactants, were then interrogated with 370 nm light. The first measurements were made as early as 0.08 sec. The analyzer was programmed with two sets of parameters so that the initial data region could be observed in expanded detail. The first measurements were taken at about 0.015-sec intervals for a total of about 0.6 sec; the remaining observations were then taken at regular intervals to a total reaction time of about 10 sec. A total of 99 data points for each of 16 cuvets was taken and recorded as absorbance values that were corrected for the 1 *M* HNO_3 reference in the 17th cuvet. A computer program using the Disspla

plotting capability was written to plot the data as absorbance vs time, ln absorbance vs time, and the reciprocal of absorbance vs time to test for zero-, first-, and second-order kinetics.

Nitrous acid displays a number of sharp absorbance peaks suitable for monitoring the concentration (Fig. 2.10). The peak at 371.5 nm was selected for our work because it is further from the UV cut-off region and thus less likely to be subject to interference by other compounds. A Beer's law plot (absorbance vs concentration) for nitrous acid in 1 *M* nitric acid was constructed using freshly prepared solutions of $NaNO_2$ in 1 *M* HNO_3 (Fig. 2.11). Absorbance was recorded as a function of time on the centrifugal fast analyzer in the time-based acquisition mode; the data were then extrapolated to zero time to correct for the loss of NO and NO_2 vapors from the solutions. The relationship of concentration of nitrous acid in 1 *M* HNO_3 to absorbance (A) with 370 nm light from the interference filter in the centrifugal fast analyzer can be expressed by the equation

$$M = \frac{A - 0.06}{21.69} . \tag{2.6}$$

Hydroxylamine. Nitrous acid was reacted with 0.25 *M* hydroxylamine nitrate in 1 *M* HNO_3 at several nitrous acid concentrations. In each case, a straight line plot of ln absorbance vs time was obtained. The slopes of the lines were essentially identical, showing that the reaction was first-order

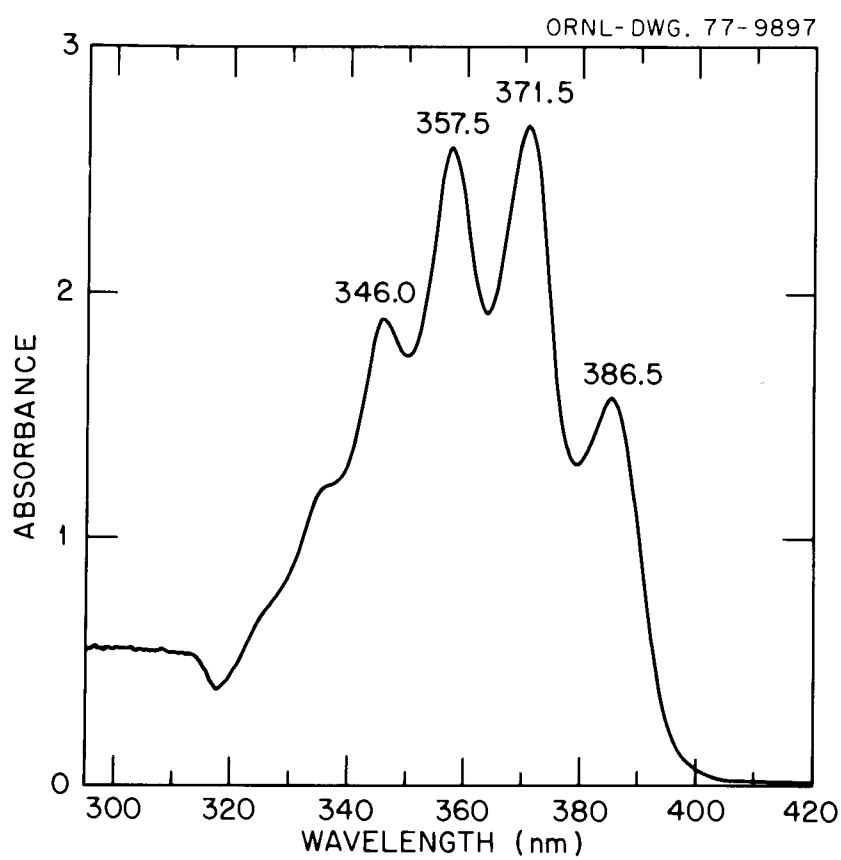

Fig. 2.10. Nitrous acid absorbance in 1 *M* HNO_3. Trace recorded on a Perkin-Elmer Hitachi model 200 double-beam grating spectrophotometer vs 1 *M* HNO_3 reference. Exact peak location determined in a separate experiment with a Cary 14 spectrophotometer.

ORNL-DWG 77-10451

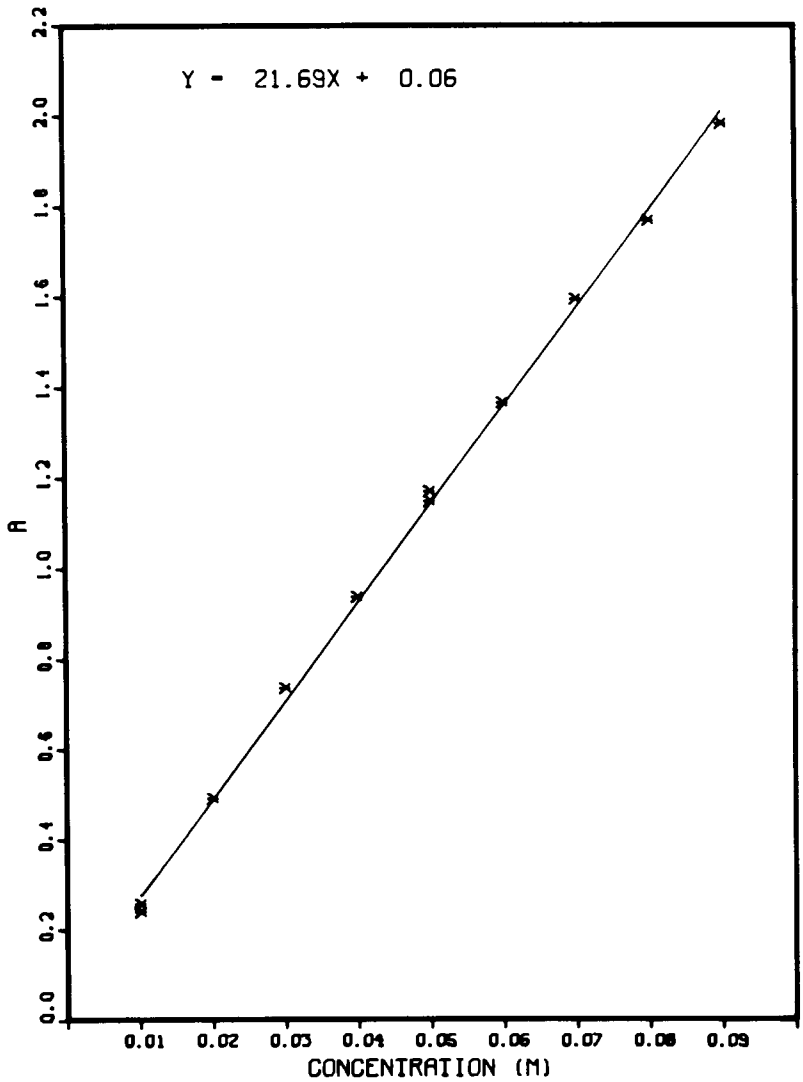

Fig. 2.11. Beer's Law plot for nitrous acid in 1 *M* nitric acid. Data obtained with a 370-nm interference filter in the centrifugal fast analyzer.

with respect to nitrous acid concentration. A typical plot is shown in Fig. 2.12. A rate constant of $1.408 \pm 0.077\ sec^{-1}$ (mean ± standard deviation) was obtained (Table 2.7). Thus nitrous acid has a half-life of 0.49 sec in 0.25 *M* hydroxylamine nitrate and 1 *M* HNO_3 at 25°C.

First-order kinetics are in agreement with the published[15] data for the reaction of nitrous acid with hydroxylamine in 0.1 *M* perchloric acid. The mechanism proposed in perchloric acid involves the intermediate formation of hyponitrous acid,

$$HNO_2 + NH_2OH \rightleftarrows H_2N_2O_2 + H_2O \ , \tag{2.7}$$

which then decomposes to the final products,

$$H_2N_2O_2 \rightarrow N_2O + H_2O \ . \tag{2.8}$$

ORNL-DWG 77-10448

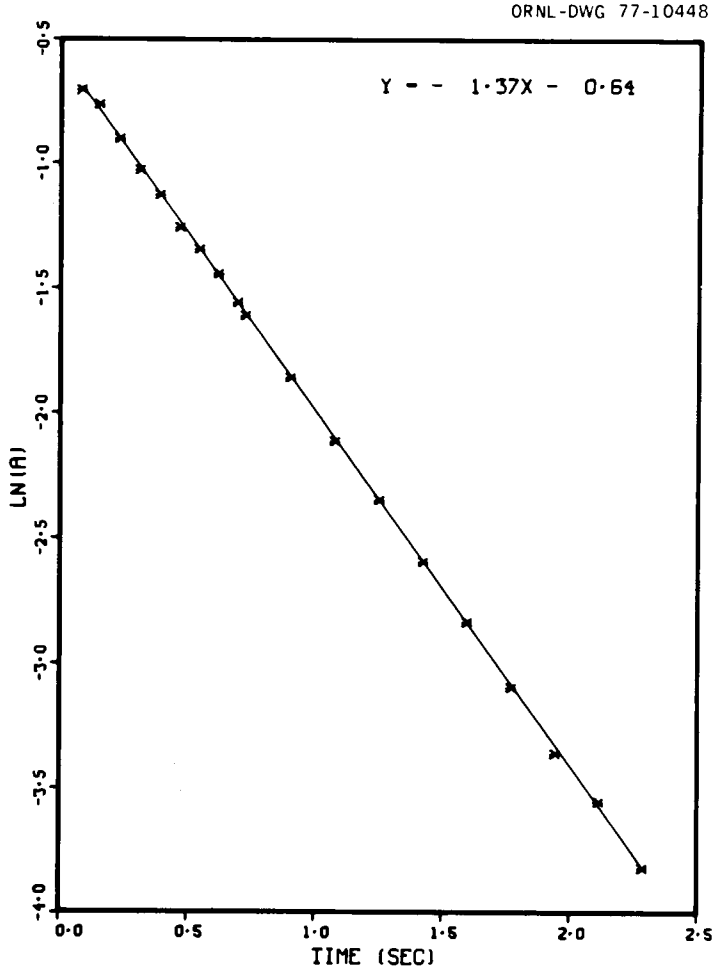

Table 2.12. First-order rate plot for the reaction of nitrous acid with hydroxylamine nitrate in 1 *M* nitric acid. Rate constant is 1.368/sec; half-life is 0.507 sec.

Table 2.7. First-order rate constant for the reaction of nitrous acid with hydroxylamine nitrate[a]

HNO_2 concentration (*M*)	*k* (sec^{-1})
0.004	1.526
0.004	1.572
0.004	1.362
0.004	1.298
0.022	1.368
0.022	1.416
0.022	1.384
0.022	1.376
0.041	1.370
0.041	1.409
0.041	1.404
Average	1.408 ± 0.077

[a]All experiments were with 0.25 *M* NH_3OHNO_3 in 1 *M* HNO_3 at 25°C.

A half-life of 18 min was reported[15] for the nitrous acid reaction with 0.01 *M* hydroxylamine in 0.1 *M* $HClO_4$. Both hydrogen ions and nitrate ions are known[16,17] to accelerate the decomposition of hyponitrous acid. Thus if the decomposition of hyponitrous acid is the rate-controlling step in the reaction of nitrous acid with hydroxylamine nitrate, the much shorter half-life obtained in our work probably is attributable to the different solvent 1.0 *M* HNO_3 instead of 0.1 *M* $HClO_4$.

Hydrazine. The reaction of nitrous acid with hydrazine was much more complex than the reaction with hydroxylamine. The general features of the reaction were: (1) a rapid decrease of the 370-nm absorbance to near zero, (2) a slower increase of absorbance to values as great as or greater than the initial nitrous acid absorbance, and (3) an even slower decrease in absorbance, again to near zero. A typical example for the reaction of 0.022 *M* nitrous acid with 0.025 *M* hydrazine is shown in Fig. 2.13. With higher concentrations of hydrazine (0.05 or 0.25 *M*), the initial decrease in

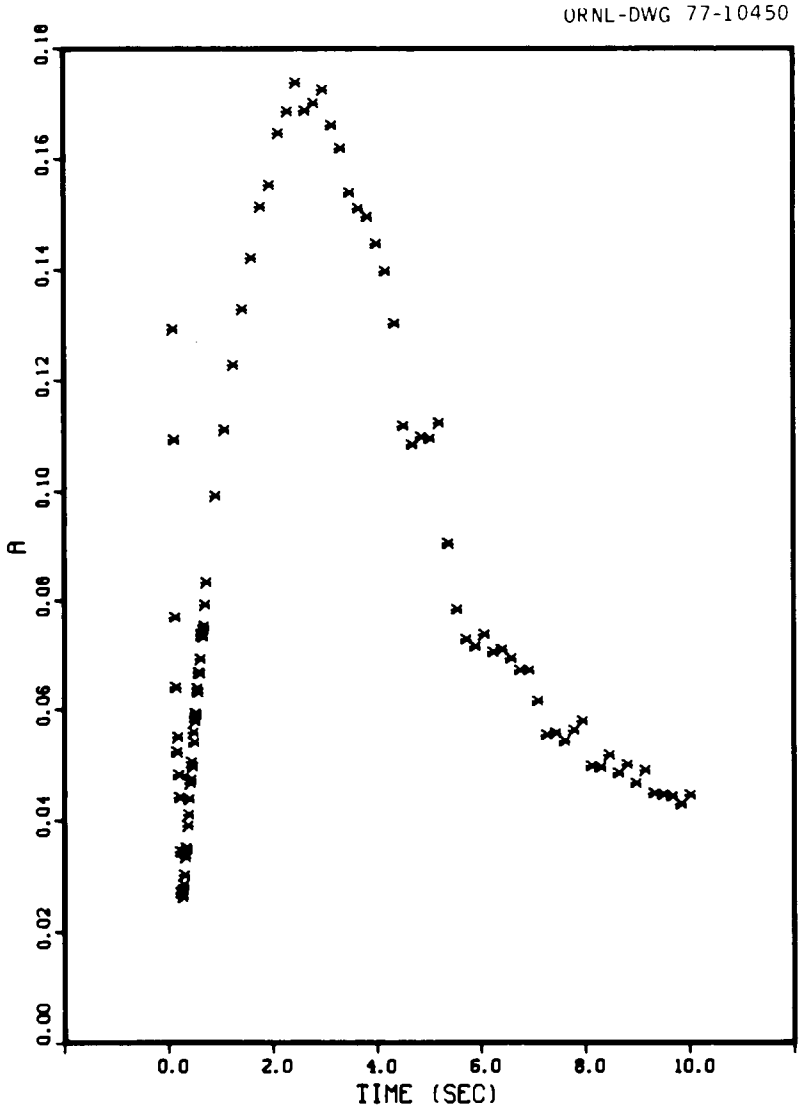

Fig. 2.13. Reaction of nitrous acid with hydrazine in 1 *M* nitric acid.

absorbance appeared to be complete before the first sample measurement at about 0.8 sec. The absorbance pattern can be rationalized on the basis of the reaction mechanism proposed by Perrott et al.[18] They propose three sequential reactions in acid media:

$$HNO_2 + N_2H_5^+ \rightarrow \underset{(A)}{NH_2NHNO} + H_2O + H^+ \tag{2.9}$$

$$\underset{(A)}{NH_2NHNO} \rightarrow \underset{(B)}{NH_2NNOH} \tag{2.10}$$

$$\underset{(B)}{NH_2NNOH} \xrightarrow{H^+} HN_3 + H_2O\ . \tag{2.11}$$

The first reaction forms intermediate A. This rearranges to intermediate B, which then decomposes to hydrazoic acid and water. If we assume that intermediate A has no absorbance in the 370-nm region (which seems reasonable because there are no double bonds or other features to permit electronic resonance) and that intermediate B does have absorbance at 370 nm (which is possible because it contains a hydroxyl group attached to a double bonded nitrogen pair), the up-and-down absorbance pattern with time (Fig. 2.13) can be explained as follows: (1) the initial rapid decrease in absorbance to near zero is a result of the reaction of HNO_2 with $N_2H_5^+$ to form intermediate A; (2) the subsequent increase in absorbance is due to the rearrangement of intermediate A to intermediate B; (3) the final decrease in absorbance is a result of the decomposition of intermediate B into hydrazoic acid and water.

The absorbance data for two experiments with dilute (0.025 *M*) hydrazine nitrate and 0.022 *M* nitrous acid were graphed in an expanded form to display the initial region of absorbance decrease. These gave an apparent first-order rate constant of about 9.6/sec, or a nitrous acid half-life of about 0.07 sec under these conditions. The data from one experiment are shown in Fig. 2.14. The situation is complicated by the possibility of an additional reaction between nitrous acid and hydrazoic acid,

$$HNO_2 + HN_3 \rightarrow N_2O + N_2 + H_2O\ , \tag{2.12}$$

which could become important when a large stoichiometric excess of hydrazine is not available. Under these conditions, the hydrazine-nitrous acid reaction might not be dominant.

It is obvious from these tests that the reaction of nitrous acid with hydrazine nitrate is very rapid, at least an order of magnitude faster than with hydroxylamine nitrate. Additional tests are needed to define the kinetics of the reactions with hydrazine.

Urea. The reaction of nitrous acid with urea nitrate gave a complex pattern of absorbance vs time. The data points were much more scattered, and duplicate experiments were much less reproducible than with the other compounds tested. A typical plot is shown in Fig. 2.15. The absorbance increased rapidly for a few tenths of a second to a value significantly higher than that caused by the initial nitrous acid concentration. Then the absorbance decreased with one or more "mountain peaks" during the down slope. Apparently one or more intermediates with absorbance at 370 nm must be formed.

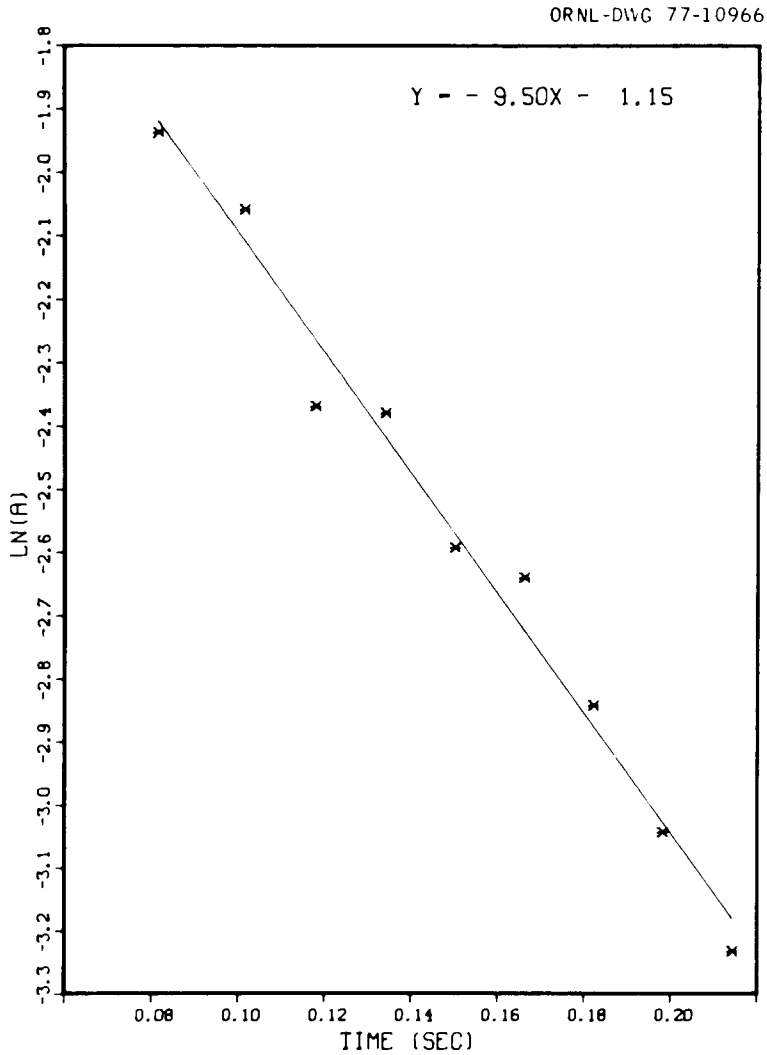

Fig. 2.14. First-order rate plot for the reaction of dilute nitrous acid with dilute hydrazine nitrate in 1 *M* nitric acid.

The mechanism of the reaction of nitrous acid with urea has not been investigated in recent years. An early article[19] suggests a two-step mechanism initially involving the formation of cyanic acid and nitrogen.

$$NH_2CONH_2 + HNO_2 \rightarrow HOCN + N_2 + 2H_2O \ , \tag{2.13}$$

followed by competing decomposition reactions,

$$HOCN + H_2O \rightarrow NH_3 + CO_2 \ , \tag{2.14}$$

$$HOCN + HNO_2 \rightarrow N_2 + CO_2 + H_2O \ . \tag{2.15}$$

This mechanism was invoked to account for the variable stoichiometry of the reaction. It could partially explain the absorbance vs time patterns that we obtained. Cyanic acid probably absorbs at 370 nm because it exists as a tautomeric pair H–O–C≡N ⇄ O=C=N–H, which present many options

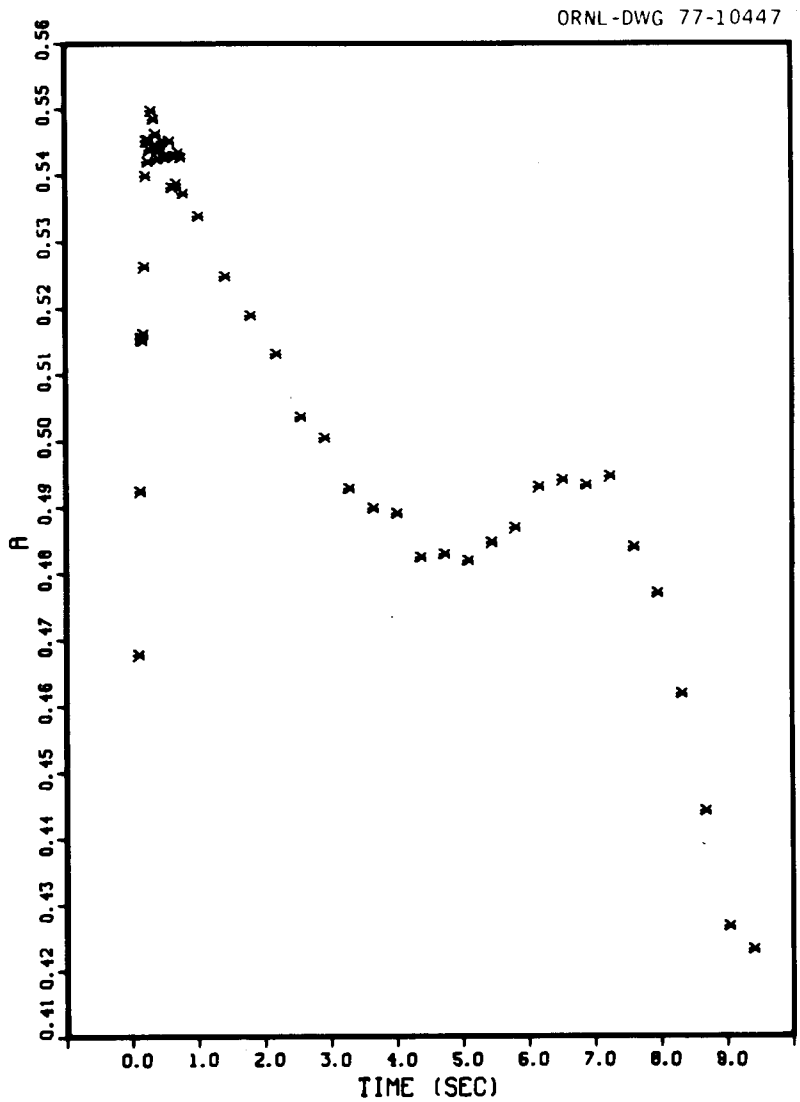

Fig. 2.15. Reaction of nitrous acid with urea in 1 *M* nitric acid.

for electronic resonance. Thus the initial rapid increase in absorbance could be caused by the formation of cyanic acid, and the more gradual decrease could be due to the decomposition of cyanic acid to ammonia, nitrogen, and carbon dioxide. This mechanism does not appear to offer any explanation for the characteristic "mountain peaks" that repeatedly appeared. It seems likely that the reaction mechanism is more complex than suggested by this model.

The data for the initial 0.28-sec time period of nine experiments were plotted in an expanded form to examine the initial absorbance increase in more detail. The data showed considerable scatter and did not fall on a straight line when plotted in a form for first-order kinetics. Because the absorbance value must be the sum of the residual nitrous acid absorbance plus the assumed absorbance of the cyanic acid formed, no quantitative data treatment was possible. A note in a recent Russian publication[20] gave a differential rate equation for the reaction of nitrous acid with urea, which indicated that the reaction should be first-order with respect to nitrous acid. No

experimental details were given in the paper, and we cannot reconcile their conclusions with our results.

Process application. The kinetic experiments completed during this report period have shown that nitrous acid reacts more than ten times as rapidly with hydrazine nitrate as with hydroxylamine nitrate under equivalent conditions in 1 *M* nitric acid. It is known from hot-cell experiments[21] that hydrazine stabilizes plutonium(III) in nitric acid solutions and that hydroxylamine does not. Our kinetic data confirm the inferred rate of the nitrous acid–hydrazine reaction relative to the nitrous acid–hydroxylamine reaction.

Urea does not appear to have been extensively tested as a holding reductant; it might be applicable. The initial reaction of nitrous acid and urea to form cyanic acid appears to be complete in about 0.25 sec. Although not as rapid as the hydrazine–nitrous acid reaction, it is considerably more rapid than the hydroxylamine–nitrous acid reaction. Glove-box tests of the efficacy of urea as a holding reductant with plutonium(III) would be of value.

Additional compounds are being screened as alternate holding reductants; the results of this work will be described in future reports.

Formation of hydrazoic acid during Purex solvent extraction steps (A. D. Kelmers, ORNL Chemistry Division). The reaction of nitrous acid with hydrazine in acid media and in the presence of excess hydrazine leads nearly stoichiometrically to hydrazoic acid.[18,22,23]

$$HNO_2 + N_2H_4 \rightarrow HN_3 + 2H_2O \ . \tag{2.16}$$

The formation of hydrazoic acid under conditions similar to those to be encountered in Purex processing was investigated briefly during this report period to estimate the degree of conversion of HNO_2 into HN_3. Nitrous acid was formed and extracted into 30% TBP in dodecane by mixing equal volumes of the organic and a sodium nitrite aqueous solution in a baffled 500-ml glass mixer or in a stainless steel beaker with a two-blade stirrer. While mixing, sufficient nitric acid was added to form HNO_2 and to make the aqueous phase 0.5 *M* in HNO_3. This method generated nitrous acid directly in contact with the organic phase and helped to minimize the loss of nitrous acid as NO and NO_2 vapors. The phases were separated after mixing for 5 min. A sample of the aqueous phase was made basic with NaOH, and a sample of the organic phase was twice stripped with 10% Na_2CO_3. These solutions were subsequently analyzed for nitrite content. The nitrous acid-containing organic solution was then returned to the mixer and contacted for 5 min with an equal volume of a strip solution containing hydrazine nitrate in 0.5 *M* HNO_3. The phases were then separated, and samples of the aqueous and organic phases were treated as above and subsequently analyzed for azide content by the addition of excess ceric sulfate, followed by back-titration with ferrous ammonium sulfate.

The results (Table 2.8) show that 66 to 92% of the nitrous acid was extracted into the organic phase with distribution coefficients of 5 to 6. Then, on contacting the nitrous acid-containing organic phase with the hydrazine nitrate–nitric acid strip solution, 36 to 93% of the nitrous acid was converted into hydrazoic acid. The highest conversion occurred in the test with approximately 0.1 *M* HNO_2, a concentration that simulates the conditions to be encountered in Purex processing.

As a first estimate, it would appear that most of the nitrous acid extracted from the dissolver solution would be converted to hydrazoic acid during plutonium reductive stripping or in other steps where hydrazine is employed. Estimates of the quantities of nitrous acid to be encountered following

Table 2.8. Conversion of nitrous acid to hydrazoic acid during solvent extraction steps

Test	HNO_2 extraction				
	HNO_2 concentration (M)			HNO_2	
	Aqueous feed[a]	After equilibration		E°a	Extracted (%)
		Organic[b]	Aqueous		
1	0.1	0.092	0.016	5.8	92
2	1.0	0.660	0.105	6.3	66[c]
3	1.0	0.713	0.144	5.0	71[c]

Test	HN_3 formation				
	$N_2H_5NO_3$ concentration in aqueous feed (M)[d]	HN_3 concentration (M)		NH_3 E°a	Conversion (%)[e]
		After equilibration			
		Organic	Aqueous		
1	0.5	0.068	0.018	3.8	93
2	2.0	0.243	0.054	4.5	37
3	2.0	0.220	0.040	5.5	36

[a]The aqueous feed was 0.5 M HNO_3 plus the indicated HNO_2 from $NaNO_2$.
[b]The organic phase was 30% TBP in dodecane preequilibrated with 0.5 M HNO_3.
[c]Some HNO_2 loss was observed as NO_2 vapors.
[d]The strip solution was 0.5 M HNO_3 plus the indicated $N_2H_5NO_3$.
[e]Sum of the HN_3 in the equilibrated organic and aqueous strip solution compared to the HNO_2 in the organic feed.

dissolution of actual spent fuel are necessary for estimating the quantities of hydrazoic acid that could be formed during fuel reprocessing.

Reaction of ammonium nitrate and nitric acid (A. D. Kelmers, ORNL Chemistry Division and D. N. Browning, GLCA student participant, ORNL Chemistry Division). The investigation of the chloride-catalyzed decomposition of ammonium nitrate in nitric acid at 100°C,

$$NH_4NO_3 \xrightarrow{Cl^-} N_2O + 2H_2O \ , \tag{2.17}$$

has been completed, and an ORNL/TM report describing the work is in preparation. The rate of disappearance of ammonium nitrate can be expressed in the form of a differential rate equation,

$$-\frac{d[NH_4^+]}{dt} = k[NH_4^+]^m[HNO_3]^n[HCl]^p \ , \tag{2.18}$$

in terms of the rate constant, k, and the molar concentrations of ammonium ion, nitric acid and hydrochloric acid, to the respective powers m, n, and p. A least-squares program for the estimation of nonlinear parameters that employs a maximum neighborhood method of iteration was used to evaluate m, n, p, and k. The data (time in seconds and ammonium ion concentration in molarity)

from a total of 32 experiments run at 100°C with 4 to 7 M HNO_3 and 0.05 to 0.25 M HCl were used in the calculations. The differential rate law obtained was

$$-\frac{d[NH_4^+]}{dt} = 6.27 \times 10^{-7}[NH_4^+]^{0.91}[HNO_3]^{4.86}[HCl^{1.14} , \tag{2.19}$$

with a standard error of fit of 5.5% for all parameters. The value of 0.91 for the $[NH_4^+]$ exponent is in good agreement with the preliminary assignment[24] of first-order kinetics for the disappearance of ammonium ion.

A reaction mechanism was proposed, based on the experimental evidence. The first reaction must involve HCl and HNO_3 to generate an active chloride component. Results of experiments, which showed that air flowing through the reaction flask vapor space did not remove chloride from the solution, indicated that the possibility is unlikely of a significant concentration of any intermediate having an appreciable vapor pressure above these nitric acid solutions at 100°C. Thus compounds such as chlorine or nitrosyl chloride are unlikely to be the active component, although they could be present in trace quantities. Also, HBr and HF showed no catalytic activity. Thus the active component is probably a stable chlorine-containing compound, and the corresponding bromine or fluorine compounds are much less stable. The hypohalous acids meet these criteria. Thus the initial reaction might be

$$2H^+ + Cl^- + NO_3^- \rightleftarrows HOCl + HNO_2 . \tag{2.20}$$

It is also possible to gain information about the reaction mechanism from the end compounds; evolution of N_2 suggests the decomposition of a compound with two interconnected nitrogen atoms. The decomposition of nitramide is well known,

$$NH_2NO_2 \rightarrow N_2O + H_2O . \tag{2.21}$$

In the chloride-catalyzed decomposition of molten ammonium nitrate at higher temperatures, chloramine has been proposed[25] as an intermediate. It is then possible to write a sequence of plausible reactions to represent the chloride-catalyzed decomposition of ammonium nitrate in nitric acid media at 100°C. The reactions are:

$$2H^+ + Cl^- + NO_3^- \rightleftarrows HOCl + HNO_2 \tag{2.22}$$

$$HOCl + NH_4^+ \rightleftarrows NH_2Cl + H^+ + H_2O \tag{2.23}$$

$$NH_2Cl + HNO_2 \rightarrow NH_2NO_2 + H^+ + Cl^- \tag{2.24}$$

$$NH_2NO_2 \rightarrow N_2O + H_2O \tag{2.25}$$

$$NH_4^+ + NO_3^- \rightarrow N_2O + 2H_2O \tag{2.26}$$

The chloride-catalyzed decomposition of ammonium nitrate could be applied only with difficulty to Purex-process fuel reprocessing plants. Such plants appear to be committed to stainless-steel apparatus; thus the introduction of chloride solutions that could lead to chloride-induced corrosion would likely be unacceptable. The reaction might be useful in waste-treatment schemes where a separate facility could be constructed and materials of suitable

corrosion resistance could be selected. The reaction appears unique, and it is unlikely that additional research would reveal a catalytic additive that would function through a similar reaction sequence and that would also be noncorrosive to stainless steel.

2.2.3 Solvent chemistry studies

L. Maya (ORNL Chemistry Division) and C. D. Bopp (ORNL Chemical Technology Division)

The zirconium distribution coefficient dependence on butyllauryl phosphoric acid concentration[26] shows that the species extracted have a ligand:metal ratio of 2, which is similar to that observed in the case of HDBP[27] or HDEHP.[28] Additional experiments were performed to elucidate the extraction mechanism and to deduce the nature of the extracted species. The hydrogen ion dependence the extraction at constant nitrate concentration and the nitrate ion dependence at a constant acid concentration were determined. The results (Fig. 2.16) indicate a complex mechanism. The slope of the hydrogen ion dependence is +2 in the range of 1.0 to 3.0 *M*, and the slope of the nitrate ion dependence is +0.5 in the range of 0.1 to 1.0 *M*, with a leveling-off effect beyond that concentration. The fractional value of the nitrate ion dependence indicates that the species extracted are possibly polymeric, and the fact that hydrogen ion participates in the extraction indicates that these polymeric species may be hydrolyzed to a certain extent. It is conceivable that the species present in the aqueous medium are of the type $[Zr(NO_3)_x(OH)_y]_n^{4-x-y}$. The relevant stability constants[29] for the complexing of zirconium by nitrate indicate that the ratio of NO_3:Zr could at most be 1; therefore, in the case of extraction by HBLPA, additional nitrate must be incorporated up to a NO_3:Zr limit of 1.5. This agrees with the NO_3:Zr values of 0.6 to 1.2 observed by Peppard and Ferraro[28] in the extraction of zirconium species by HDEHP. Furthermore, those species proved to be oxygenated, having a composition corresponding to $[ZrO_{0.5}NO_3(DEHP)_2]_n$.

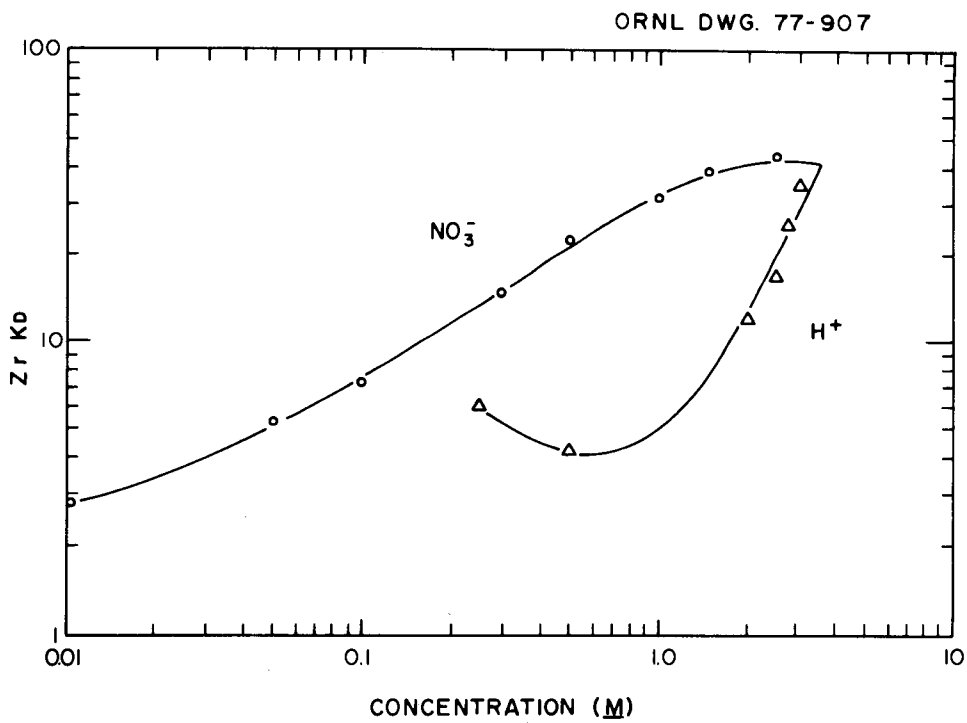

Fig. 2.16. Nitrate and hydrogen ion dependence of zirconium distribution coefficient with 10^{-4} *M* HBLPA in dodecane.

A study of the TBP dependence of zirconium extraction by HBLPA (Fig. 2.17) shows that TBP has an antagonistic effect, as previously deduced[26] from comparison of K_D values of the HBLPA–dodecane and HBLPA–TBP-dodecane extraction mixtures. The TBP dependence indicates that there is a 1:1 complex formed between HBLPA and TBP. The following equation describes the extraction mechanism in the presence of TBP:

$$Zr^{4+} + 2L^{-} + 2HBLPA{\cdot}TBP \rightarrow ZrL_2(BLP)_2 + 2TBP, \tag{2.27}$$

where L is OH^- or NO_3^-.

Previous results[26] obtained in the absence of other metals indicated strong complexing of zirconium by HBLPA. The relative stability of the Zr·2HBLPA complex has been established in the presence of macroamounts of uranium under conditions that are representative of the Purex process. It was found that uranium depresses the extraction of zirconium, possibly by formation of a $UO_2(NO_3)_2(HBLPH)_n$ complex. However, the stability of the uranyl complex must be lower than that of the zirconium complex, because the latter is still extracted to a considerable extent in spite of the presence of uranium at concentration levels that are 10^5 times larger than that of zirconium (Table 2.9).

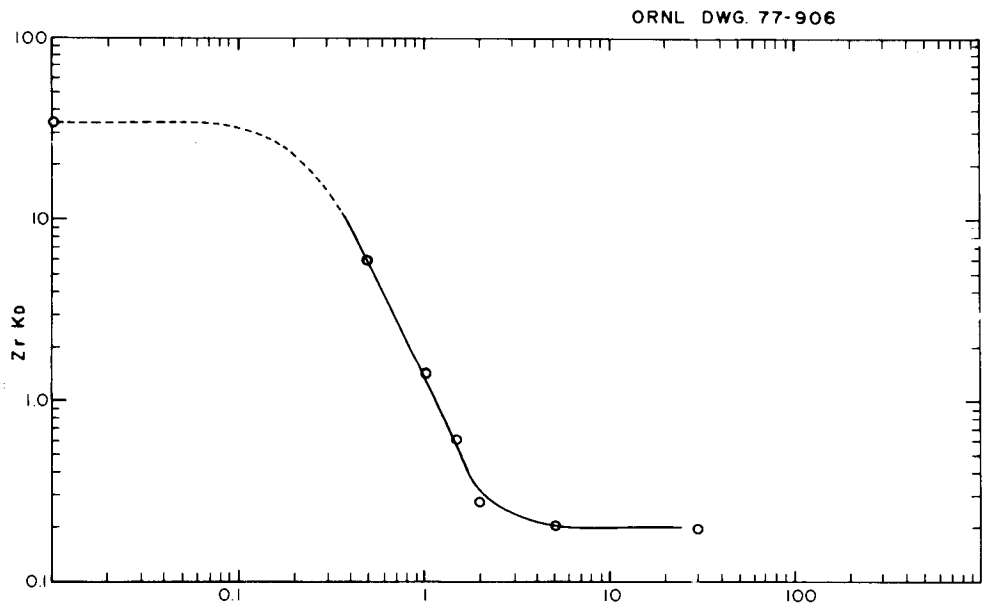

Fig. 2.17. TBP dependence of zirconium distribution coefficient with 10^{-4} M HBLPA in dodecane.

Table 2.9. Zirconium distribution in the presence of uranium

Aqueous solution	Extractant	Zr K_D
3 M HNO_3, 2.5 M $LiNO_3$, 10^{-5} M Zr	30% TBP–dodecane containing 10^{-3} M BLP	2.9
3 M HNO_3, 1.25 M $UO_2(NO_3)_2$, 10^{-5} M Zr	Same as above	0.21
Same as above	30% TBP–dodecane	0.015

The removal of HBLPA from 30% TBP–dodecane by alkaline washes was studied. The following compounds were examined: sodium carbonate, sodium hydroxide, potassium carbonate, ammonium carbonate, hydrazine, and guanidine. It was found that under typical Purex operating practices, that is, a wash with 0.2 *M* Na_2CO_3 at an O:A ratio of 50, very little NaBLP could be removed. Similarly, use of hydrazine removed little BLP^- from the solvent. There is a strong effect of the sodium ion concentration on the distribution of NaBLP between the aqueous and organic phases. The removal of NaBLP at a given base concentration is proportional to the volume of aqueous phase used. The relation is not linear, as would be expected if only one species were participating in the equilibration. The relation becomes linear when plotted on a semilog graph (Fig. 2.18). The displacement of line C with respect to line A reflects the salting out effect of sodium ion concentration. It is seen that NaBLP is much more soluble in 0.05 *M* Na_2CO_3 than in 0.2 *M*

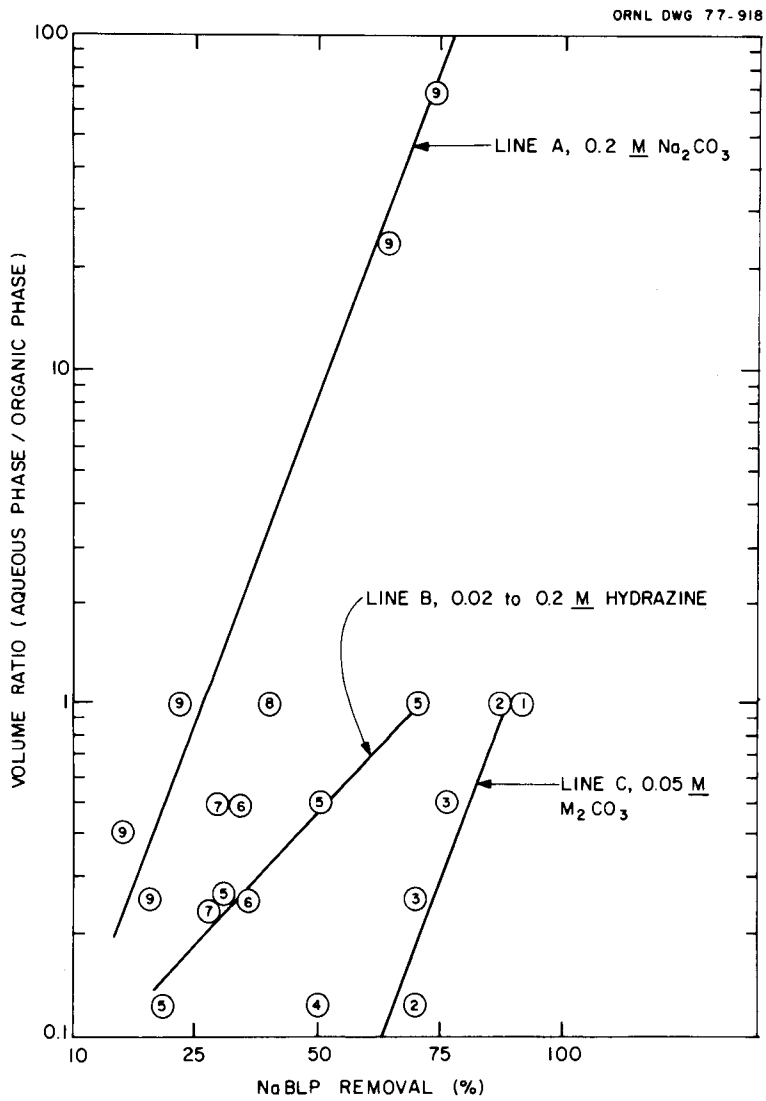

Fig. 2.18. Butyllauryl phosphate removal from 30% TBP–dodecane. Alkaline washes: (1) 0.025 *M* Na_2CO_3, (2) 0.05 *M* Na_2CO_3, (3) 0.05 *M* K_2CO_3, (4) 0.1 *M* NaOH, (5) 0.2 *M* hydrazine, (6) 0.1 *M* guanidine, (7) 0.05 *M* $(NH_4)_2CO_3$, (8) 0.1 *M* Na_2CO_3, (9) 0.2 *M* Na_2CO_3.

Na_2CO_3. The distribution from an aqueous solution containing hydrazine, guanidine, or ammonium ions falls on a line with a slightly different slope. This might be an indication of a different extraction mechanism because all these ions can hydrogen bond to the transferring species.

The data for 0.2 *M* Na_2CO_3 are also presented as a Martin plot[30] (Fig. 2.19), which indicates the presence of two species. At low NaBLP concentrations in the aqueous phase, the distribution coefficient has a value of 7.1; however, as the concentration increases, there is an abrupt change and a marked decrease of the distribution coefficient to a value of 0.8. This break is apparently a consequence of the formation of aggregates of NaBLP in the aqueous phase as the NaBLP concentration increases, and it reflects the "critical micelle concentration"[31] for this surfactant system.

Preliminary tests show that zirconium has little effect on the removal of HBLPA by alkaline washes. However, these tests were performed on freshly formed Zr·2BLPA complexes. Hydrolytic changes after aging might have an effect; this will be examined.

The observation that NaBLP can be completely removed from TBP–dodecane solutions by a water wash suggests that degradation products similar to HBLPA might also be removed after

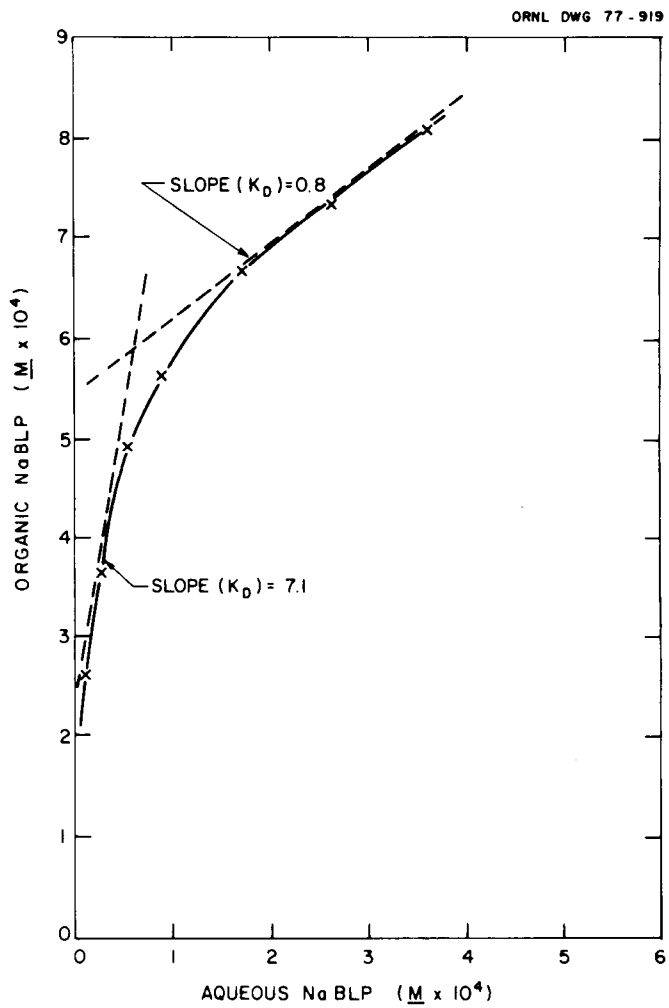

Fig. 2.19. Sodium butyllauryl phosphate distribution between 0.2 *M* Na_2CO_3 and 30% TBP–dodecane initially containing 10^{-3} *M* HBLPA.

formation of the sodium salt. Thus in Purex processing, a water wash following a basic wash could be effective in removing many radiolytic degradation products.

Future work will examine the removal of HBLPA by column treatments such as those proposed by German workers.[32]

2.2.4 Reduction of Pu(VI) with NO_2 and NO gases

M. R. Bennett and A. D. Kelmers (ORNL Chemistry Division)

The reduction of plutonium (VI) to plutonium (IV) by NO_2 gas was described in the previous quarterly report.[33] Tests with about 3 g/liter of Pu in 3 *M* HNO_3 at 26° and 40°C showed no detectable reduction. At 60° and 70°C, essentially complete reduction was obtained as measured by the disappearance of the Pu(IV) absorption peak at 831 nm; however, the amount of NO_2 added to the system was 12 to 22 times that required to satisfy the assumed stoichiometry of 0.5 mole of Pu(VI) reduced per mole of NO_2 added.

During this report period, the use of NO gas was investigated. Nitric oxide had been briefly tested,[34] and the reaction was assumed to be

$$2NO + 3PuO_2^{2+} + 4H^+ = 3Pu^{4+} + 2NO_3^- + 2H_2O \ , \tag{2.28}$$

or 1.5 mole of Pu(VI) reduced per mole of NO. Following the same experimental procedure used with NO_2, the NO gas was sparged through solutions of about 3 g/liter of Pu(VI) in 3 *M* HNO_3. In these tests, the plutonium reduction was followed by counting the TTA–inextractable Pu(VI) in a 1-ml aliquot of the reaction mixture.[33] The results (Fig. 2.20) again show only a very slow reaction at

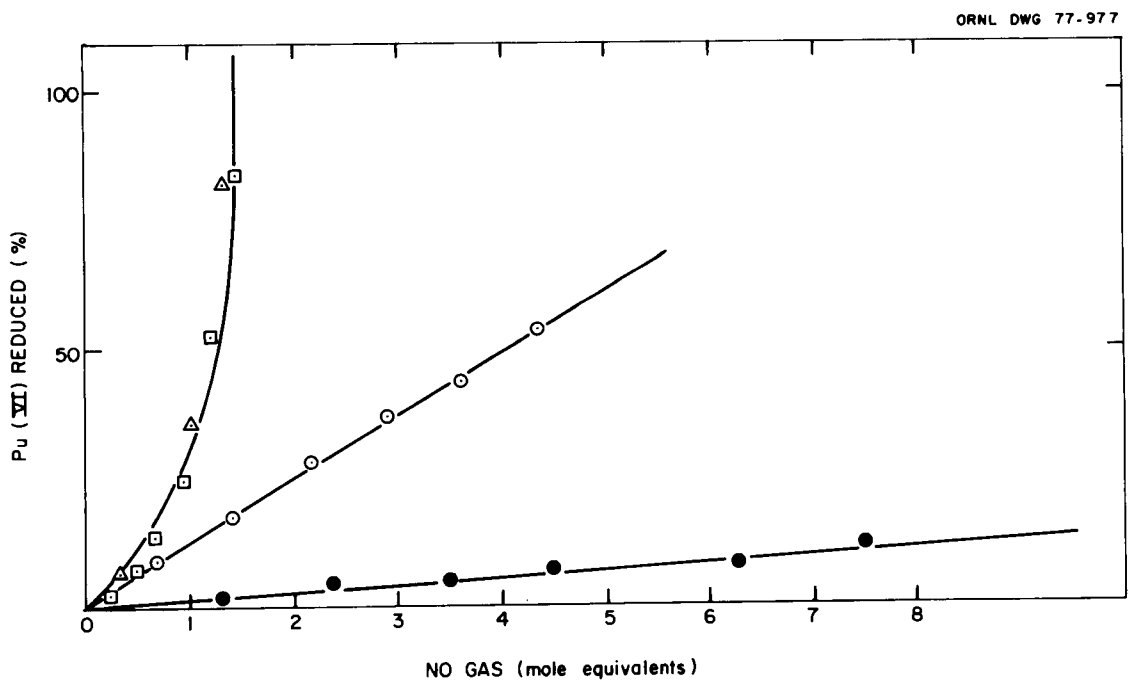

Fig. 2.20. Reduction of plutonium(VI) to plutonium(IV) with NO gas. All tests in 3 *M* HNO_3, △ 60°C, ⊡ 60°C (50–50 NO–NO_2 gas mixture), Θ 55°C solution presparged with NO, ● tests at 26, 40, and 45°C.

26 to 45°C. At 60°C the reaction was much more rapid, and the percent of Pu(VI) reduced appeared to be independent of the NO partial pressure. At this temperature only about 1.5 times the stoichiometric amount of NO was required; thus NO is much more effective than NO_2 under these conditions.

Reactions in the system under investigation are affected by the classical nitric acid production equilibrium,

$$3NO_2 + H_2O \rightleftarrows 2HNO_3 + NO \ , \tag{2.29}$$

which has been extensively investigated over many years. The NO:NO_2 ratio is of interest, and the equilibrium is frequently[35-37] expressed in terms of an equilibrium quotient,

$$K = \frac{{}^{p}NO}{({}^{p}NO_2)^3} . \tag{2.30}$$

Under our experimental conditions for plutonium reduction, K is large ($\log K = \sim 4$ to ~ 7); thus, at equilibrium essentially all of the gas would be NO. However, the rate of conversion of NO_2 to HNO_3 and NO is highly dependent on temperature and nitric acid concentration and is relatively slow compared to the contact time of the gas in our experiments. Thus in our experiments when NO gas was bubbled through the solution, it remained essentially all NO; when NO_2 was bubbled through the solution, some minor portion reacted to form NO.

It seems likely that the plutonium(VI) ion, PuO_2^{2+}, reacts with dissolved nitrous acid rather than with dissolved NO or NO_2 gases. Nitrous acid formation from NO has been fully investigated[38] and the reactions involved are:

$$HNO_3 + HNO_2 \rightarrow N_2O_4 + H_2O \text{ (rate controlling)} \tag{2.31}$$

$$N_2O_4 + 2NO + 2H_2O \rightleftarrows 4HNO_2 \tag{2.32}$$

$$HNO_3 + 2NO + H_2O \rightarrow 3HNO_2 \tag{2.33}$$

The formation of HNO_2 is autocatalytic and depends on the HNO_2 and HNO_3 concentrations, but is independent of the NO partial pressure,[38]

$$\frac{[dHNO_2]}{dt} = k[HNO_2][HNO_3] \ . \tag{2.34}$$

In agreement with this fact, we observed (Fig. 2.20) that at 60°C a 50–50 mixture of NO–NO_2 gave the same plutonium reduction rate as did pure NO.

The kinetics of the reduction of plutonium(VI) to plutonium(V) by nitrous acid in <1 M HNO_3 has been investigated.[39] The reaction,

$$2PuO_2^{2+} + HNO_2 + H_2O \rightarrow 2PuO_2^{+} + HNO_3 + 2H^+ \ , \tag{2.35}$$

is rapid in dilute HNO_3 at room temperature and is accelerated in more concentrated nitric acid or at higher temperatures. Thus under our experimental conditions, it should be fast. The disproportionation of plutonium(V) is also known[40] to be rapid at HNO_3 concentrations greater

than about 1 *M* or at elevated temperatures. Thus it is possible to construct a sequence of probable reactions to represent the reduction of plutonium(VI) to plutonium(IV) by NO gas. These are:

$$2NO + HNO_3 + H_2O \rightarrow 3HNO_2 \text{ (rate limiting)} , \tag{2.36}$$

$$6PuO_2^{2+} + 3HNO_2 + 3H_2O \rightarrow 6PuO_2^{+} + 3HNO_3 + 6H^+ , \tag{2.37}$$

$$6PuO_2^{+} + 12H^+ \rightarrow 3Pu^{4+} + 3PuO_2^{2+} + 6H_2O , \tag{2.38}$$

$$2NO + 3PuO_2^{2+} + 6H^+ \rightarrow 3Pu^{4+} + 2HNO_3 + 2H_2O . \tag{2.39}$$

This stoichiometry shows that 1.5 mole of Pu(VI) would be reduced per mole of NO utilized. It is also interesting that none of these reactions is reversible.

In light of the above discussion, it appears likely that the rate-limiting factor in our experiments might be the rate of formation of nitrous acid from NO or NO_2. Experimental work has been initiated to demonstrate that nitrous acid formation is the rate-limiting reaction.

2.2.5 Pu(IV) polymer reaction in aqueous solutions

H. A. Friedman, M. M. Osborne, and L. M. Toth (ORNL Chemistry Division)

A spectrophotometric study of Pu(IV) polymerization in aqueous nitric acid solutions has been initiated to assess the influence of uranyl nitrate on the reaction. Immediate attention has been focused on the polymerization reaction in solutions of 0.5 *M* $UO_2(NO_3)_2$ and 0.05 *M* plutonium at 50°C as a function of HNO_3 concentrations of 0 to 0.6 *N*. A major problem that precludes the presentation of detailed results at this time has been in achieving agreement between expected and analytically determined acid concentrations. In general, we have found that Pu(IV) disproportionation and polymerization reactions increase markedly at higher temperatures; considerable polymerization occurs at 50°C in approximately 0.1 *N* HNO_3, whereas almost none occurs at 22°C.

2.2.6 Materials compatibility studies

J. C. Griess (ORNL Metals and Ceramics Division)

A materials evaluation program was initiated to identify the most suitable materials for process equipment to be installed in the IPET and the Hot Pilot Plant. As the first step in this program, a critical review of the literature and plant experience will be made, and available pertinent corrosion data will be summarized. This state-of-the-art survey will serve as a basis for preliminary choices of materials and for planning an experimental program to obtain additional corrosion data where needed. A subcontract for the survey, to be completed in FY 1977, was negotiated with Battelle Columbus Laboratories.

2.3 PRODUCT CONVERSION

B. L. Vondra

The primary effort during this quarter was the initiation of a scoping study to be carried out by General Electric Corp. (Vallecitos). The contract covers evaluation of the various options for product conversion processes.

REFERENCES FOR SECTION 2

1. Los Alamos Scientific Laboratory, *Quarterly Progress Report on the Advanced Plutonium Fuel Program, Apr. 1 to June 30, 1972,* LA-5067-PR (1972).

2. W. D. Burch et al., *LMFBR Fuel Reprocessing Program Progress Report for Period April 1 to December 31, 1974,* ORNL/TM-4836 (April 1975), pp. 75–90.

3. O. K. Tallent and J. C. Mailen, *Study of the Dissolution of Refractory PuO_2 in Nitric-Hydrofluoric Acid Dissolvents at 100° C,* ORNL/TM-5181 (March 1976).

4. W. D. Burch et al., *LMFBR Fuel Reprocessing Program Progress Report for Period October 1 to December 31, 1976,* ORNL/TM-5768 (February 1977).

5. W. D. Burch et al., *LMFBR Fuel Reprocessing Program Progress Report for Period January 1 to March 31, 1976,* ORNL/TM-5463 (June 1976).

6. J. W. Mellor, *A Comprehensive Treatise on Inorganic and Theoretical Chemistry,* vol. XII, Longmans, Green and Co., New York (1942), p. 91.

7. R. Bernard, J. I. Bullock, B. J. Gellatly, and L. F. Larkworthy, "Chemistry of the Trivalent Actinides. Part III. Some Chemical and Physical Properties of Hydrated Uranium(III) Fluoride and the Anhydrous Chloride, Bromide, and Iodide. The Stability of Uranium(III) in Aqueous Solution and in Organic Solvents," *J. Chem. Soc., Dalton Trans.* **1973,** 604.

8. J. O. Tveekrem and M. S. Chandrasekharaiah, "The Standard Free Energy of Formation of UI_3 from EMF Measurements on a Solid Electrolyte Galvanic Cell," *J. Electrochem. Soc.* **115,** 1021 (1968).

9. M. Handa, "Kinetic Studies of the Oxidation of Uranium Iodides by Oxygen," *Bull. Chim. Soc. Jpn.* **39,** 1869 (1966).

10. J. Fuger and D. Brown, "Thermodynamics of the Actinide Elements. Part IV. Heats and Free Energies of Formation of the Tetrachlorides, Tetrabromides, and Tetraiodides of Thorium, Uranium, and Neptunium," *J. Chem. Soc., Dalton Trans.* **1973,** 428.

11. J. G. H. duPreez, R. A. Edge, M. L. Gibson, H. E. Rohwer, and C. P. J. van Vuuren, "The Chemistry of Uranium. Part X. Octahedral Pentahalouranate(IV) Complexes," *Inorg. Chim. Acta* **10,** 27–32 (1974).

12. R. Gradl and N. Edelstein, *Reactions of Dithiolate Ligands with Uranium(IV) Halides,* LBL-4000, TID-4500-R62 (1974), p. 344.

13. W. D. Burch et al., *LMFBR Fuel Reprocessing Program Progress Report for Period April 1 to June 30, 1976,* ORNL/TM-5556 (August 1976).

14. J. E. Mrochek, et al., *Clinical Chem.* **23,** in press (1977).

15. M. N. Hughes and G. Stedman, *J. Chem. Soc.,* **1963,** 2824.

16. J. R. Buchholz and R. E. Powell, *J. Am. Chem. Soc.* **85,** 509 (1963).

17. J. R. Buchholz and R. E. Powell, *J. Am. Chem. Soc.* **87,** 2350 (1965).

18. J. R. Perrott, G. Stedman and N. Uyssal, *J. Chem. Soc., Dalton Trans.* **1976,** 2058.

19. E. A. Werner, *J. Chem. Soc.* **111,** 863 (1917).

20. I. V. Shilin and D. P. Adaev, *Kinet. Catal.* **16,** 965 (1975).

21. G. L. Richardson and J. L. Swanson, HEDL-TME-75 (1975), 31.

22. A. Sabanejeff, *Z. Anorg. Chem.* **20,** 21 (1899).

23. J. R. Perrott and G. Stedman, *J. Inorg. Nucl. Chem.* **39,** 325 (1977).

24. D. N. Browning and A. D. Kelmers, *LMFBR Fuel Reprocessing Program Progress Report for Period October 1 to December 31, 1976,* ORNL/TM-5768 (February 1977), p. 3–28.

25. G. Guioehon, *Ann. chim.* **5,** 295 (1960).

26. L. Maya and C. D. Bopp, *LMFBR Fuel Reprocessing Program Progress Report for Period January 1 to March 31, 1977,* ORNL/TM-5879 (May 1977), pp. 3–25.

27. C. J. Hardy and D. Scargill, *J. Inorg. Nucl. Chem.* **17,** 337 (1961).

28. D. F. Peppard and J. R. Ferraro, *J. Inorg. Nucl. Chem.* **10,** 275 (1959).

29. R. E. Connick and W. H. McVey, *J. Am. Chem. Soc.* **71,** 3182 (1949).

30. F. S. Martin and G. M. Gillies, *The Chemistry of Ruthenium,* AERE-C/R-816 (1951).

31. A. W. Adamson, *Physical Chemistry of Surfaces,* J. Wiley & Sons, New York 1976, pp. 476–480.

32. H. Goldacker, et al., *Kerntech.* **18,** 426 (1976).

33. M. R. Bennett, *LMFBR Fuel Reprocessing Program Progress Report for Period January 1 to March 31, 1977,* ORNL/TM-5879 (May 1977), p. 3–26.

34. D. E. Horner and D. J. Crouse, *Laboratory Development of Solvent Extraction Processes for Spent LMFBR Fuels,* ORNL/TM-5729 (1977), p. 6.

35. J. J. Carberry, *Chem. Eng. Sci., Genie Chim.* **9,** 189 (1959).

36. H. Theobald, *Chem.-Ing. Technol.* **40,** 763 (1968).

37. L. Ya. Tereshchenko, V. P. Panov and M. E. Pozin, *J. Appl. Chem. (USSR)* **41,** 474 (1968).

38. G. Schmid and G. Bahr, *Z. Phys. Chem.* **41,** 8 (1964).

39. V. S. Koltunov and G. I. Zhuravleva, *Soviet Radiochem.* **10,** 648 (1968).

40. J. M. Cleveland, *The Chemistry of Plutonium,* Gordon and Breach, New York (1970), p. 26.

3. ENGINEERING RESEARCH

W. S. Groenier

The various engineering research studies reported here represent the first phase of the equipment development program and provide a basis for further design and development of specific engineering test components. An emphasis is placed on the identification, study, selection, development, and characterization of unit processes through the application of basic or fundamental experimental engineering techniques.

Studies of the voloxidation, NO_x scrubbing, iodine evolution, selective absorption, and Iodox processes are in progress, and development efforts are described. Work directed toward dissolver and solvent extraction equipment development and toward the development of instrumentation and control equipment and methods is also reported.

3.1 VOLOXIDATION

M. E. Whatley

The voloxidation process is being developed as a head-end method for removing tritium from fuel prior to aqueous processing. Based on experimental work, it appears that this objective can be met by reacting the oxide fuel with oxygen or air in a temperature range from 450 to 650°C (723 to 923 K). Release of tritium and, to a lesser extent, some of the other fission products occurs when UO_2 is restructured during oxidation to U_3O_8. Early removal of the tritium from the fuel into a relatively small volume is desirable to avoid mixing the tritium (as water) with aqueous streams in subsequent process steps. A secondary benefit of voloxidation is the oxidation of residual sodium in the fuel prior to dissolution.

The investigation of the applicability of rotary kilns to the voloxidation process is being continued. These studies are described and reported as part of the LWR Fuel Reprocessing and Recycle Program,[1,2] which now provides funding for voloxidation work. Because the results are directly applicable to either LWR or LMFBR fuels, highlights of recent work are provided below.

1. A dimensional analysis was performed using all relevant variables to organize the data obtained in the experimental program for measuring the dispersion coefficient of material in rotating kilns.

2. Heat transfer studies were continued using a computer model to predict the temperature profile in a rotary kiln.

3. The influence of kiln diameter, slope, feed rate, and feed size on the residence time distribution (RTD) of rotary kilns was determined. The effects of varying the flight configuration are under study; initial runs with a smaller flight-width-to-diameter ratio show a definite decrease in the RTD spread.

4. Layout design drawings for the 0.5-metric ton/day voloxidizer were received from C. E. Raymond/Bartlett-Snow Company for review and comment. All changes have been resolved except the flight cartridge design, which is being reviewed. The design of auxiliary equipment is proceeding on schedule.
5. Test equipment was assembled to determine the effect of iodine on the operation of a water-vapor removal system (molecular sieves) for the treatment of voloxidizer off-gases. Preliminary runs are under way at the Tennessee Technological University.

3.2 DISSOLUTION

The objective of the dissolution task is to ensure that LMFBR fuels can be dissolved in HNO_3 to give high metal recoveries. Dissolution characteristics of the fuels can vary widely, depending on plutonium content, method of preparation, and irradiation history. Consequently, extensive leaching data will be obtained in the overall program to determine the effects of such variables. Other efforts are directed toward understanding the behavior of iodine in the dissolver system. Criticality control and off-gas considerations call for dissolver design and operation to be performed within rather narrow limits. Continuous dissolving methods are being emphasized which appear to offer superior solutions to these problems.

During this report period, major emphasis was on the ongoing development of a continuous, rotary dissolver. Because a large amount of NO_2 in dissolver off-gas streams might have a deleterious effect on the performance of the Iodox process for iodine removal from gas streams, emphasis has also been on the development of a method for removing nitrogen oxides from the off-gas streams associated with dissolvers and feed preparation vessels.

3.2.1 Four-foot-diameter dissolver prototype

B. E. Lewis

Operational testing of the 4-ft-diam rotary dissolver prototype is continuing. During this report period, rinsing studies were continued, detailed designs and plans were made for corrosion-erosion tests, and work was started on development of an analytical model for the liquid flow characteristics in the rotary dissolver.

Rinsing studies. Experiments to determine the rinsing efficiency of the dissolver have been continued. In these experiments, −325 mesh nickel powder was used to represent fission products and slowly soluble fuel.[3] The powder feed material and the simulated sheared fuel hulls and shroud were added to the dissolver through the flapper isolation valves to minimize the loss of metal powders by dusting. The water flow from the dissolver was filtered to remove all solids. The hulls and shrouds were contacted by a countercurrent water flow in the three dissolver sections and then collected in a receiver. The nickel powder remaining on these solids was dissolved in 8 *M* nitric acid for analysis. This 4-ft-diam dissolver contains an inlet section, a dissolution section, and an outlet section.

Determination of the nickel content in the leach solution allowed the rinse efficiency to be calculated using the following equation:[4]

$$\text{Rinse efficiency} = \left[1 - \frac{M_f}{M_i}\right](100) \ , \tag{3.1}$$

where M_f = mass of the nickel powder remaining with the discharged hulls and shroud, and M_i = mass of the powder added to the dissolver. The amount of nickel leaving with the liquid stream was determined by weighing the filter. This value was used only to calculate a material balance and to aid in determining steady-state operation.

The first series of rinsing tests was conducted at a 2-gal/min water feed rate, 3-rpm drum rotational speed, 5-min stage holdup time (time between reverse rotations), and a nickel addition rate of 100 g approximately every 10 min (at alternate reverse rotations). An apparent steady-state operating condition was attained after about 150 nickel additions. The experimental single-stage rinse efficiency obtained in this series of tests was in the range of 65 to 70%. An overall rinse efficiency for a multistaged machine can be calculated using the following equation:

$$\text{Rinse efficiency} = \left[1 - \left(1 - \frac{IE}{100}\right)^N\right] (100) \ , \tag{3.2}$$

where IE = rinsing efficiency for a single-stage dissolver, and N = number of dissolution stages. Thus a dissolver having three dissolution sections would be expected to exhibit an overall rinse efficiency in the range of 95.7 to 97.3%. The rinsing experiments previously conducted in a 1-ft-diam, 3-stage (5-section) rotary dissolver yielded rinse efficiencies of 99.6 to 99.95% using nickel powder and fuel hulls, but without shroud pieces.[4] These experiments were run, however, using longer stage holdup times (up to 60 min).

We are preparing to investigate the effects of increasing the liquid flow rate, stage holdup time, and percentage of fines in the feed material on the observed rinse efficiency.

Corrosion-erosion tests. Plans are being made for the corrosion-erosion testing of various dissolver construction materials. In these tests, we plan to expose specimens of various candidate alloys to an environment of falling and sliding sheared materials in 8 M HNO_3 at 100°C. The following list of materials has been established from which priorities for the tests will be set: titanium, zirconium, 309 SCb, 316 L, 304 L, E-Bright 26-1, Corronel 230, Incoloy 800, Incoloy 825, Carpenter A-283, Multimet Alloy (N-155), Haynes Alloy No. 188, Hastelloy G, Haynes Alloy No. 20, Inconel 690, Stellite 6-B, and Haynes Alloy No. 25.

The tests will be conducted in the 4-ft-diam dissolver after modifications are made for the addition of specimens and use of HNO_3 at 100°C. Support equipment is being located for use in these tests.

Impulse–response model. Ideally, the liquid flow through a rotary dissolver should approach the flow pattern through several mixed tanks in series. Several months ago, the actual flow patterns for the 4-ft-diam dissolver were obtained by using the tracer-injection technique. In these tests, a small quantity of nitric acid was placed in a reservoir installed in the inlet water line and injected into the dissolver along with the water stream. A conductivity meter and recorder were used to record the electrical conductivity of the outlet liquid stream. A computer program is under development that will model the liquid flow through the dissolver according to the data obtained by these tests. The computer model performs well for the simple case of only liquid flowing through the dissolver. The presence of solids in the dissolver and periodic reverse drum rotations greatly complicate modeling of the system. More work is planned to develop the model for use in more

realistic cases with solids transfer and reverse rotations. Potential uses of this model include design calculations for a multistage dissolver and problem diagnosis.

3.2.2 Operational testing of ferrofluidic seals

B. E. Lewis

The operational testing of ferrofluidic seals has been initiated to show their feasibility as a possible backup sealing system for the main concept of a purged housing for the rotary dissolver. A ferrofluidic seal is composed of a ferrofluid and permanent magnets. The ferrofluid fills the gap between the stationary and rotating parts and is held in place by permanent magnets mounted in the seal housing. The radiation resistance testing of the fluorocarbon-based ferrofluid chosen for these tests has been completed. Two portions of ferrofluid were exposed to ^{60}Co gamma rays at a level of about 5.1×10^5 R/hr for times sufficient to give integrated doses of 4.96×10^7 and 3.04×10^8 R. The ferrofluid showed no signs of deterioration at the lower radiation level. However, the higher dose produced marked changes, including breakage of the suspension, formation of a layer of solids, and a large increase in liquid viscosity.[5] Therefore, it does not appear suitable for exposure to radiation levels in excess of 10^8 R.

We intend to use the fluorocarbon-based ferrofluid to evaluate the ferrofluid seal concept and its potential usefulness for a variety of reprocessing plant applications. All seal test instrumentation has been installed and is being operationally checked. Experimentation should begin in July.

3.2.3 Nitrogen oxide scrubbing

R. M. Counce

Engineering studies have been continued to measure the removal of nitrogen oxides from a gaseous mixture of nitrogen oxides, air, and steam. During this report period, the following experiments were conducted:

1. measurement of the $NO_2 + 2N_2O_4 + NO(NO_x)$ absorption efficiency of a sieve-plate column with a 0.432-m plate spacing;
2. measurement of the NO_x absorption efficiency of a packed column under varied operating temperatures;
3. measurement of the NO_x absorption efficiency of a packed column with varied air-sparge rates of the liquid hold-up tank, with and without recycle of this off-gas through the column;
4. removal of HNO_2 from the scrubber liquid.

Using the packed column, the concentration of NO_x has been reduced from 30 vol % to less than 2 vol %. However, the effects of desorbing NO_x species from the recirculating scrubber liquid obscure the actual NO_x removal efficiency of the packed column; eliminating these effects should increase removal efficiencies.

A flowsheet of the experiment is shown in Fig. 3.1. The absorption columns, installed in parallel, are a three-stage sieve-plate column and a packed column. The plate column is as has been previously described[6] except that the plate spacing has been increased 0.432 m. The packed column is a 0.0762-m-diam device packed to a height of 1.524 m with 1/4-in. Intalox saddles. The scrubber liquid is recirculated through a liquid hold-up tank that has an overflow line to allow the maintenance of a constant liquid inventory. This tank may be sparged with air with the resultant

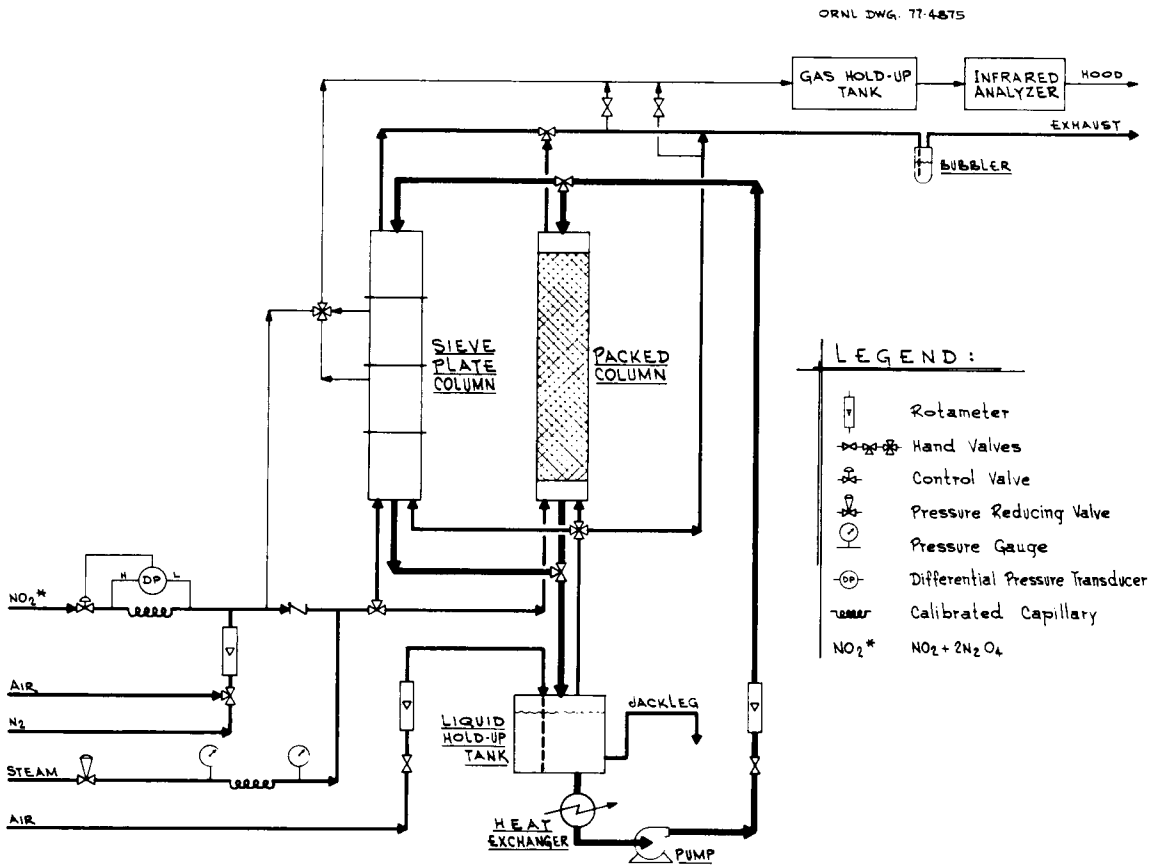

Fig. 3.1. Flow diagram of equipment used in NO_x removal study.

effluent gas recycled to the column in use or routed to the hood exhaust. A gas feed stream of NO_2+ $2N_2O_4(NO_2^*)$, air, and steam is blended and metered to the column being tested. Gas samples may be taken continuously of the feed and effluent gas streams of either column as well as of the gas in each stage of the sieve-plate column. The gas sampling system consists of a rotameter to meter the flow of a small sample stream, a gas hold-up tank to allow time for sufficient oxidation of NO to NO_2^*, and an infrared analyzer that is sensitive to NO_2^*. Liquid samples are taken for HNO_2 and HNO_3 analyses.

The overall NO_x removal performance and relevent operating parameters for the reported experiments are shown in Table 3.1. Some gaseous NO_x analyses presented were made by the Analytical Chemistry Division. The conversion of NO_x (NO_x absorbed–NO_x entering) in the sieve-plate column with a 0.432-m plate spacing, experiment ER2-4, was 87%. This compares with an 80% NO_x conversion obtained in ER1-42 under similar conditions but with a 0.229-m plate spacing.[7] The effect of operating temperature on the performance of the packed column was investigated over a temperature range of from 24 to 46.5°C (experiments ER2-10, ER2-11, and ER2-13). The removal efficiency of the system decreased with increased temperature. The effect of the air-sparge rate of the liquid hold-up tank was investigated in experiments ER2-10, ER2-14, and ER2-15. Increasing the sparge rate resulted in increased NO_x removal efficiency. Recycle of the off-gas from the liquid hold-up tank under varied sparge rates (ER2-6 and ER2-16) resulted in

Table 3.1. Experimental run conditions and results of NO_x removal in a three-stage sieve-plate column and a column packed with $^1/_4$-in. Intalox saddles

Run[a]	Column gas phase conditions: Inlet: Total flow rate (m^3/sec) $\times 10^4$	Column gas phase conditions: Inlet: Partial pressure of NO_2*[d] (atm)	Column gas phase conditions: Inlet: Steam flow (kg $mole^{-1}$ sec^{-1}) $\times 10^5$	Column gas phase conditions: Outlet: Partial pressure of NO_x[e] (atm)	Sparge gas from liquid holdup tank: Added to feed gas	Sparge gas from liquid holdup tank: Flow rate (m^3/sec) $\times 10^5$	Sparge gas from liquid holdup tank: Partial pressure of NO_x[e] (atm)	Column liquid phase conditions: Inlet[c]: Temperature (°C)	Column liquid phase conditions: Outlet: Temperature (°C)	Column liquid phase conditions: Outlet: HNO_3 (*M*)	Column liquid phase conditions: Outlet: HNO_2 (*M*)	Overall column efficiency[b]
2-4	2.00	0.330	2.82	0.044	Yes	0.0		24	47	2.85	0.20	0.87
2-6	2.00	0.330	3.38	0.011	Yes	0.0		24	53	2.95	0.15	0.97
2-10	1.78	0.235[f]	3.35	0.015[f]	No	0.0		24	50	1.77	0.10	0.94
2-11	1.73	0.212[f]	3.36	0.023[f]	No	0.0		34	59	1.90	0.08	0.89
2-13	1.71	0.201[f]	3.84	0.026[f]	No	0.0		46.5	70	1.81	0.05	0.87
2-14	1.70	0.195[f]	3.83	0.006[f]	No	1.35	0.006	26	52	1.78	0.06	0.97
2-15	1.77	0.228[f]	3.79	0.013[f]	No	0.78	0.012	28	52	1.49	0.06	0.95
2-16	1.71	0.200[f]	3.48	0.012[f]	Yes	0.78	0.014	24	52	1.44	0.06	0.93

[a]Run 2-4 was conducted in the sieve-plate column; all others were conducted in the packed column.
[b]Efficiency = (NO_x absorbed–NO_x entering).
[c]Inlet flow rate was 1.75×10^{-5} m^3/sec in all runs.
[d]$NO_2^* = NO_2 + 2N_2O_4$.
[e]$NO_x = NO_2^* + NO$.
[f]Gas analysis by Analytical Chemistry Division.

little change in the system performance. With either recycle or nonrecycle of off-gas from the liquid hold-up tank, increased NO_x removal efficiency coincided with decreased HNO_2 concentration in the scrubber liquid.

At the conclusion of ER2-11, the steam and NO_2* flows were stopped while continuing to contact the air and scrubber liquid countercurrently. The concentration of NO_x in the off-gas decreased very slowly over the next 30 min from the steady-state value achieved during the run. This effect is believed to be the result of desorbing HNO_2; however, liquid-phase analyses were inconclusive.

The stripping of HNO_2 from the scrubber liquid was the object of experiment ER3-1. Prior to the experiment, the scrubber liquid remained in the liquid hold-up tank for about 16 hr after completing experiment ER2-13. The scrubber liquid, containing approximately 0.1 *N* HNO_2 originally, was countercurrently contacted with air while sampling the incoming and outgoing gas and liquid phases. The results, given in Table 3.2, show that nitrous acid was removed from the liquid phase in the packed column and resulted in the production of approximately 1 mole of NO_x per mole of HNO_2 decomposed. This desorption of NO_x tends to obscure the results of the actual NO_x removal study as described.

Table 3.2. The removal of HNO_2 from recycle scrubbing liquid by contact with air in a packed column.

Run ER3-1: Feed gas flow rate: 2.0×10^{-4} m^3/sec;
liquid flow rate: 1.75×10^{-5} m^3/sec;
liquid inventory: 1.83×10^{-2} m^3;
temperature: 20°C

Run time (sec)	HNO_2 in liquid phase (*M*)		Partial pressure of NO_x[a] (atm)	
	Inlet	Outlet	Inlet	Outlet
0	0.103	0.080	0.0	0.050
900	0.087	0.067	0.0	0.040
1800	0.071	0.055	0.0	0.026
2700	0.060	0.047	0.0	0.020
3600	0.050	0.042	0.0	0.018

[a] $NO_x = NO_2^* + NO; NO_2^* + NO_2 + 2N_2O_4$.

In conclusion, the results have demonstrated gaseous NO_x removal to an acceptable level (<2 vol %) in the equipment described. However, the actual NO_x removal efficiency of the column tested is somewhat obscured by the desorption of NO_x compounds, which are apparently formed by the dissociation of liquid HNO_2. In order to optimally size NO_x scrubbing equipment, the absorption of gaseous NO_x and the destruction of liquid HNO_2 appear to require separate investigations. The first of these investigations is planned and will deal with determining the number of stages or height of packing required for adequate gaseous NO_x removal. Later studies will be necessary to understand the destruction of HNO_2 in the liquid phase.

3.3 FEED PREPARATION

The aqueous feed discharged from the primary dissolver system contains solids (undissolved fission products, corrosion products, etc.) and therefore requires clarification prior to solvent extraction. Preparation of the feed for solvent extraction also includes adjustment of the plutonium valence and HNO_3 concentration as well as treatment to remove iodine. This task also includes the development of secondary dissolution methods to feature more corrosive reagents for fuel constituents not soluble in the primary dissolver.

Proposed iodine-removal methods include the use of NO_2–H_2O_2 or NO_2–O_3 gas mixtures in addition to steam as sparge streams in the digestion and feed preparation tanks. Development of this unit process is emphasized.

3.3.1 Iodine evolution

J. G. Morgan

A series of small-scale engineering tests are planned to study iodine evolution from a nitric acid stream, using steam stripping in a packed column. Equipment has been received during this quarter for installation; it is hoped that the preliminary checkout runs will begin during the next reporting period.

Previous laboratory studies showed that iodine is evolved during fuel voloxidation[8] and dissolution in nitric acid.[9] The primary uncertainty is the formation of nonvolatile iodine compounds formed from organic impurities in the recycle solutions. Even when using reagent grade nitric acid and distilled water, nonvolatile organic iodides are formed. This formation appears to be associated with the oxidation step from elemental I° to IO_3^- (Ref. 10). The amount of organic iodides formed is acid-concentration dependent. At 4 *M* HNO_3, the following compounds have been identified: CH_3I, C_2H_3I, C_2H_5I, n-C_3H_7I, and n-C_4H_9I. Several methods have been used to effect iodine volatility on a laboratory scale. One method is sparging of the isotopically diluted solution with an ozone mixture prior to distillation.[11] Improved results were obtained by also sparging with N_2O_3 during distillation. Another method involved autoclaving ^{131}I with a carrier solution at 120°C prior to distillation and N_2O_3 sparging.[12] A third method,[13] and one that will be used in our experiments, involves adding a dilute solution of H_2O_2 to the boiling HNO_3; the iodine is evolved as HI.

3.4 FLUOROCARBON ABSORPTION STUDIES*

M. J. Stephenson

This task consists of the accelerated development of the krypton absorption process. The program includes expansion of the pilot-plant development, performance of a system reliability analysis, and a study of the chemical effects of impurities in the fluorocarbon solvent on the process and equipment.

3.4.1 Pilot-plant operation

B. E. Kanak, R. S. Eby, V. C. Huffstetler, and J. L. Patton (ORGDP)

Pilot-plant tests are continuing to investigate further the process behavior of various feed gas components. The current test series is part of campaign 4. Fractionator column concentration

*Jointly funded by LWR Fuel Reprocessing and Recycle Program and Advanced Fuel Recycle Program.

profiles were presented in the last progress report to show the quantitative effect of solvent flow rate and column pressure on the fractionator operation. An interesting krypton-85 concentration peak was measured in each case, using an external gamma-scintillation scanning device. It was determined that the internal krypton buildup was brought about by a complex sorption-desorption phenomenon centered about a soluble gas-pinch point. Additional tests demonstrated that the location of the pinch point could be manipulated within the column and subsequently forced to locate at any interior point simply by adjusting relative heat contents of the two phases. It was found that, when the pinch point was raised high in the column, enough stripping stages became available to effectively strip all of the dissolved gases from the solvent. If sufficient contact stages were provided both below and above the pinch point, the more soluble components could be greatly concentrated within the column because of the repeated sorption-desorption activity. In fact, during tests with krypton, fractionator internal concentration buildups in excess of 10,000 were measured. Figure 3.2 shows a typical column concentration profile that was established during one such test. Specifically, this figure presents the concentration ratio of krypton at various places within the column to the amount of krypton at the top or inlet section of the column. It is of significance to point out that the concentration peak always occurred precisely where the column temperature gradient was maintained. Furthermore, in one test, the temperature gradient was established at a section of the column where a gas sampling point was located, and the highly concentrated krypton product was withdrawn from the system to demonstrate the feasibility of pulling the captured fission gas from the system as a side-stream product.

Preliminary tests have been completed to evaluate the effectiveness of the feed-gas cooler as a batch cold trap for water removal from a saturated process feed. The introduction of water into the fluorocarbon process is of particular interest because of its limited solubility in refrigerant-12. The initial phase of testing was conducted over a continuous 4-day period in which 15.3 scfm of air containing 12,500 ppm (by volume) of water was first compressed to an absorber pressure of 150 psig and then fed through the feed-gas cooler. By cooling the gas stream down to an outlet temperature of near −20° F, the water content was reduced to a level of 55 ppm, which is equivalent to a removal efficiency of 99.6%. This resulting gas stream concentration was approximately one-third the maximum allowable concentration (that that would saturate the absorber solvent). It is important to point out that a large quantity of water was condensed in the intermediate and final compressor receiver tanks, which indicates a potential need to perform at least some feed-gas pretreatment or to allow the compressor to run hotter, with little or no interstage or afterstage cooling. Additional water-removal tests have been conducted and are under analysis. These tests support the earlier results and show that, even under a broad range of operating conditions, the water content of the gas leaving the feed-gas cooler will remain below the process solvent saturation limits.

Currently, plant tests are being conducted with nitrogen dioxide. Preliminary results indicate that significantly better solvent cleanup can be achieved in the modified solvent still with improved reflux capability. Although maintaining a moderate distillate-to-reflux ratio of 0.75 and a nitrogen dioxide feed concentration of 2000 ppm, only 30 ppm was detected in the process off-gas. the current series of tests will continue for approximately one month and will be summarized in the next progress report.

Recurring intermediate hydraulic and liquid flow check-valve problems forced premature replacement of the solvent metering pump with a more reliable regenerative turbine pump. Unlike the metering pump, however, the new unit requires external pressure and flow controls. Approximately 500 hr have been logged on the new pump without incident. Compared with the diaphragm type, the regenerative pump is easier to start and maintain because the impeller is the

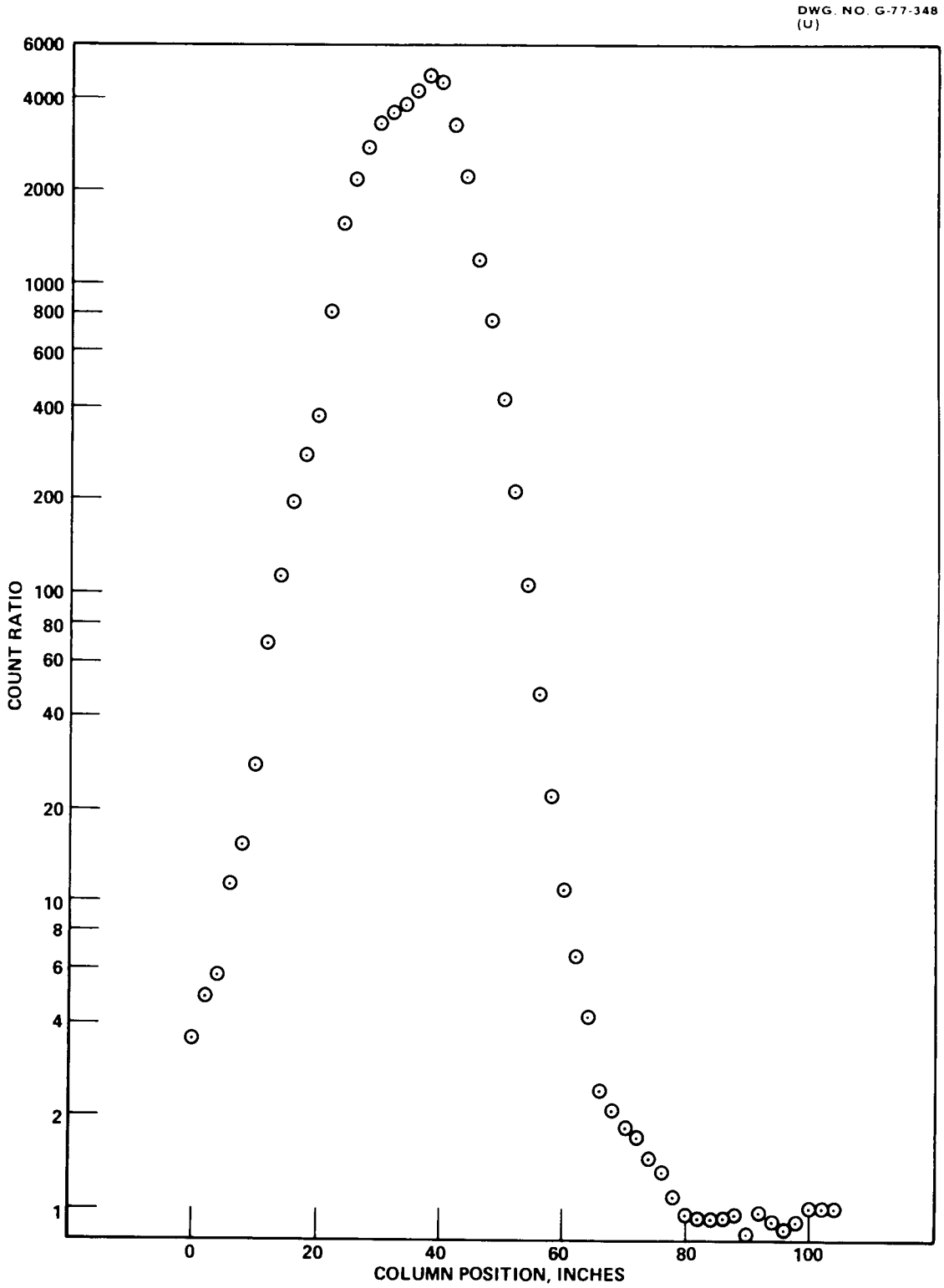

Fig. 3.2. Fractionator column concentration profile during internal column concentration test.

only moving part. A mechanical shaft seal is used and, consequently, will have to be carefully evaluated. Other modifications to the pilot plant include the installation of a miniabsorber and product cold trap.. The miniabsorber will allow the evaluation of packed-column diameter and height parameters on overall performance and a comparison of different types of packings. The product cold trap will give the plant sufficient capability to effect a krypton–xenon–carbon dioxide product separation.

3.4.2 Process application

R. S. Eby and M. J. Stephenson (ORGDP)

One of the objectives of this work is to identify flowsheet options and simplifications that lead to a more economical and/or reliable process. Recently, a new process flowsheet based on a combination absorber-fractionator was proposed. The intrinsic operating and economic advantages of this particular flowsheet were obvious. Figure 3.3 is a schematic of a greatly simplified process based on a combination absorber-fractionator (-stripper column. This flowsheet is well founded on fractionator) data taken to quantify the unusual pinch-point phenomenon and exploits the internal column concentration buildup behavior shown in Fig. 3.2. Unlike its predecessor, the new process contains only a single packed column to conduct the necessary process functions of absorption,

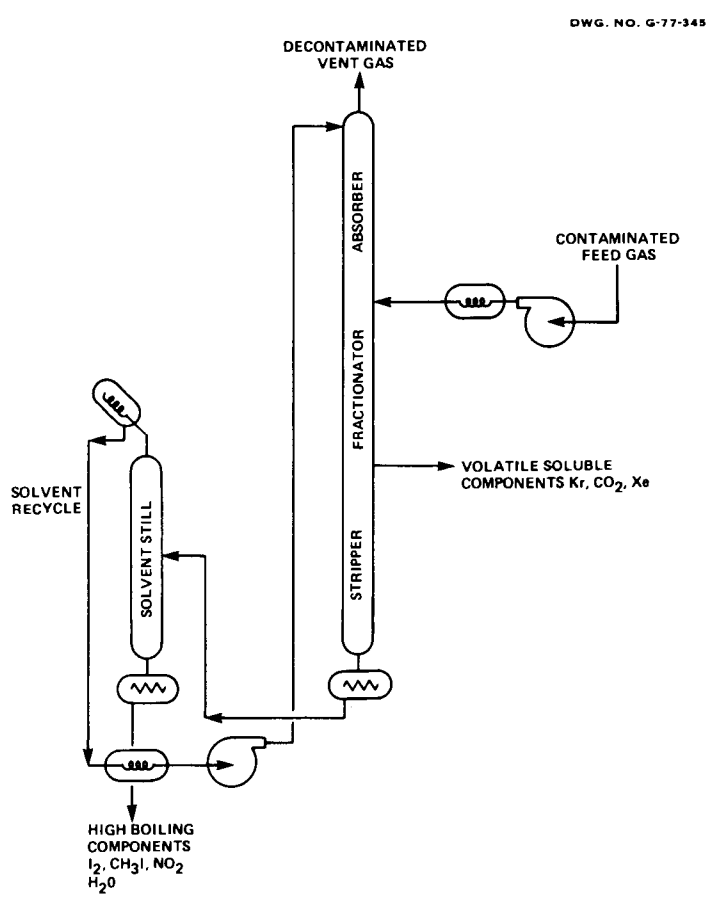

Fig. 3.3. Schematic of the fluorocarbon process based on a combination absorber-fractionator-stripper column.

fractionation, and stripping. A solvent purification still is needed if the feed-gas contains significant amounts of high-boiling components such as water, nitrogen dioxide, and iodine. Decontaminated off-gas flows from the top of the combination column and regenerated solvent from the bottom, while the fission product gases are collected as a side stream. The top part of the column (i.e., that part above the feed-gas point) is the absorption section of the process. The middle section (i.e., that part of the column between the product takeoff and the feed-gas point) serves as the fractionator. The bottom section including the reboiler makes up the stripper. Figure 3.4 shows a possible instrumentation scheme that might be employed for column control. Like the conventional process, the individual sections of the modified plant operate at different solvent-to-gas flow-rate ratios. In fact, in the absence of a pressure gradient, the modified process relies even more heavily on varying L/G ratios to achieve the three-regime operation. The dependence of the equilibrium distribution coefficient on temperature also contributes to the success of the combined operation. The absorber L/G is established by the solvent flow rate that is needed to achieve the desired removal of fission products from the feed-gas. The fractionator L/G is fixed primarily by the temperature of the downflowing solvent and total pressure of the system. The stripping section L/G is established by the boilup rate required to strip the dissolved gases from the solvent. Product is withdawn at a column position near the pinch point. An inline column condenser can be added as part of the combination column between the stripper and fractionator zones as shown in Fig. 3.4 to give the process a greater operating flexibility when the heat content of the required stripping vapor flow is greater than the heat content of the cold downflowing solvent. Specifically, when higher process removals of very soluble components such as xenon and carbon dioxide are needed, it might become necessary to use a higher boilup rate in the stripper to get a more complete cleanup of the recycle solvent.

The new selective absorption process will require substantially less equipment and control instrumentation than the standard version; because it is a simpler process, one can easily assume that the simplified process will be more economical, easier to control, and more reliable. Also, the simplified plant will obviously occupy less space.

3.4.3 Chemical studies of contaminants in LWR off-gas processing
L. M. Toth and D. W. Fuller

Carbon dioxide distribution coefficients in the R-12 gas-liquid system have been analyzed as a function of temperature for CO_2 concentrations of $\leqslant 4$ mole %. The distribution coefficient, $D = X^L/X^V$ (where X is the mole fraction in the liquid (L) and vapor (V) phases respectively), has been fit by least squares to

$$\log_{10} D = -0.4397 - 174.1/T \ , \tag{3.3}$$

where T is degrees Kelvin. These data are shown in Fig. 3.5. The standard errors of each of the latter two terms in the above expression are 0.0486 and 12.77 respectively. Distribution data have also been obtained for higher CO_2 concentrations (up to $X^L_{CO_2} \approx 0.9$); but, because these solutions are considerably removed from the dilute solution limits, the corresponding R-12 concentration in each phase must be known before a distribution coefficient expression similar to the one given above can be determined. These R-12 concentration data will be obtained during the coming month.

With the installation of a new high-pressure spectrophotometric cell and improved rocker system, we have returned to the I_2–H_2O–304 stainless steel corrosion studies discussed earlier.[14] A

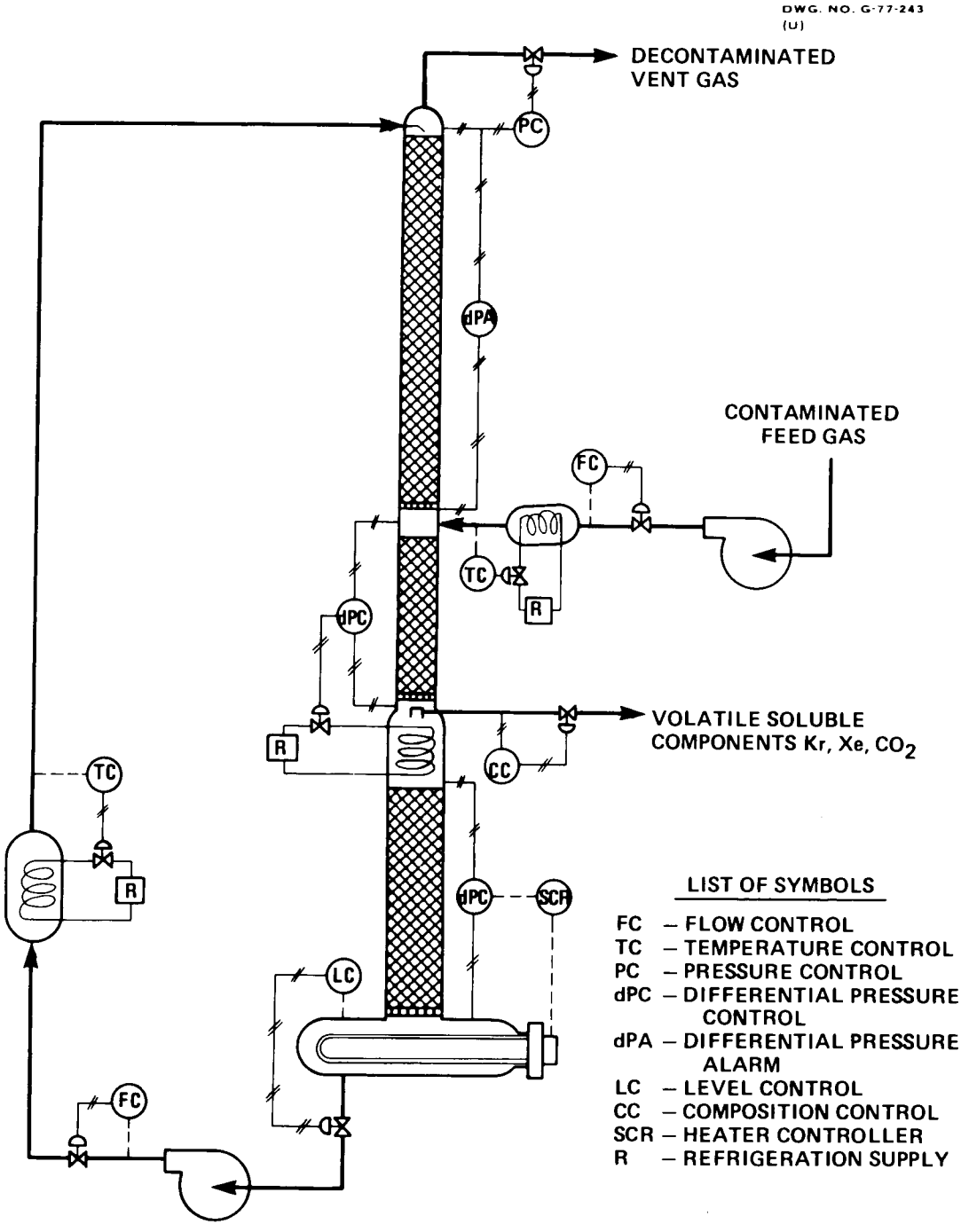

Fig. 3.4. Required control instrumentation for combination column.

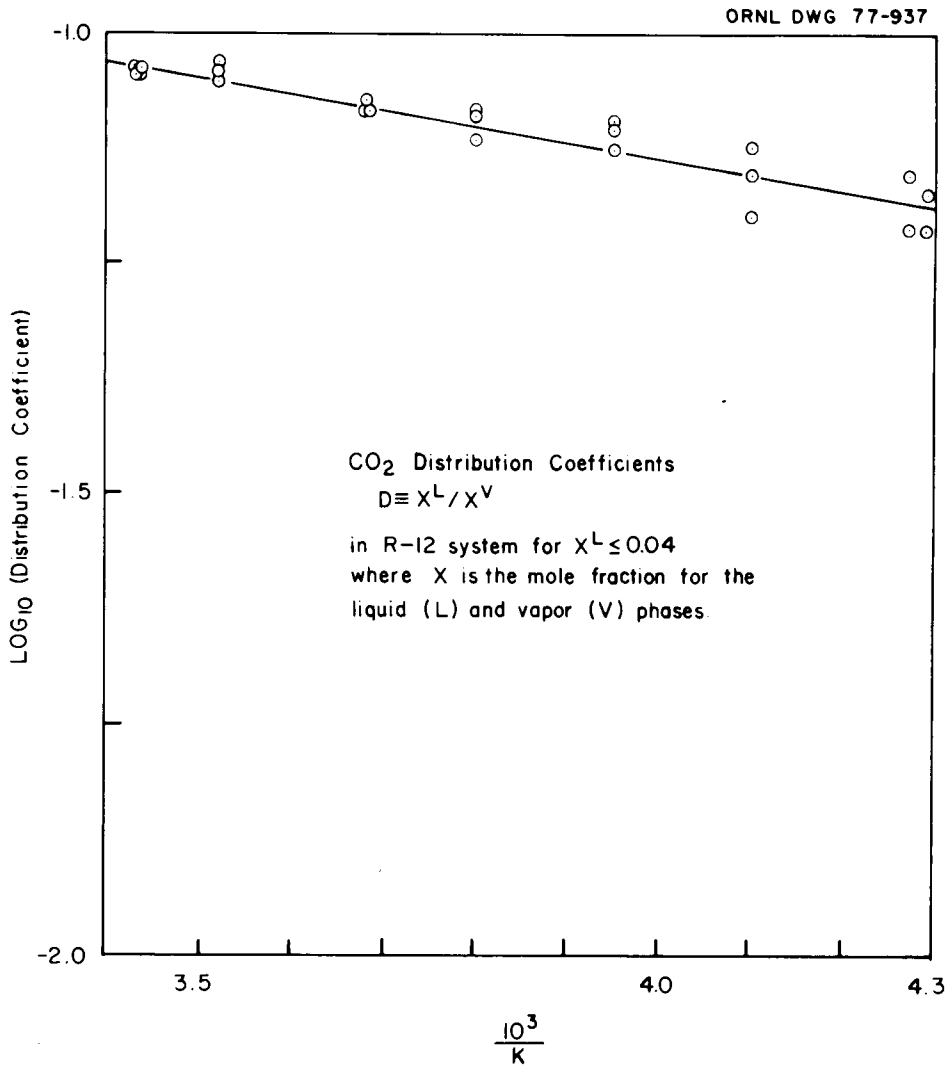

Fig. 3.5. CO_2 distribution coefficients.

principal point that we wished to verify was the possibility that the loss of I_2 from liquid R-12 as a result of corrosion was a first-order reaction rate process, independent of the added water as long as the R-12 remained saturated; that is, there was a constant activity of water in solution. We have recently found that the I_2 loss rate at 0°C decreases as water is added for water concentrations equivalent to 50 to 100 ppm. This finding suggests that the corrosion rate is determined by the rate at which water dissolves in R-12. Other aspects of the corrosion mechanism that will be sought in the near future are: (1) the difference in the corrosion rate and mechanism caused by temperature changes; (2) the maximum acceptable concentration limits of water in the system.

Further aspects of the I_2 solubility have been considered in view of comments from J. R. Merriman[15] suggesting that our entropies of solution for I_2 in R-12 deviated from similar entropies derived by Hildebrand et al.[16] These entropies can be derived from the solubility data, realizing that the entropy of solution is given by $R\, d(\ln X^L)/d(\ln T)$. Therefore, by differentiating our expression for the I_2 solubility, we obtain a value of 23.7 eu (entropy units) at 298 K where a value

approximately 2 entropy units higher is expected. The major source of error in our measurement of I_2 solubility rested with the determination of the molar extinction coefficient, ϵ, for the 520 nm band of I_2. We had previously used a value of 832 liters mole^{-1} cm^{-1}, which was suspiciously about 10% high in comparison with I_2 in other solvent systems. Recalibration led to an improved value of ϵ = 759 liters mole^{-1} cm^{-1}. When this value was used to correct the data given earlier, a proportional increase in the I_2 solubility was obtained. These corrected data are shown in Fig. 3.6 and are plotted as open circles along with the least-squares line (dashed) from the original solubility expression.[14] A repeat of the solubility measurements with the improved spectrophotometric cell and rocker system produced essentially the same results (shown as crosses in Fig. 3.6) as found earlier. A least-squares fit of all these data yields

$$\log_{10}(I_2) = 2.575 - 1620/T \ . \tag{3.4}$$

The 95% confidence limits on these data are shown as bars in Fig. 3.6 at each limit of the data. Within the error in the measurements, we find no serious disagreement in the measured and

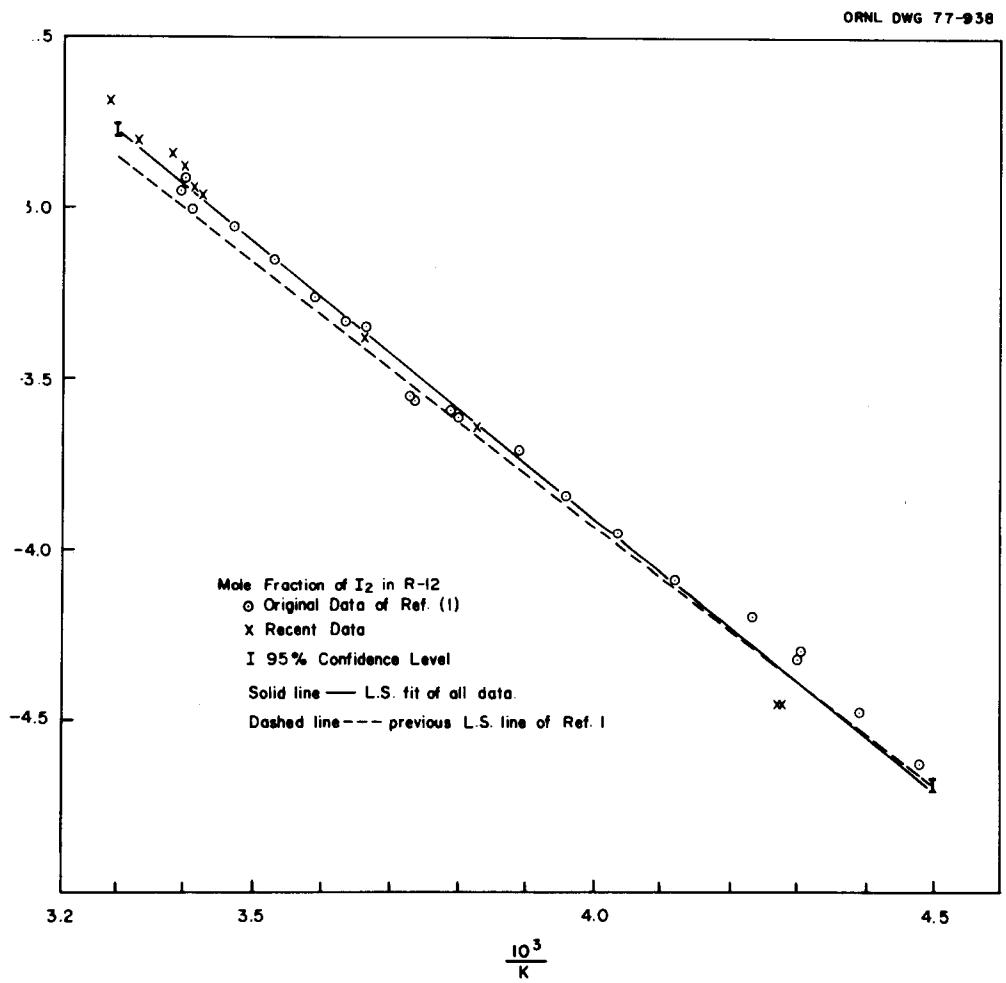

Fig. 3.6. Mole fraction of I_2 in R-12.

predicted entropies of solution. It is probable that further repetition of these measurements could reduce the error still more if greater precision were necessary. Because the molar extinction coefficients cancel out of the distribution coefficient expression (assuming $\epsilon_L - \epsilon_V$), no change in the distribution coefficient data is warranted.

3.5 IODOX PROCESS

B. A. Hannaford

The removal of volatile fission products from process and effluent streams is an important part of LMFBR fuel reprocessing. Iodine retention factors approaching 10^7 are desired when processing 90-day-decayed fuel. The Iodox demonstration system incorporates iodine scrubbing, collection of the solid pentavalent iodine, and acid recovery. Studies were continued of the Iodox process, which uses hyperazeotropic HNO_3 to scrub volatile iodine compounds from air and to convert the iodine to the nonvolatile pentavalent form.

A continuous 43-hr Iodox experiment, IXD-10, was carried out for verifying that decontamination factors measured in earlier 8-hr experiments represented steady-state results. Preparations for the experiment included installation of a stainless-steel feed acid storage tank and production of about 38 liters of about 23 *M* HNO_3 to offset the deficit that would occur during the experiment.

Iodine-131 concentrations for IXD-10 (Fig. 3.7) were determined by postrun counting of samples in glass (as in other recent experiments) to avoid the background from ^{131}I that accumulates in the flow cell. Sample frequency was less than in earlier experiments because of the projected duration of the experiment. It is probable that the simultaneous drop in ^{131}I concentration for all plates, which occurred at 2100-min run time, was caused by the increased acid concentration on plate 1. This acid concentration change caused a fluctuation in performance for that plate, presumably from an observed decrease of about 0.4 g H_2O/min in the flow of humidifying water to the gas feed stream over the time interval of 2050 to 2220 min. The decontamination factor for plate 1 responded to changes in acid concentration, as expected from previous experiments; this factor was verified by calculation of plate 1 decontamination factors at run times of 1310, 1900, 2100, 2250, and 2490 min and relating the results to acid concentration.

The ^{131}I concentrations on plates 2 through 5 moved in parallel with each other throughout the experiment, reflecting the change in the decontamination factor for plate 1. The relative constancy of decontamination factors for plates 2, 3, and 4 are illustrated by Table 3.3. The greater variability for the plate 5 decontamination factor was caused by poor counting statistics for plate 6. The overall column DF of 2.7×10^4 was comparable to the value of about 2×10^4 measured in an 8-hr experiment (IXD-7) under nearly identical conditions. The DF calculated on the basis of gas samples only (4.6×10^6) was implausibly high, because the corresponding plate-to-plate DF would be about 13, as compared with an observed average of about 5.5. Taking the observed plate-to-plate average as the most reliable basis for calculation, the DF of 2.7×10^4 should have produced an average concentration of 0.5 counts min^{-1} $liter^{-1}$ in the final off-gas. The resulting accumulated ^{131}I activity in the silver-zeolite off-gas trap would have been easily measurable. A postrun experiment in which concentrated ^{131}I-traced CH_3I was fed to a test trap containing silver-zeolite from the batch used in run IXD-10 confirmed that the sorbent effectively trapped iodine. Therefore, no suitable explanation has yet been found for the extremely low ^{131}I count in the off-gas traps.

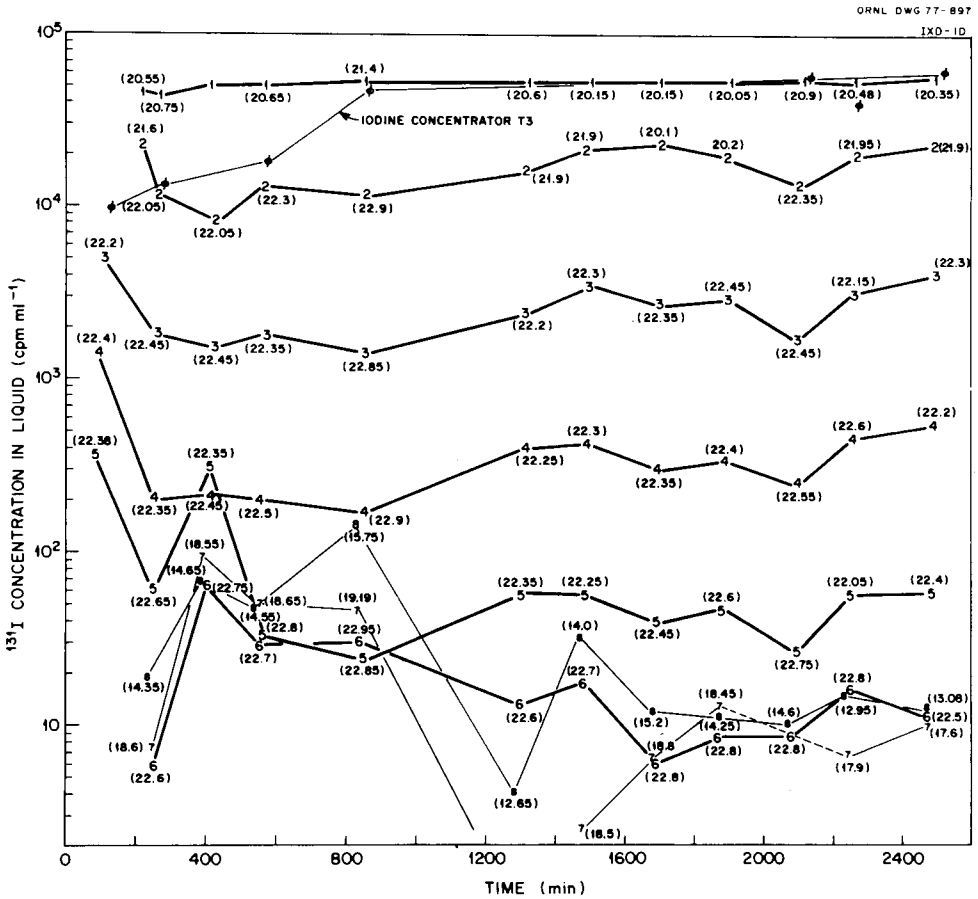

Fig. 3.7. Run IXD-10. Concentration of iodine in liquid and gas streams vs time for scrubbing ^{131}I–traced CH_3I from air–1.9% NO_2–2.1% H_2O with fuming nitric acid [feed rate of gas mixture = 98 std liters/min (1.62×10^{-3} m^3/sec); feed rate of 23.4 *M* HNO_3 = 45 ml/min (7.50×10^{-7} m^3/sec); feed rate of water = 6.1 ml/min (1.02×10^{-7} m^3/sec); concentration of CH_3I in feed gas = 0.000264 g of I per liter; nitric acid concentrations are given in parentheses; temperature: 22 to 26°C, plate 1; 27°C, plate 6; 50°C, plate 8].

Table 3.3. Run IXD-10: decontamination factors (DF) for ^{131}I–traced CH_3I in air–1.9% NO_2–2.1% H_2O

Plate	Decontamination factor[a]
1	2.94 ± 0.64 (±22%)
2	6.59 ± 0.86 (±13%)
3	7.11 ± 0.93 (±13%)
4	8.27 ± 1.12 (±14%)
5	4.37 ± 1.04 (±24%)
6[b]	–
Average[c]	5.49
Column, overall	2.7×10^4
Column, overall[d]	4.6×10^6

[a]Average and standard deviation for five time periods: 1310, 1900, 2100, 2250, 2490 min.

[b]Counting statistics for plates 6, 7, and 8 were too scattered for reliable calculation.

[c]Average = $[(DF)_1 \times (DF)_2 \times \ldots (DF)_5]^{1/5}$.

[d]Based on ^{131}I concentrations and flow rates of gas streams only, taking the average of four feed-gas samples (13,580 ± 1110 counts min^{-1} $liter^{-1}$) divided by the average of five final off-gas samples (0.00293 ± 0.0035 counts min^{-1} $liter^{-1}$).

The iodine balance for the experiment was unsatisfactory, based on a few selected solution samples from the iodine concentrator (T3) and plates 1 and 2 of the Iodox column. For plate 1, reported iodine concentrations averaging 0.15 g of I per liter represented about 30% of the expected concentration and about 20% of the solubility value, although the presence of precipitate showed that all plate 1 samples were saturated. The specific ^{131}I activities for plate 1 samples were high by a factor of about 5, based on comparison with specific activity calculated from the inputs to the feed gas cylinder (3 mCi ^{131}I, 80 g CH_3I). In future experiments some special treatment of the plate 1 samples will be provided to stabilize the iodine pending postrun ^{131}I counting and wet analysis of the solution.

For the first time in the demonstration of Iodox, the solution was continuously transferred from the iodine evaporator to the iodine concentrator over a period of about 35 hr. Resulting condensate flowing to the acid recycle system contained about 1200 counts/min of ^{131}I, providing a retention factor of about 1060 for the evaporators based on an input of about 1.3×10^6 counts/min of ^{131}I. This reproduced the value measured earlier in run IXD-7. Samples taken from the acid recycle system showed a relatively smooth increase in ^{131}I concentration in the recirculating salt inventory during the first half of the experiment with increasing scatter in the second half. Only about 5% of the ^{131}I reported to the raffinate, and about $25 \pm 20\%$ to the recycle product acid.

Preparations were begun for an experiment in which a transient will be produced in the methyl iodide feed rate to the Iodox column; these include (1) an improved metering system for water vapor, (2) installation of two all-Teflon pumps for delivering fuming nitric acid to the specific gravity monitors, and (3) upgrading the 20-position sample valve with replacement of nylon components by machined Kel-F parts.

3.6 INSTRUMENTATION AND CONTROL SYSTEMS

W. R. Hamel and N. C. Bradley

The overall objectives of this task are to develop instrumentation systems and engineering techniques for the fuel reprocessing program and to provide a basic instrumentation and control technology for application to commercial plants. In addition, instrumentation and control systems are required to support laboratory experiments and highly specialized tests associated with the components and process development tasks in the Advanced Fuel Recycle Program.

3.6.1 Nondestructive assay of spent fuels

G. L. Ragan, C. W. Ricker, T. J. Burns, D. T. Ingersoll, J. D. Jenkins, F. R. Mynatt, and J. E. Rushton

During this quarter, all effort on this subtask has been directed toward the design and construction of a proof-of-principle experiment. This experiment is expected to confirm the validity of the active neutron interrogation method for the nondestructive assay of the total fissile content of spent fuel and blanket subassemblies.

The engineering design for the proof-of-principle experimental equipment has been completed, and fabrication of the equipment is underway.

The storage shield facility for the four 100-Ci antimony-beryllium sources required for the proof-of-principle experiment has been fabricated and installed at Building 7930. The source

monitor and interlock system associated with the storage shield facility has been constructed and is ready for installation. The components for the four antimony-beryllium sources have been received from the Amersham-Searle Company. The holders required for the activation of the antimony in the Oak Ridge Research Reactor have been designed and fabricated.

Test samples for the proof-of-principle experiment have been procured. Enriched (7.1% ^{235}U) MH1A (U.S. Army reactor) fuel subassemblies will be used in conjunction with Dresden pins (1.5% ^{235}U) for the assay investigations. Although these test samples will be adequate, the quality of the experimental measurements could be enhanced by incorporating fuel having higher enrichment. Therefore, efforts are being made to procure 18% enriched fuel for use with the fuel now available.

During this quarter, a decision was made on the basis of analyses to use methane-filled proton recoil neutron detectors, rather than helium-3 detectors or fission counters, for the detection of fission neutrons. Also, it was decided that two ^{235}U fission chambers were to be used to monitor the interrogation neutrons produced by the antimony-beryllium sources. The methane-filled proton recoil detectors and associated electronics for the proof-of-principle experiment have been received. The fission counters used for source monitoring during the experiment and the electronics associated with these detectors are scheduled for delivery early in August.

3.6.2 Process sensors and control

N. C. Bradley, D. N. Fry, J. M. Googe (University of Tennessee consultant), J. O. Hylton, J. M. Jansen, Jr., W. F. Johnson, G. N. Miller, W. P. Murray, H. H. Ross, A. A. Shourbaji, C. M. Smith, J. E. Strain, and R. M. Tate

Vibration analysis instrumentation for the rotary dissolver. The analysis of recorded vibration signals from accelerometers mounted on the pillow-block bearing supports of the 4-ft-diam rotary dissolver is continuing. The identification of characteristic vibration signatures for each phase of dissolver operation is one step in the development of a method for dissolver blockage detection. After the identification of these characteristic signatures, any change might be useful for detecting the presence of a mechanical anomaly or an incipient blockage.

We have established a characteristic vibration signature for most phases of dissolver operation. A single revolution of the dissolver was divided into 16 segments for analysis because it was found that the vibration is dependent upon dissolver position. A power density spectrum was obtained for each orientation. By using all of the power spectral density (PSD) values within a specified bandwidth of frequencies of each power spectrum, a single root-mean-square (rms) value was formed for each orientation of each dissolver revolution. By plotting this rms value versus dissolver orientation during different phases of dissolver operation, we have established various characteristic signatures.

Characteristic vibration signatures are now established for (1) the inlet of simulated chopped fuel hulls, (2) the mixing of these hulls in the dissolution section, (3) the transfer of hulls from the dissolution to exit sections, and (4) the transfer of hulls from the exit section. Figure 3.8 presents the characteristic vibration signature for the input of hulls into the dissolver. The signature is a peak in the rms value that was formed from PSD values within the 4 to 5 kHz frequency range. The peak is caused by the vibrations caused by the impaction of the hulls as they enter the dissolver and occurs only at the time when the hulls are introduced. Figure 3.9 presents the signature for the transfer of the hulls from the exit section of the dissolver to the outside. This signature is characterized by multiple peaks in the rms value (4- to 5-kHz frequency range) and is caused by impacting of the hulls as they are dropped from the four exit transfer baffles into the exit chute. Figure 3.10 presents

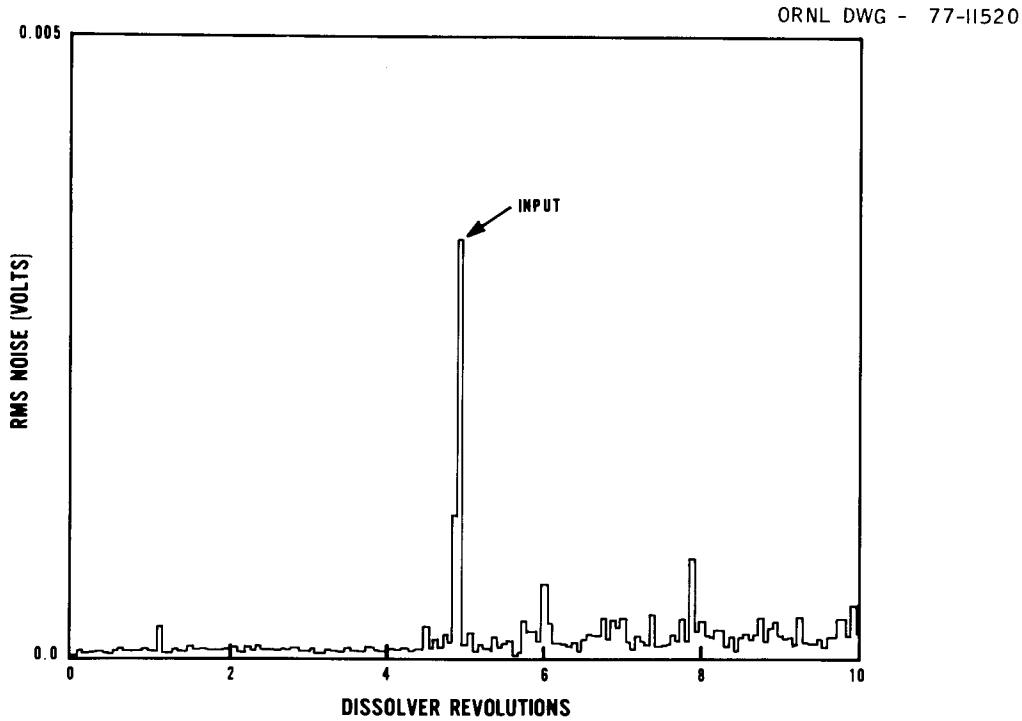

Fig. 3.8. RMS noise for 4 to 5 kHz frequency band showing characteristic peak due to input of hulls.

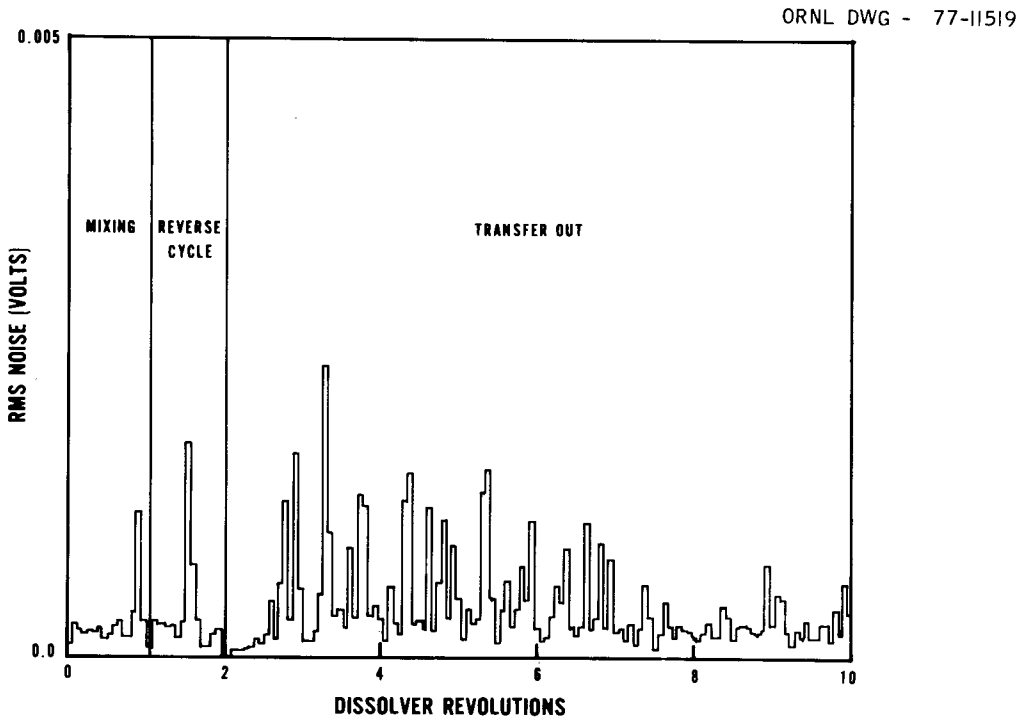

Fig. 3.9. RMS noise for 4 to 5 kHz frequency band showing characteristic peaks due to hull transfer out of the exit section.

ORNL DWG - 77-11523

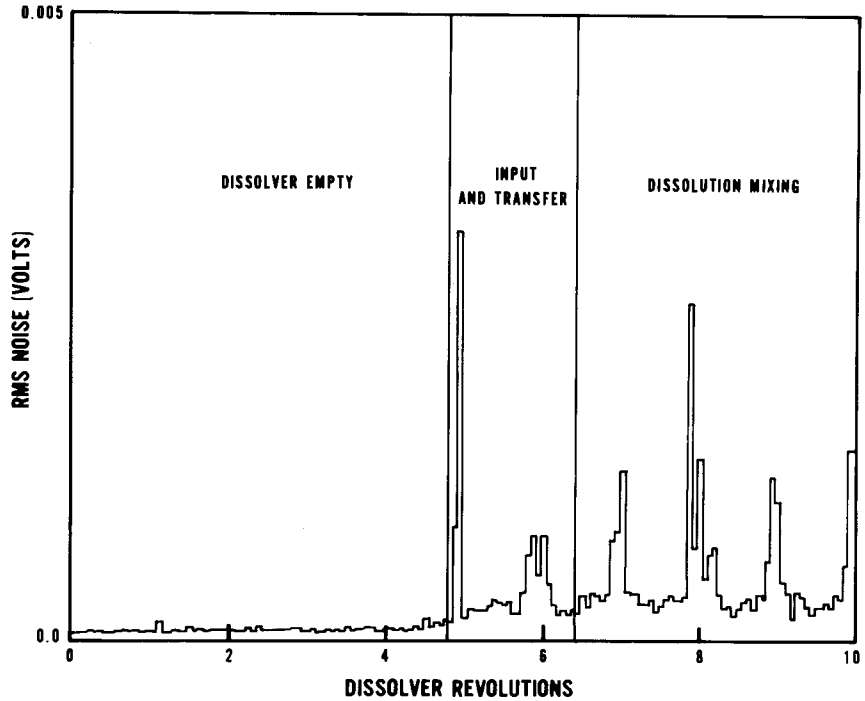

Fig. 3.10. RMS noise for 2 to 3 kHz frequency band showing characteristic one per revolution peaks due to hull mixing in the dissolution stage.

the signature for mixing of hulls in the dissolution section. The signature is characterized by a single peak in the rms value (2- to 3-kHz frequency range) near the end of each revolution, caused by the agitation baffle in the dissolution section lifting the hulls until they fall over the back of the transfer chute to the bottom. Figure 3.11 presents the signature for the transfer of hulls from the dissolution section of the exit section. This transfer occurs during a reverse revolution of the dissolver. The signature is a single peak in the rms value (2- to 3-kHz frequency range) near the middle of the reverse revolution and is similar to that of mixing in the dissolution section, but it occurs at a different orientation in a revolution and only during a reverse revolution.

Through the use of the characteristic vibration signature for the transfer of hulls from the dissolution section to the exit section, we believe that we will be able to detect a blockage in the transfer chute between these two sections. This signature is characterized by a peak at approximately the middle of the revolution. A blockage should cause a change in the location of the peak within the revolution, or a secondary peak will occur when the hulls that have failed to transfer through the chute to the exit section fall from the chute back into the dissolution section.

As reported in a previous quarterly report, we have been able to detect a resonance caused by a flared V-roller in the dissolver.[17] Through additional analysis, the presence of this mechanical anomaly has been separated from the characteristic vibration signatures. In accelerometers that are located near the point of the effects of the anomaly, the characteristic vibration signatures are influenced by these effects. However, in accelerometers removed from the point of the effects of the anomaly, the characteristic vibration signatures are still distinguishable. Because the anomaly produces effects several times during each dissolver revolution, it is best characterized by a PSD frequency spectrum rather than the rms value (which is large—0- to 2-kHz frequency range) each time the effect occurs. Figure 3.12 shows PSD spectra for the dissolver operating during mixing in

ORNL DWG - 77-11522

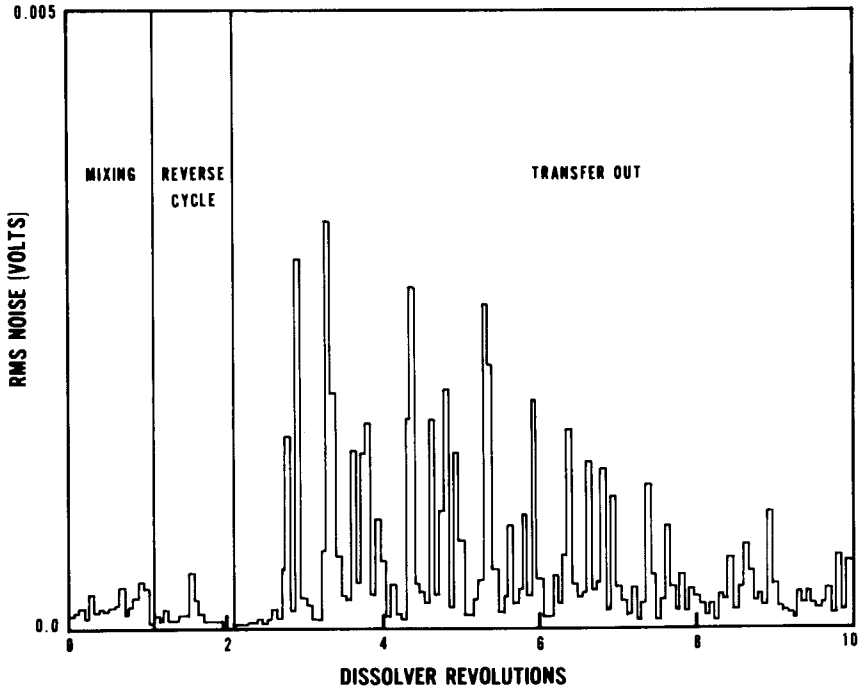

Fig. 3.11. RMS noise for 2 to 3 kHz frequency band showing peaks near center of reverse cycle.

ORNL DWG - 77-11521

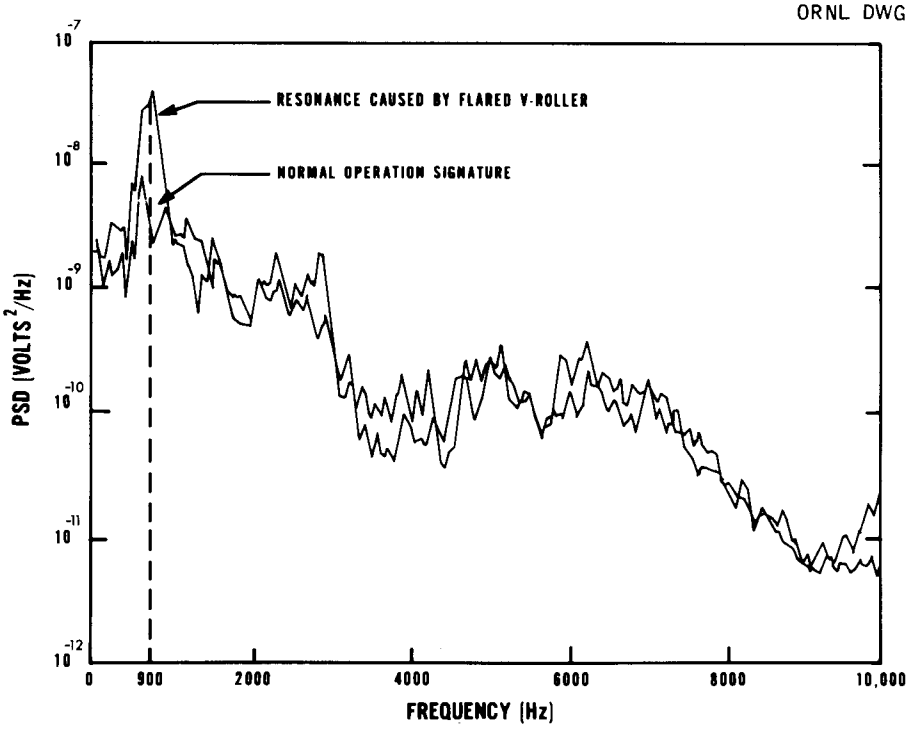

Fig. 3.12. Frequency spectrum of dissolver vibrations during dissolution mode showing effect of flared V-roller.

the dissolution section with and without the mechanical anomaly present. A large peak at approximately 900 Hz is apparent when the anomaly is present.

Sensor development for process analysis. Work is being carried out to characterize the spectral properties of uranium, plutonium, and mixed fission products in nitric acid solutions. Since nitrate ion is a strong, broad-band absorber in the uv spectral region, our effort is restricted to visible radiation. The major objective here is to determine the absorption spectra of the dissolver solution components and to study how these spectra change with different dissolution–digestion conditions. These data will be used to define a multiwavelength "absorption matrix" that will be used in the prototype monitor design. Present work is being carried out with cold uranium solutions and simulated fission products (rare earths). Concurrently, we are preparing for the installation of a quality spectrophotometry system in a hot-cell facility. This equipment will allow us to study "hot" dissolver solutions as well as other anticipated fuel-related materials. Completion of this facility is expected in the next quarter.

Optical components for the monitor are also being evaluated. Multiple wavelength detection is being studied with a vidicon-polychromator system. Computer strategies for optical data processing are being developed. Other detectors (diode array, charged-coupled detector, charge-induced detector) are also being assessed for this application. A ten-channel filtered diode array appears promising.

An effort has also been initiated to develop a continuous free-acid monitor based upon equilibrium vapor-phase measurement where changes in vapor-phase acid concentration are related to the liquid-phase free nitric acid concentration. Very preliminary tests indicate a strong, consistent relationship between the two phases in the region between 2 and 6 *M* nitric acid. Two areas of investigation are in progress: (1) the liquid-vapor phase equilibria in dissolver solutions and (2) possible measurement techniques for the vapor phase. A successful vapor-phase measurement system appears to be applicable in virtually any nuclear fuel processing operation.

One-fourth-scale dissolver seal test instrumentation. Upon receipt of the temperature control system, instrument mounting and fabrication were completed. The two-rack control system was moved to the seal test site, where field wiring was completed. Presently, the programmable logic controller (PLC) program is being tested and readied for operation.

Four-foot-diameter dissolver prototype dissolver corrosion test instrumentation. A Dynatrol specific gravity measurement instrument was selected and an order placed for a unit with titanium-wetted parts. Delivery is expected in August. This instrument will act as the sensor portion of a loop-control system to maintain the dissolver solution at 8 *M* HNO_3.

Eddy current probes measurement system. The eddy current probes for the measurement of dissolver rotating drum deflections have been received, and the mounting hardware has been fabricated. The probes have been calibrated, and temperature tests have been run on these devices. They are to be installed in July when the 4-ft-diam dissolver is shut down for a short period of time.

Prototype voloxidizer. The design of the instrumentation package for the prototype voloxidizer is almost complete. Preliminary drawings that show the interconnections of the unit process controller to the remainder of the instrumentation and to the voloxidizer system have been completed by drafting and are being reviewed. The majority of the instruments have been specified and ordered.

Infrared temperature measurement. The infrared temperature measurement system for use with the voloxidizer has been purchased and is being evaluated. The periscope design has been reviewed, and indicated changes are being made.

Iodine evolution experiment. Preliminary control system design has been completed and is being reviewed. Some of the instruments are on order, and the selection of others is in progress.

Digital unit process controller evaluation and development. Work on the Bristol UCS-3000 has concentrated on communicating with peripheral devices by means of the universal asynchronous interface board. Tests are under way to establish reliable communication links with a supervisory computer (PDP-11/40) and an analog data multiplexer (a Burr-Brown "Micro Mux"). A color cathode ray tube operator interface purchased for use with the UCS-3000 has been received and will be tested as soon as the above examinations are completed.

3.7 SOLVENT EXTRACTION

M. E. Whatley

An effort has begun at Argonne National Laboratory to emphasize the development of a critically (nuclear) safe centrifugal solvent extraction contactor for LMFBR fuel reprocessing. The primary objective of the program is to design, fabricate, and test a centrifugal contactor suitable for reprocessing LMFBR fuel at a rate of approximately 0.5 metric-ton/day. The design of the contactor is based on the annular mixing concept conceived at ANL several years ago. A number of these contactors will be operated in multistage Purex solvent extraction systems.

The contactor is sized to provide about 3 gpm throughput, based on a concentrated feed solution. The dimensions were selected for this throughput at a rotor speed of 1750 rpm, while retaining overall critically safe dimensions for all concentrations of ^{239}Pu.

The design comprises a hollow rotor coupled directly to a motorized spindle and rotating within a fixed casing. The rotor is about 3.5 in. in diameter and 10 in. high (8-in. settling section and 2-in. weir section). The motorized spindle is a 1-hp commercial precision unit that operates at about 1750 rpm. The spindle is bolted to a heavy 90° machine bracket to permit vertical mounting on a support plate. A rotary air seal is mounted on the upper end of the hollow spindle shaft and supplies air for the rotor weir control system. The contactor casing is mounted on the underside of the support plate. Two pipe lines are connected at the sides of the casing for feeding aqueous and organic solvent streams to the annulus where they are mixed by skin friction between the rotor and the casing. The mixed phases enter an opening in the bottom of the rotor and are separated by centrifugal force as they move upward through the rotor. Suitable weirs direct the separate streams to collector rings in the casing from which they flow through discharge lines.

Fabrication drawings are essentially complete and are being reviewed. A purchase order has been issued for the motorized spindle. The support bracket and rotary air seal have been received from vendors.

At proposed flow rates, residence time in the mixing zone of a contactor will be about 2 sec and in the separating rotor, about 5 sec. Concern has, at times, been expressed that such short residence in the mixing zone might be inadequate to complete reactions that are relatively slow, such as the reduction of Pu(IV) to Pu(III) for the partitioning of uranium and plutonium. One relatively simple way to increase the residence time in the mixing zone is to extend the length of the casing while

retaining the same rotor design. A recent test was performed by use of the original ANL centrifugal contactor, which has a 4-in.-diam rotor. In this test, a plastic (methacrylate) pipe extension was attached to the casing with tangential exit lines at the bottom of the mixing annulus. These lines were then connected near the bottom of the extension. In this arrangement, the mixed phases could be removed from the annulus and reinjected into the extended casing. A preliminary test with water showed that vigorous mixing persisted throughout the extended casing. In the test arrangement, the volume of the mixing zone was increased by about a factor of 10 over the normal mixing zone volume. Larger increases in mixing zone volume are possible with this design.

Preparations are under way for tests to measure kinetics of extraction and scrubbing of ruthenium and zirconium in a single-stage miniature annular centrifugal contactor.

REFERENCES FOR SECTION 3

1. B. L. Vondra, *LWR Fuel Reprocessing and Recycle Program Quarterly Report for Period January 1 to March 31, 1977,* ORNL/TM-5864 (May 1977).

2. B. L. Vondra, *LWR Fuel Reprocessing and Recycle Program Quarterly Report for Period April 1 to June 30, 1977,* ORNL/TM-5987 (August 1977).

3. J. H. Goode, C. L. Fitzgerald, and V. C. A. Vaughen, *The Dissolution of Unirradiated and Irradiated (U, Pu)O_2 in Nitric Acid,* ORNL-5015 (February 1975).

4. W. D. Holland, C. O. Reiser, R. B. Heimdahl, and W. S. Groenier, *Nuclear Fuel Dissolution and Rinsing Studies Using a Continuous Rotary Dissolver,* ORNL/TM-5566 (March 1977).

5. Personal correspondence from J. C. Mailen to B. E. Lewis, May 26, 1977.

6. W. D. Burch et al., *LMFBR Fuel Reprocessing Program Progress Report for Period April 1 to June 30, 1976,* ORNL/TM-5556 (August 1976).

7. R. M. Counce and W. S. Groenier, *Nitrogen Oxide Absorption into Water and Dilute Nitric Acid—Description of a Mathematical Model and Preliminary Scrubbing Results Using an Engineering-Scale Sieve-Plate Column,* ORNL/TM-5910 (in preparation).

8. J. H. Goode, *Voloxidation—Removal of Volatile Fission Products from Spent LMFBR Fuels*, ORNL-TM-3723 (January 1973).

9. D. O. Campbell, *LWR Fuel Reprocessing and Recycle Program Quarterly Report for Period April 1 to June 30, 1976,* ORNL/TM-5547 (July 1976).

10. K. Nakamura et al., "Formation of Organic Iodides upon Heating Nitric Acid Solutions Containing Carrier-Free Iodine-131," *J. Nucl. Sci. Technol.,* **10**(6), 367–373 (1973).

11. G. I. Cathers et al., *Method for Removing Iodine from Nitric Acid,* U.S. Patent 3,803,295, Apr. 9, 1974.

12. G. I. Cathers et al., *Removal of Iodine from Nitric Acid Solutions,* U.S. Patent 3,792,154, Feb. 12, 1974.

13. G. I. Cathers et al., *Volatilization of Iodine from Nitric Acid Using Peroxide,* U.S. Patent 3,914,388, Oct. 21, 1975.

14. L. M. Toth, D. W. Fuller, and J. T. Bell, "Chemical Studies of Contaminants in LWR Off-Gas Processing," *LWR Fuel Reprocessing and Recycle Program Quarterly Report for Period April 1, 1976 to June 30, 1976,* ORNL/TM-5547 (July 1976).

15. Personal communication, J. R. Merriman, Paducah Gaseous Diffusion Plant, to L. M. Toth, May 1977. See also J. R. Merriman, *The Solubility of Gases in CCl_2F_2; A Critical Review,* Paducah Gaseous Diffusion Plant, Report KY-G-400 (March 1977).

16. J. H. Hildebrand, J. M. Prausnitz, and R. L. Scott, "Regular and Related Solutions," Van Nostrand Reinhold Co., New York (1970), p. 145.

17. W. D. Burch et al., *LMFBR Fuel Reprocessing Program Progress Report for Period October 1 to December 31, 1976,* ORNL/TM-5768 (February 1977).

4. ENGINEERING SYSTEMS

M. J. Feldman

Reflected in this issue of the Advanced Fuel Recycle Program progress report is a regrouping of subject areas that indicate the functional thrust of the program planning. The program has been organized into three functional areas. The Engineering Systems Section is one of these areas; we have, therefore, revised the report format to present the work of the engineering systems group in one section.

The Engineering Systems Section of the Advanced Fuel Recycle Program has a basic responsibility of the analysis, definition, design, fabrication, and operation of engineering-scale reprocessing components, systems, and a pilot plant. The group represents an integral part in the classical progression of the development of a major technical area. Its inputs are the activities of the research and development of chemical concepts as represented by the work presented in Section 2 and the engineering modeling, analysis, research, and experimental work presented in Section 3.

In the Enginering Systems Section, the progression of work is furthered in four subsections. The Engineering Analysis group is responsible for analysis on the effect of modification, change, or revision of major reprocessing parameters as applied to the design and operation of plant-scale activities. The analysis section is also responsible for defining research and development areas necessary to understand the actual effects of parameter modifications.

The Component Development group is responsible for the definition, design, fabrication, and operation of major reprocessing equipment items. Although this group functions as a part of program progression, it has two unique missions: the development of full-scale equipment (as measured by throughput) and remote operation and maintenance. The introduction of these two controlling parameters coupled with the ongoing technical reprocessing parameters characterize this area.

The Systems Development area contributes to program progression by incorporating major processing component developments into operating systems or subsystems. In addition, development areas that are generic in nature and have application to broad areas of reprocessing are also studied.

The efforts of Engineering Analysis, Component Development, and Systems Development are focused in a fourth area known as the HEF conceptual design group. Here, ongoing efforts are to culminate in the conceptual design of a reprocessing plant that will demonstrate environmentally acceptable and financially efficient spent fuel reprocessing. The components and systems are integrated into an operating facility that, in addition to an acceptable demonstration of initial goals, has a longer-range goal of providing an adequately flexible test bed to house future (30-year) developments in the reprocessing field.

4.1 ENGINEERING ANALYSIS

A. R. Irvine

A report dealing with the solubility of plutonium-bearing mixed-oxide fuels was completed and is now in press. The report (ORNL/TM-5903) is entitled *The PuO_2 Dissolution Problem for LWR Plutonium Recycle and LMFBR Fuels: Fabrication and Reprocessing Problems and Their Resolution* and was prepared by E. L. Nicholson; the abstract follows:

> "A survey was made of the information reported to date for laboratory-scale dissolution experiments on PuO_2-UO_2 fuels, of reprocessing plant problems that might be encountered with these fuels, and of the fabrication methods for producing these fuels. The possibility of producing fuels that will be highly soluble in pure nitric acid without resorting to the use of corrosive fluorides for complete dissolution is examined. The report concludes that production of highly soluble fuel is possible, that it is probably economically justifiable, and that fluorides are not necessary for dissolution. Highly soluble fuel would likely have minimal impact on reprocessing criticality and waste disposal problems. Reactor specifications for PuO_2-UO_2 fuels seemingly permit a greater degree of nonhomogeneity than is desirable for achieving high solubility. A fuel solubility criterion is therefore proposed that would limit the amount of insoluble PuO_2 in irradiated fuels to $\leqslant 0.01\%$ of the total amount of plutonium present."

The change in U.S. policy on nonproliferation as it affects the Advanced Fuel Recycle Program will be a major undertaking in the Engineering Analysis group. The addition of the thorium reprocessing cycle to the existing uranium-plutonium reprocessing cycle requires that an analysis of present program criteria and objectives be conducted to indicate required changes and necessary additional areas of development.

4.2 COMPONENT DEVELOPMENT

N. R. Grant

The component development effort is a general follow-on to the engineering research effort. Chemical concepts applicable to the effort, which are projected by the research and development area and subjected to model testing in the engineering research area, are screened for engineering application to the program. In the component development area, both capacity and remote maintenance and operation criteria are applied. The design, fabrication, and operation of full-scale, remotely operable process equipment are component development goals.

Beginning this quarter, component development will address only those tasks that are directly process related and essentially deal with one major component. Other tasks will be reported in Sect. 4.3, Systems Development. Ultimately, component development will include disassembly and cutting, voloxidation, dissolution, feed preparation, solvent extraction, and product conversion. To date, only two tasks (disassembly and cutting, and dissolution) have progressed to the component development stage. The other four tasks will be added to this section as component development work is initiated during the next two years.

4.2.1 Disassembly and fuel cutting–contracted work

C. D. Watson and B. S. Weil

The component development effort in disassembly and shearing is charged with the mechanical preparation of fuel materials for the succeeding steps of voloxidation and dissolution. The work is being carried out with in-house effort and with a subcontract to the Gulf + Western (G+W)

Advanced Development and Engineering Center. Both short-range development and testing and longer-range process improvement technologies are being pursued, with the major effort in those activities directed toward HEF design.

During this quarter, G+W has engaged in design assistance activities on (1) tooling for the ORNL shear; (2) tooling for the Hill-Acme alligator shear; (3) participation in plasma-arc cutting tests at the Linde Welding Products Division, Florence, South Carolina; (4) participation in electric-arc saw cutting tests at Retech, Inc., Ukiak, California; (5) observation of the s tests at Saturn Manufacturing Co., Tualatin, Oregon; (6) completion of the roll cutting tests of the outlet nozzle of dummy LMFBR fuel and its documentation in a report; (7) performance of in-house rotary-shearing tests at the G+W Folcraft-2 installation; and (8) continuation as a major effort the detailed design of the disassembly system, including the necessary liaison involved in the fabrication of a one-fourth scale model and the required design activities to interface the model with the ORNL straight-sided Birdsboro shear.

Items 1 through 5 are included in ORNL activities; however, they are mentioned here to acknowledge G+W's assistance and participation in the program. A summary of G+W activities of items 6, 7, and 8 follow.

Subassembly cutting tests. Subassembly cutting tests were performed on stainless steel hex shroud sections with commercial roller-pipe cutters to determine (1) the cutting time and (2) the approximate magnitude of roller cutter life. The test rig consumed two sets of 7.3-cm ($2^7/_8$-in.)-diam commercial pipe cutters during shakedown trails. The roll cutters were opposed by two backup noncutting rollers applying an average cutting force of 1180 kg (2600 lb). The test setup is shown in Fig. 4.1. The last set of cutters made 112 cuts without appreciable dulling with the shroud rotating at

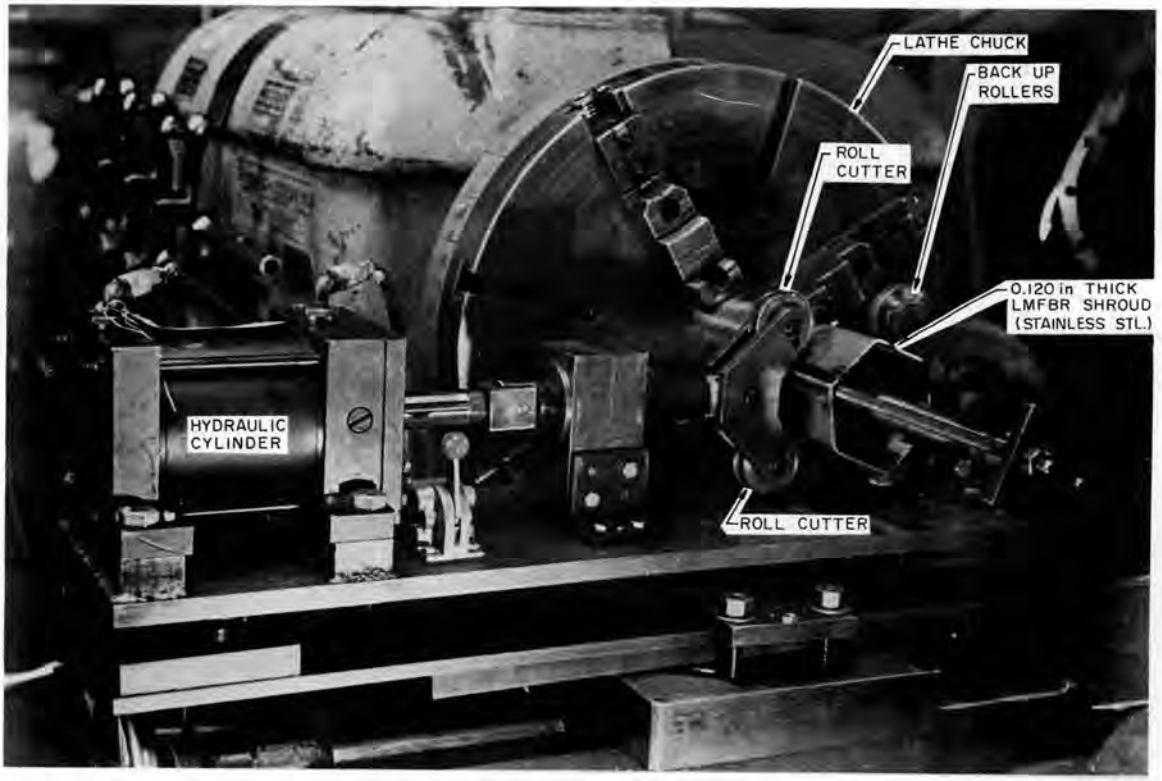

Fig. 4.1. Test setup – general assembly.

20 rpm. A detailed summary of test results are presented in a G+W report *Technical Report on Test of Roller Cutter* (ORNL/SUB-4362-10), April 21, 1977. Some additional testing is planned using 18-cm-(7-in.)-diam roll cutters, the next largest commercial size available.

Rotary shearing (machining). Recently, a second test of rotary shearing or machining of dummy LMFBR fuel was made at the G+W Folcraft 2 facility. The results were very poor for shrouded fuel and only fair for unshrouded fuel. These results are similar in nature to the two test series performed with a milling machine at the Valeron Corporation in Detroit, Michigan. Basically, when the shroud is severed by a cutter the shroud segment appears to act as a shear blade instead of the cutter segment acting as a true cutter. Clogging of the cutter teeth the first time around eliminated any change of good cutting the second time around. The machining program has been dropped from further consideration as an alternative to shearing. The equipment used in these tests is shown in Figs. 4.2 and 4.3.

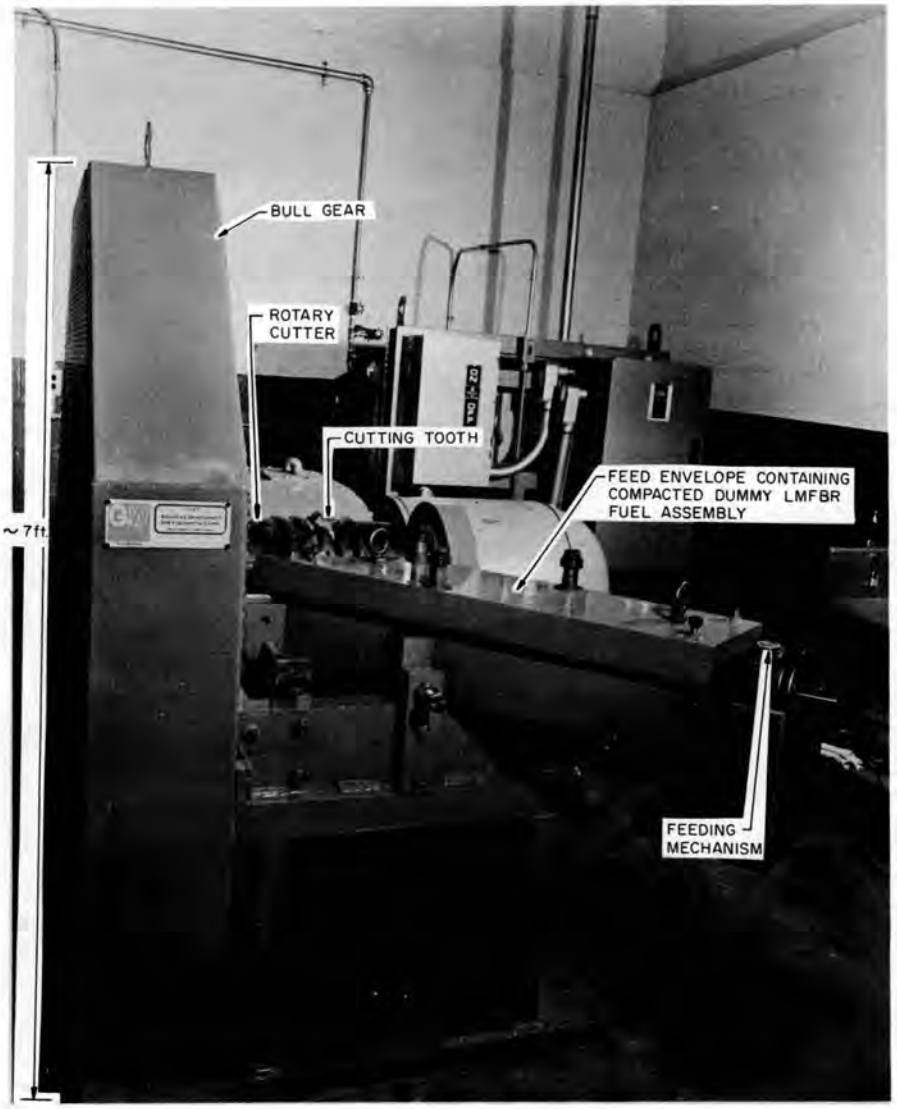

Fig. 4.2. Rotary machining (shearing) rig; view A.

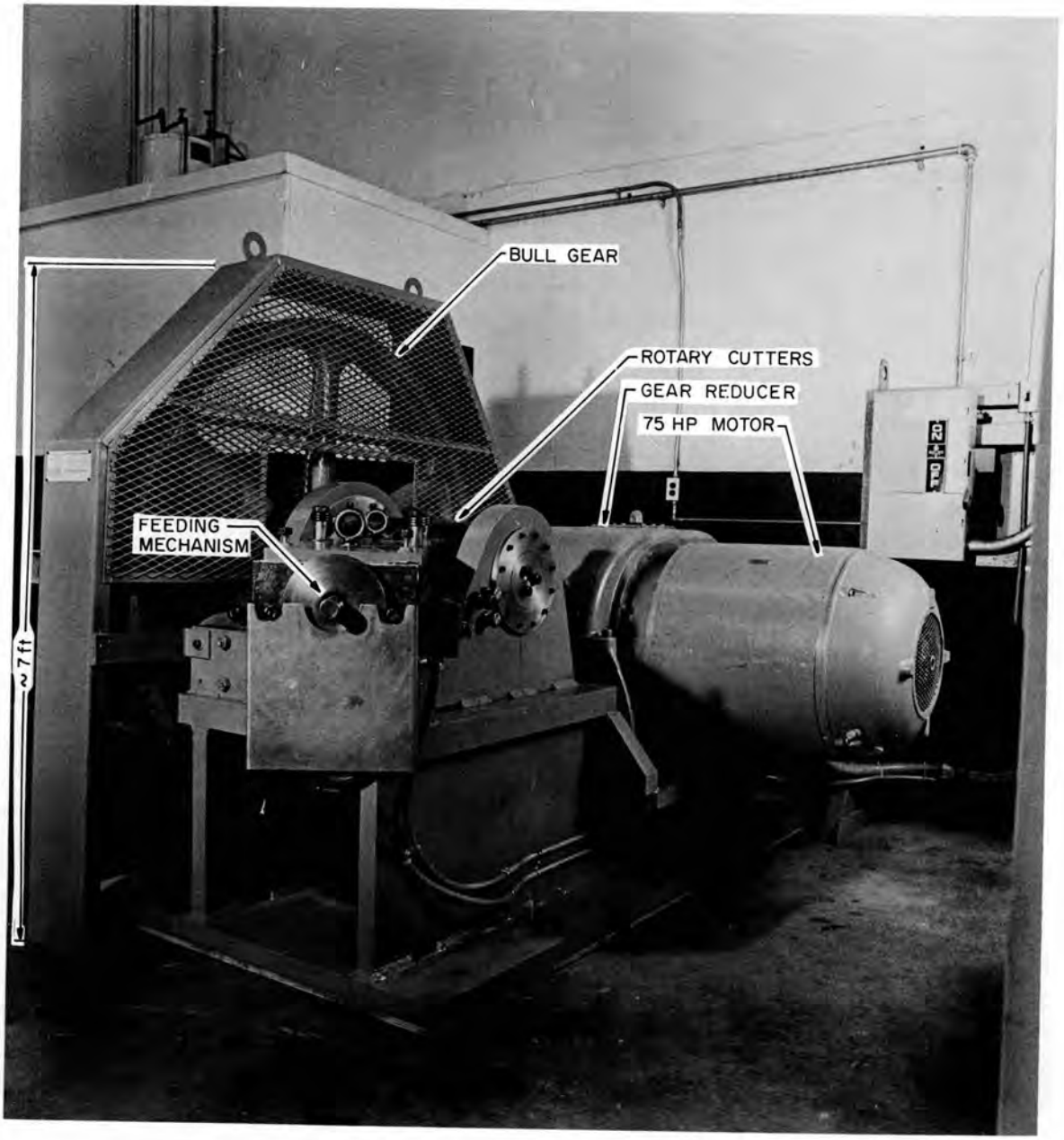

Fig. 4.3. Rotary machining (shearing) rig; view B.

Disassembly. The detail design of the disassembly machine to interface with the ORNL straight-sided shear has progressed very slowly (~30% complete). The completion date is now projected for mid-August. Part of the delay is due to a lack of manpower to accomplish the detail design, and the balance of the delay is due to the complexity of the job.

The schedule for completion of the one-fourth-scale model of the disassembly machine has slipped seriously. The model is now promised for mid-June, which is a delay of about eight weeks. The major problem is that the model proved more complicated than originally estimated.

Gulf + Western is proceeding with the plan to use a Modicon 384 programmable logic controller as the basic control device for the disassembly machine. Communication between ORNL

and G+W has been concerned with the definition of sensor elements for control needs, the requirements for experimental data recovery, and the shear and computer interface.

4.2.2 Disassembly and cutting—ORNL program
C. W. Watson, B. S. Weil, and M. E. Clifton

Experimental work this quarter has included testing a new plasma torch design at Florence, South Carolina, shredding tests at Tualatin, Oregon, and electric-arc sawing tests at Ukiah, California. The shearing task has experienced several setbacks in the modification and field installation of new equipment components for the 250-ton shear. Errors in the dimensions of replacement parts have contributed to the delays. Surveying crews have taken measurements of the shear area in preparation for the future installation of the disassembly machine; meanwhile, reliable as-built reference drawings of the shear are being prepared.

ORNL shearing. Modifications to the ORNL shear casting are complete, and reference, as-built drawings of the shear are being made. The ORNL Civil Enginering Department is preparing a shear area drawing to be used for the integration of future mechanical equipment with the existing shear. Benchmark monuments are being anchored to the floor as permanent reference points in the area.

All new equipment for the mechanical head-end has been installed (Fig. 4.4), and the shear is being wired to the newly fabricated control system.

A new optical periscope for the closed-circuit TV system was built and adapted to the new compound ram. This new periscope provides direct optical viewing of the shearing operation and also playback capability via a video tape recorder.

A new tooling design, which is a spin-off of the uniform slice technique, has been fabricated (Fig. 4.5). The design provides the best features of both dogbone and M-shaped compaction tools. The concept was developed to provide a ductile product comprised of hulls, wire, and one piece of shroud with a predictable size and shape. The embrittled product to be produced with the design will contain many shroud fragments; however, the design should prevent the uncontrolled cracking that commonly occurs with the compaction of fuel into the dogbone shape. Modifications to the new 200-ton compactor interrupted the preliminary tests of this tooling design. The design changes were necessary to prevent interference between the compactor die and the moving shear blade while the shear is under load. Testing of all the new shear tooling and the control system will begin early next quarter.

Alligator shear. A customized model 45H Hill-Acme alligator shear has been ordered and is scheduled to be received July 1, 1977. This unit will permit tests to be made that can be compared with the results of tests using the ORNL Birdsboro shear on LMFBR dummy fuel.

Tooling for the modified alligator shear, now being scheduled for fabrication in ORNL shops, was a joint design effort between G+W and the UCC-ND Experimental Engineering Design Section.

Subassembly cutting

Plasma torch. A new PCM 250 plasma torch was tested at Union Carbide Linde in Florence, South Carolina. The PCM-250 plasma torch cutting machine was coupled to the plasma torch

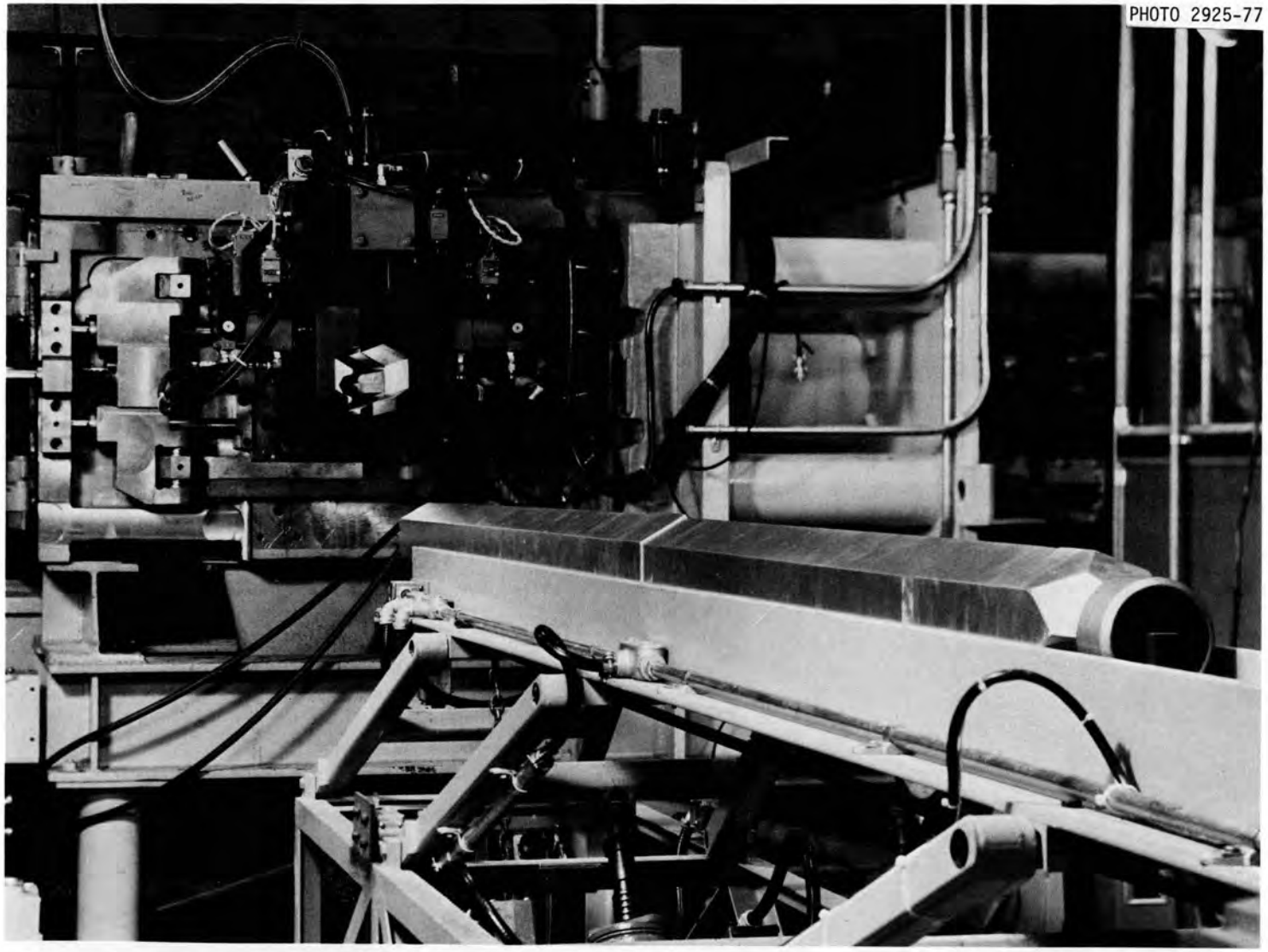

Fig. 4.4. Equipment for the mechanical head-end; the new fuel positioner is shown in the down position, whereas the black feed and withdraw mechanism is shown ready for operation.

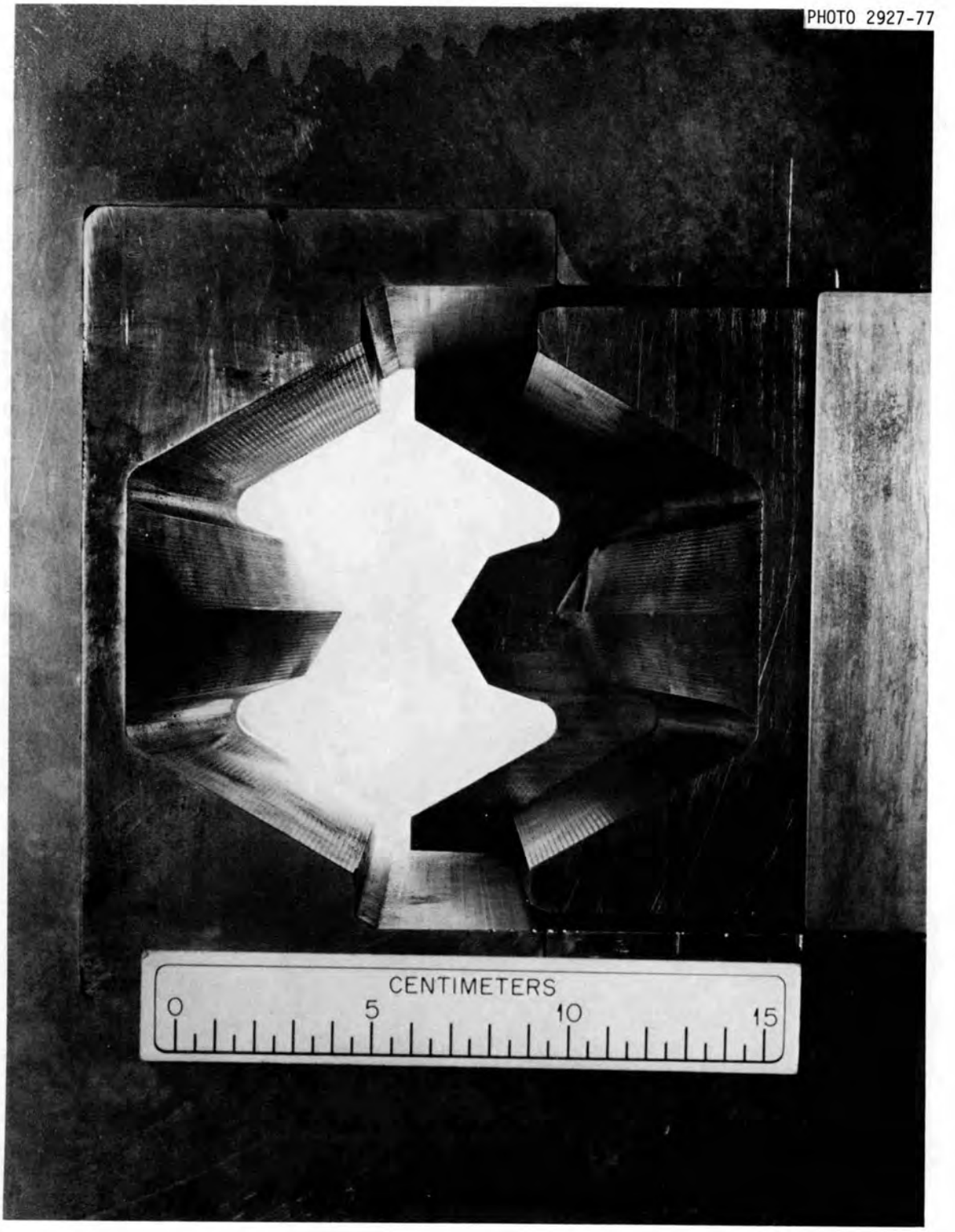

Fig. 4.5. New design V tooling shown installed in the shear.

cropping equipment used previously with a PT-7 plasma torch (see Fig. 4.6). The new torch incorporates the latest controlled power supply technology. This power supply produces a constant power level at the cut while varying the arc length to adjust for an irregular surface. The torch is capable of cutting a thickness of metal at a much lower input power than conventional units. A unit is being purchased for additional in-house tests, and it is likely that this unit will be mounted to the G+W disassembly machine.

Electric-arc saw cutting demonstration. Electric-arc saw cropping of LMFBR fuel is being investigated as a backup method to the plasma-arc torch and mechanical roll cutters. In time, all three methods will be installed and evaluated on the disassembly machine.

Recently, demonstration cutting tests were made on dummy LMFBR sections at Retech Inc., Ukiah, California. The equipment consisted of a 2500-A, 100-V dc power source owned by ORNL and a rebuilt electric-arc saw. (The original saw was designed and fabricated by Max P. Schlienger Inc., now Retech Inc., and was rebuilt with ORNL supplied funds.) The cuts were made remotely in air and under water.

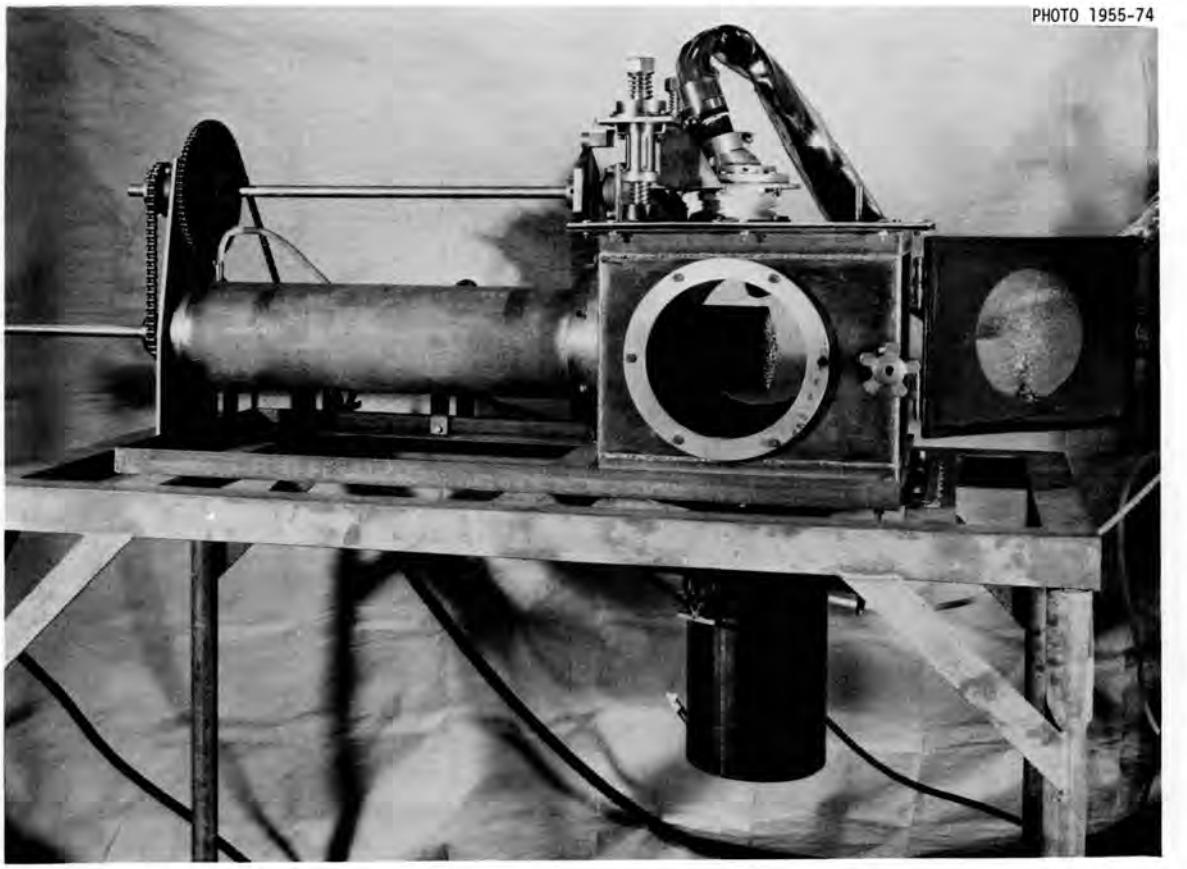

Fig. 4.6. Fuel cropping equipment used for testing the PCM-250 at Florence, S.C.

Successful demonstration cuts were made on the following kinds of dummy LMFBR subassembly sections:

1. empty LMFBR stainless steel shroud 0.3 cm (0.120 in.) thick,
2. embrittled (less than 1% elongation) stainless steel shroud as in 1 above,
3. ductile shroud within a shroud with 0.8 mm (0.03 in.) clearance,
4. shrouded wire-wrapped empty fuel rods,
5. shrouded wire fuel rods filled with springs,
6. shrouded wire-wrapped solid stainless steel fuel rods 0.63 cm (0.25 in.) in diameter,
7. an LWR assembly comprised of 17 × 17 Zircaloy-4 empty fuel tubes 0.95 cm (0.374 in.) OD cut in water and air.

The carbon steel saw blade 76 cm (30 in.) in diameter by 0.25 cm (0.1 in.) thick was operated at 1000 rpm, 25 V, and 1000 A. The kerf width underwater is 0.28 cm (0.11 in.) and is about 0.63 cm (0.25 in.) for an air cut. All water cuts were acceptable and accomplished in 7 to 25 sec, showing little or no sign of rewelding. In some cases, however, side arcing prevented completion of the cut on the first try. The 2500-A power source would "kick out" when side arcing of up to 3000 A would occur. The manufacturer plans to alter the source to make it "stiffer" and not as sensitive to the ampere surges or spikes. It is now obvious, however, that Retech underdesigned the power unit and that it should have been at least 5000 to 7500 A.

The Zircaloy dummy PWR fuel was easily cut with the electric-arc saw operating under water. However, when the cut was made in air the dummy subassembly ignited and began to burn at a rapidly increasing rate. The burning assembly was easily extinguished by flooding it with water. No explosion or eruptions occurred as the flooding was completed.

G+W is processing the cutting data and cut specimens at this time and a detailed report is in preparation.

Shredding as an alternative to shearing. A shredding machine used in the reclamation of tires, wet-cell batteries, radiators, beer cans, etc., was evaluated at Saturn Manufacturing Company, Tualatin, Oregon, as an alternative to a shear for fragmenting LMFBR fuel and as a method for disposal of stainless steel scrap. Typical shredding cutters are shown in Fig. 4.7. The tests made with a variety of dummy LMFBR fuel sections were very disappointing; therefore, this type of unit was eliminated from further consideration. In fact, the performance of the unit was so unsatisfactory that its applicability as a contender for shredding LWR Zircaloy-clad fuels is questionable. To resolve the issue, an ORNL/Savannah River Laboratory (SRL) test is planned during the coming quarter.

Prototype fuel. The radial blanket pellet sorter was delivered and checked out this quarter; part counters were installed in both pellet sorters for inventory control. The fuel rod wire-wrap machine has been designed, and fabrication bids have been extended. Long-lead-time prototype fuel materials have been ordered for development work, and a computer-based inventory system is being set up to help in future prototype fuel requirement estimates. The pellet loader machine is in the final design stages and should be ready for review and comment during the next report period.

ORNL DWG 77-5988

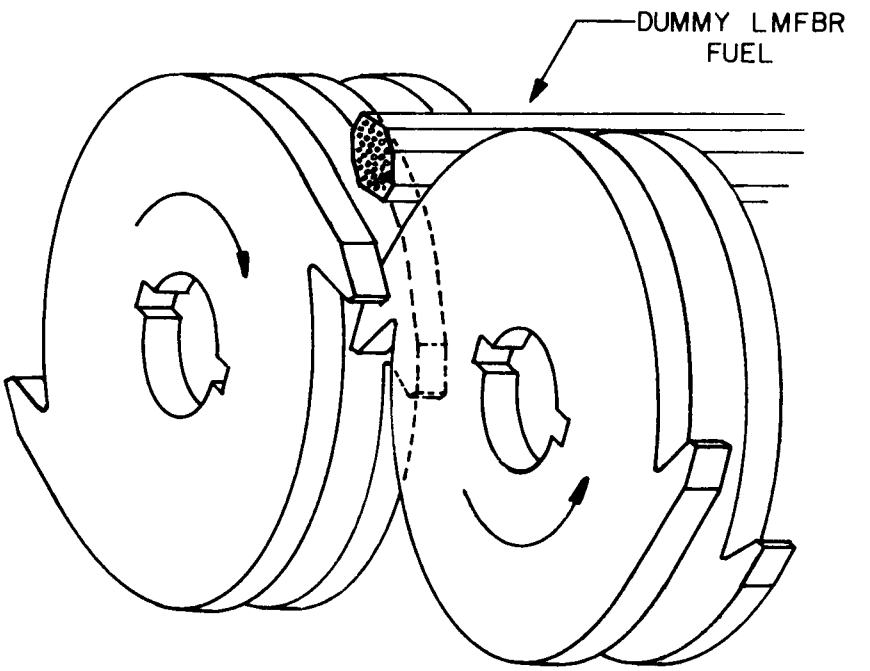

Fig. 4.7 Typical shredding cutters.

Instrumentation and controls

W. R. Hamel, N. C. Bradley, W. F. Johnson, J. M. Jansen, D. D. McCue, G. N. Miller, A. A. Shourbaji, and R. M. Tate

Shear instrumentation and control. The control panel and instrumentation package has grown from one rack to three. This growth is largely attributable to the consolidation of auxiliary instrumentation and the inclusion of control equipment for the temporary fuel loader. Field wiring was installed to incorporate a central junction box to facilitate anticipated relocations of major items of control equipment. A second programmable logic controller (PLC) was included to handle any required program overflow as well as to act as a shear simulator for program debugging and modifications. It is expected that the new control system will be in full operation by the end of this quarter.

Data acquisition computer for ORNL shear. Difficulties have been encountered with the memory expansion and magnetic tape additions to the PDP-11/40. Efforts are being made to resolve the problems satisfactorily. The digital input system is overdue but should be received soon. Software efforts have been concentrated on the development of a driver to handle the digital input system that would be compatible with the RSX11M version 3 operating system. Following several discussions with Purchasing, it now appears that an order may be issued to the vendor selected to produce the Analog I/O system.

Shear blade analyzer. Bids have been received from three vendors for proposals to build pneumatic- or fluidic-blade integrity measurement sensors. The bids were reviewed and a contract was let for the purchase of a phase 1 minimum test system, consisting of two chnnels of digital indication and one channel of analog measurement.

Multirod Shear instrumentation. The control system design is complete. The instrument control panel is being fabricated and will be complete by early July. The PLC program has been written and will be tested when fabrication is completed.

Shear dust particle size analyzer. A control system has been designed and fabricated for a dust-sample analyzer. This system will allow sequential sampling of dust from the shear cavity and from six individual filters. This data will provide a time-related dust analysis for the shearing operation.

4.2.3 Dissolution

J. Q. Kirkman and J. P. Drago

Component development effort in the dissolution area is directed toward designing, constructing, and testing a 0.5-metric ton/day, pilot-plant-scale dissolver system. This unit consists of a remotely maintainable rotary dissolver integrated with the support equipment necessary to produce a functional dissolution system.

Prototypical rotary dissolver. Fabrication work on the pilot-plant-scale rotary dissolver, initiated in January 1977, continued throughout the report period. Work is progressing on schedule, and the dissolver should be completed in August 1977.

Figure 4.8 is a cut-away isometric drawing of the dissolver presently being fabricated. The unit is approximately 6 m (19 ft) in overall length, 1.2 m (4 ft) wide, and about 1.6 m (5 ft) in height from bedplate to shroud top.

Major emphasis has been placed on completing the fabrication and assembly of the 75-cm-diam (30-in.) cylindrical dissolver drum. Figure 4.9 shows the drum positioned for automatic welding, with eight of the nine stages completed. The taped-over openings in each stage are circular inspection ports. The drum assembly procedure has consisted of welding the drum cylindrical shells and drum internals in a fixed sequence of steps beginning at the solids feed-end of the drum. With this procedure, each stage is entirely completed before assembly of the next stage begins. Figure 4.10 gives a view of the eight acid transfer ducts and the circular bulkhead of the solids-rinsing stage (final stage) of the dissolver. The cylindrical shell for this stage is not in place in this view. The acid transfer ducts are unique to the final dissolver stage and function essentially to bypass strong acid feed around the rinsing stage. The circular bulkhead is typical of the piece used to separate each stage of the dissolver from adjoining stages. The large semicircular opening in the bulkhead is connected to the conical transfer duct in the previous stage and provides for solids transfer between stages. The circumferential row of slots in the bulkhead establishes the liquid dissolvent flowpath between stages and will be countercurrent to the solids flow. The radial location of the bulkhead slots maintains an approximate 10-cm (4-in.) liquid depth in each dissolver stage. Figure 4.11 shows the completed nine-stage drum assembly; the overall length is approximately 2.4 m (8 ft). Work is under way to assemble the two bearing rings that position the drum on the roller supports and to attach the drum-end flange that supports the main gear ring.

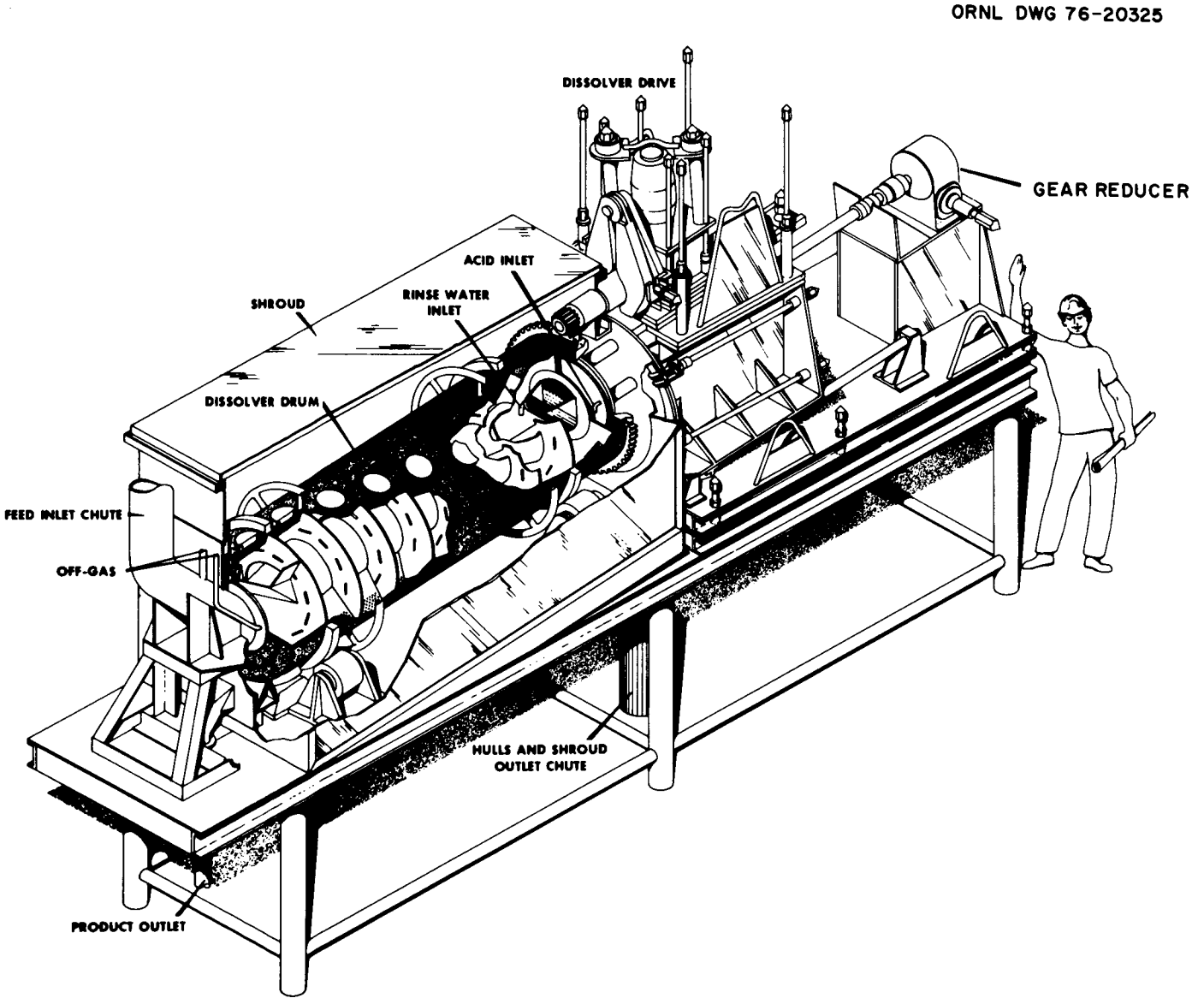

Fig. 4.8. Dissolver.

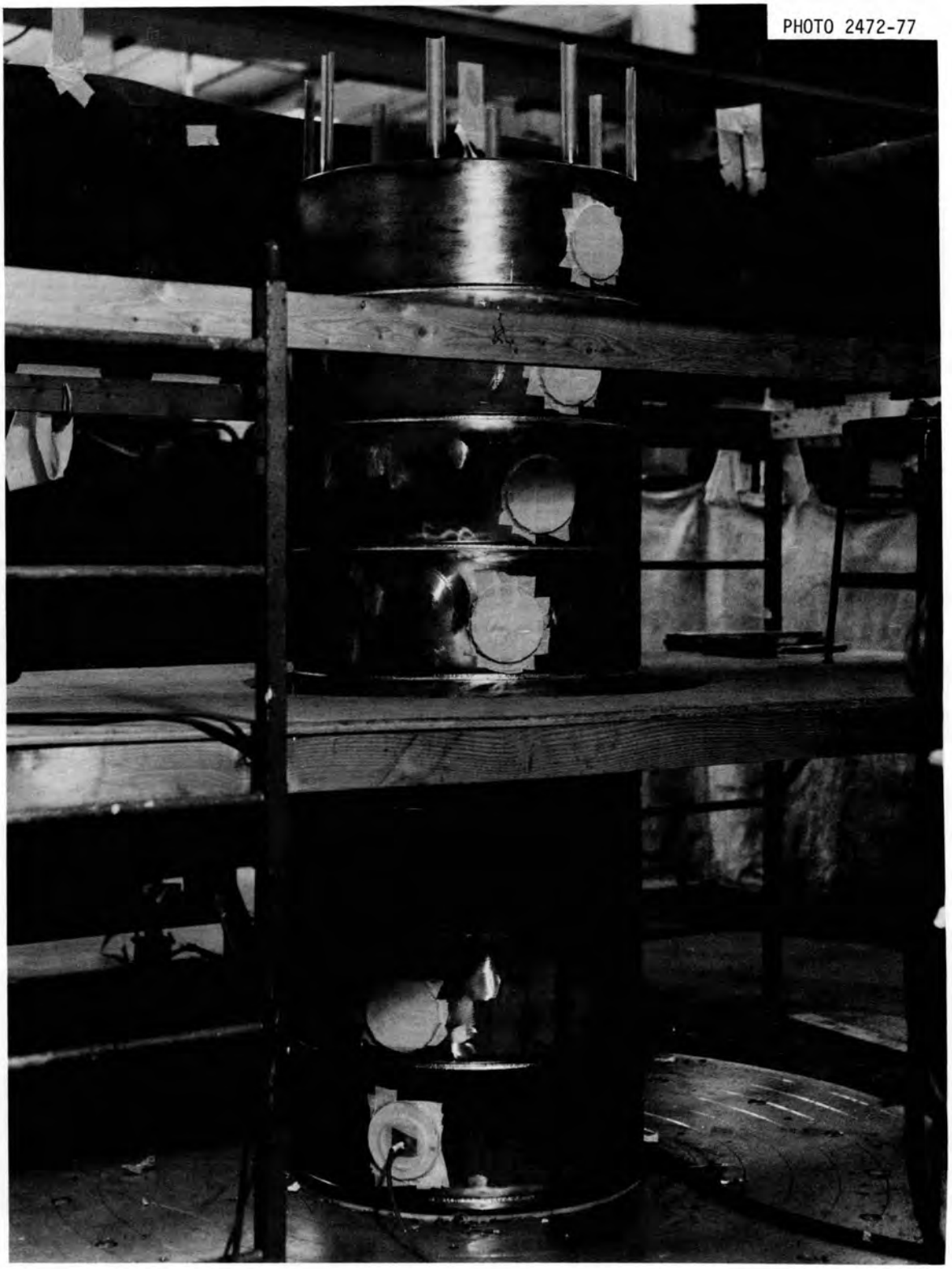

Fig. 4.9. Dissolver drum positioned for welding.

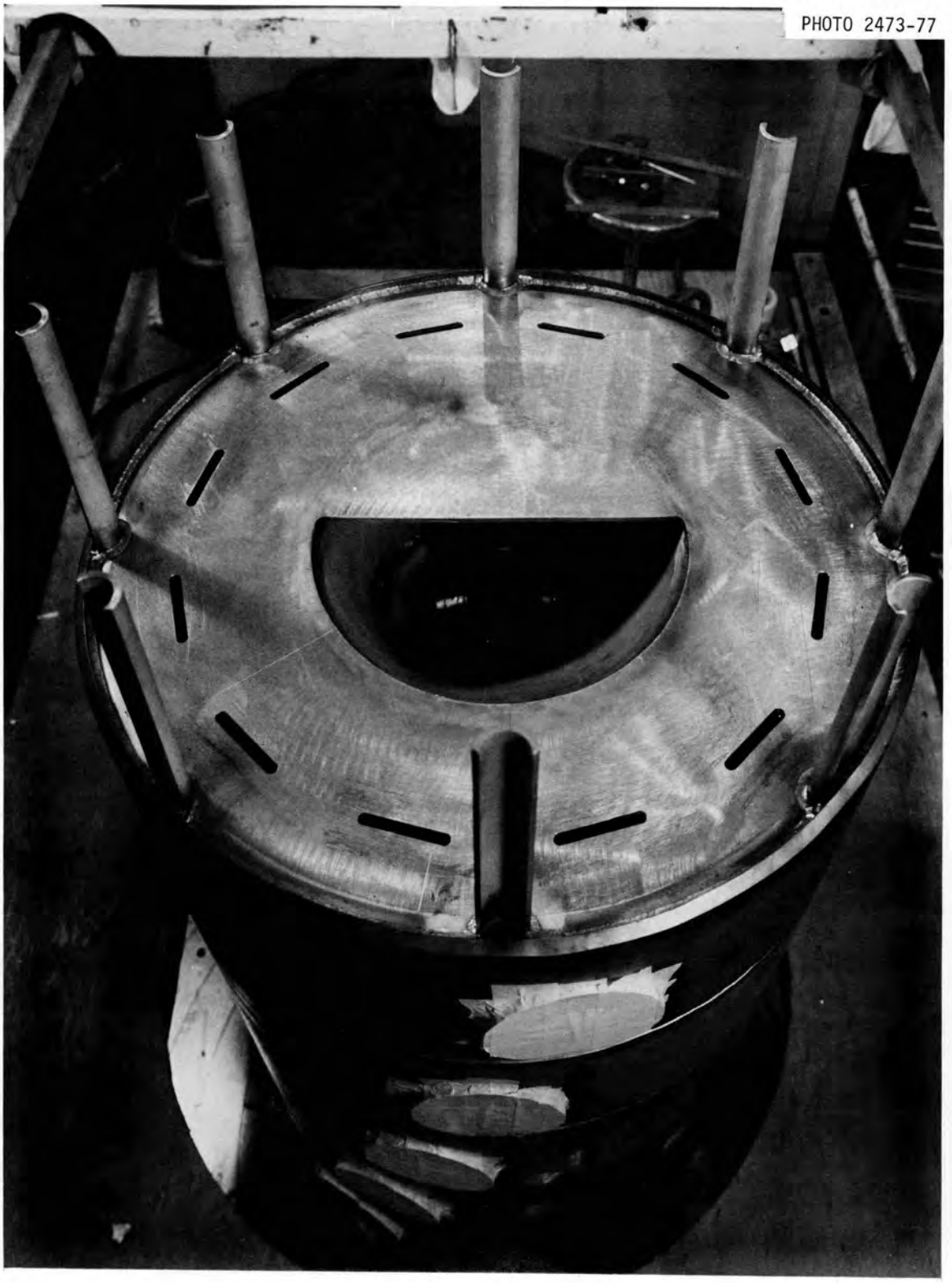

Fig. 4.10. Acid transfer ducts and circular bulkhead of the solids-rinsing stage.

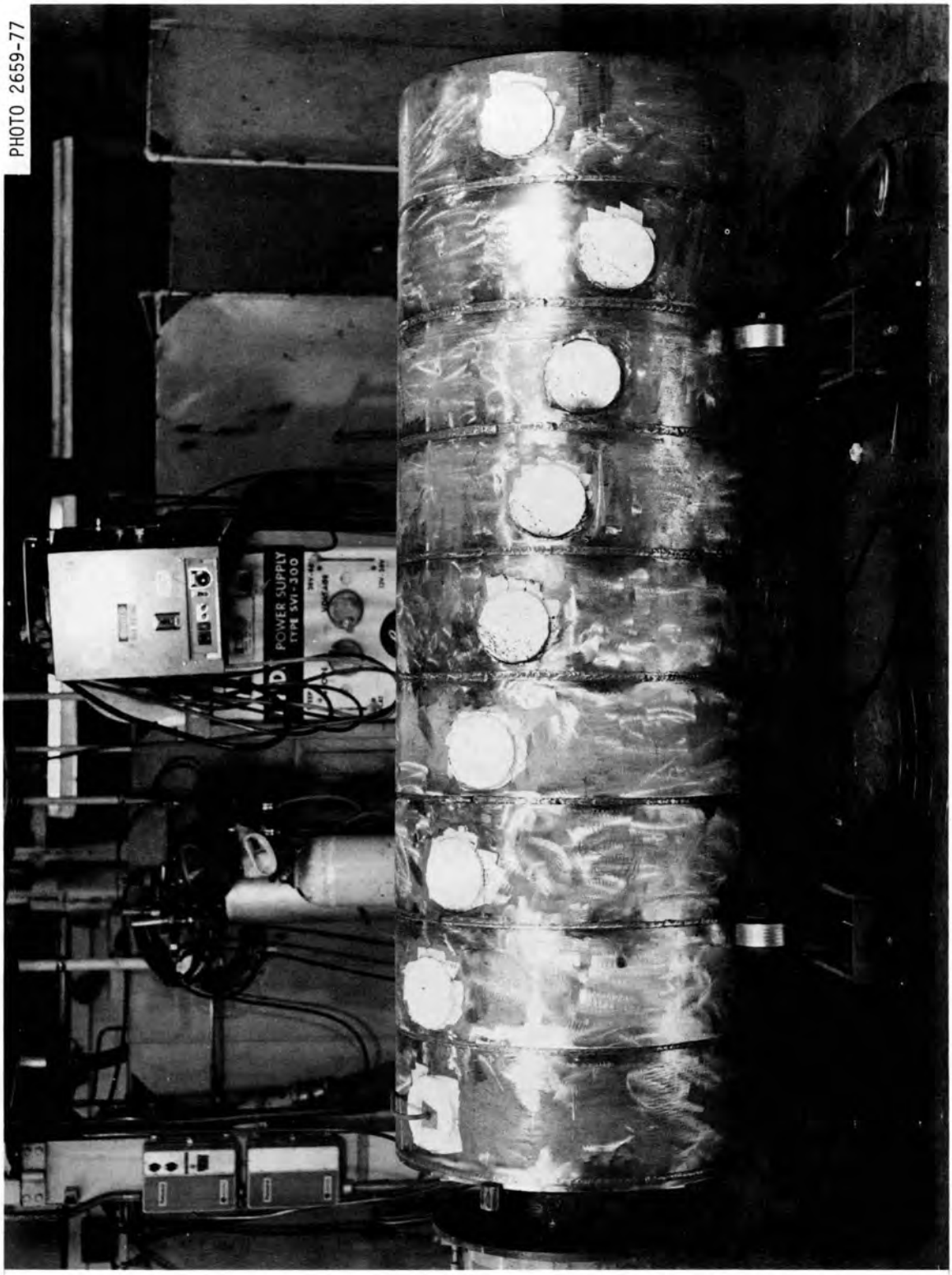

Fig. 4.11. Nine-stage dissolver drum.

A variety of machined-parts work and structural-fabrication work has been completed in parallel with the drum assembly effort.

Dissolver support system and process equipment. Figure 4.12 is a flowsheet showing the support equipment associated with the rotary dissolver. This system breaks down naturally into a set of functional subsystems necessary to provide dissolver off-gas scrubbing, recovered acid recycle, liquid dissolvent additions, shroud steam purge, product collection and handling, and solids feeding.

Accomplishments during this report period included completion of the system installation package and delivery of several process components.

The system installation package is essentially a set of design drawings defining the detailed work necessary to produce an integrated, operational dissolution system. The package contains an equipment arrangement drawing, a detailed piping drawing, and an electrical and instrumentation drawing. One June 1, 1977, the installation drawings were certified for construction and transmitted to the cost-plus-fixed-fee contractor for review and estimate. Installation work should start in July 1977.

Procurement-fabrication work associated with accumulating the process components needed in the dissolver support systems has proceeded through both ORNL shops and outside vendors. ORNL-fabricated components completed this period include the NO_x scrubber bottoms hold tank (Fig. 4.13), the iodine stripper, the recovered acid cooler, the recovered acid head tank, the acid flow control loop, and process steam jets. ORNL fabrication work continued on the liquid product diversion valve and the hulls collection equipment. The feed isolation valves, designed to segregate the atmosphere of the dissolver from that in the voloxidizer, were started June 1, 1977.

Delivery of some process components supplied by commercial vendors has slipped approximately two to three weeks from previous estimates. The NO_x scrubber column, stainless steel process tanks, stainless-steel-jacketed tanks, and process heat exchangers are now expected to arrive during July 1977. This delivery schedule should not adversely affect the installation work. Process pumps and a majority of the process piping, valves, and fittings were delivered on schedule this period.

Instrumentation and controls (W. R. Hamel, W. F. Johnson, and G. N. Miller). The fabrication drawings for the instrumentation package for the prototype dissolver system were completed during this period and have been distributed for construction. All the instrumentation components for this project have been specified and placed on order. Some have already been received, have had their calibrations verified, have been given Instrumentation and Controls numbers for the quality assurance records, and have been delivered to the job sites. Construction of the panelboard is under way in the panel shop and will accelerate as more of the instrumentation is received.

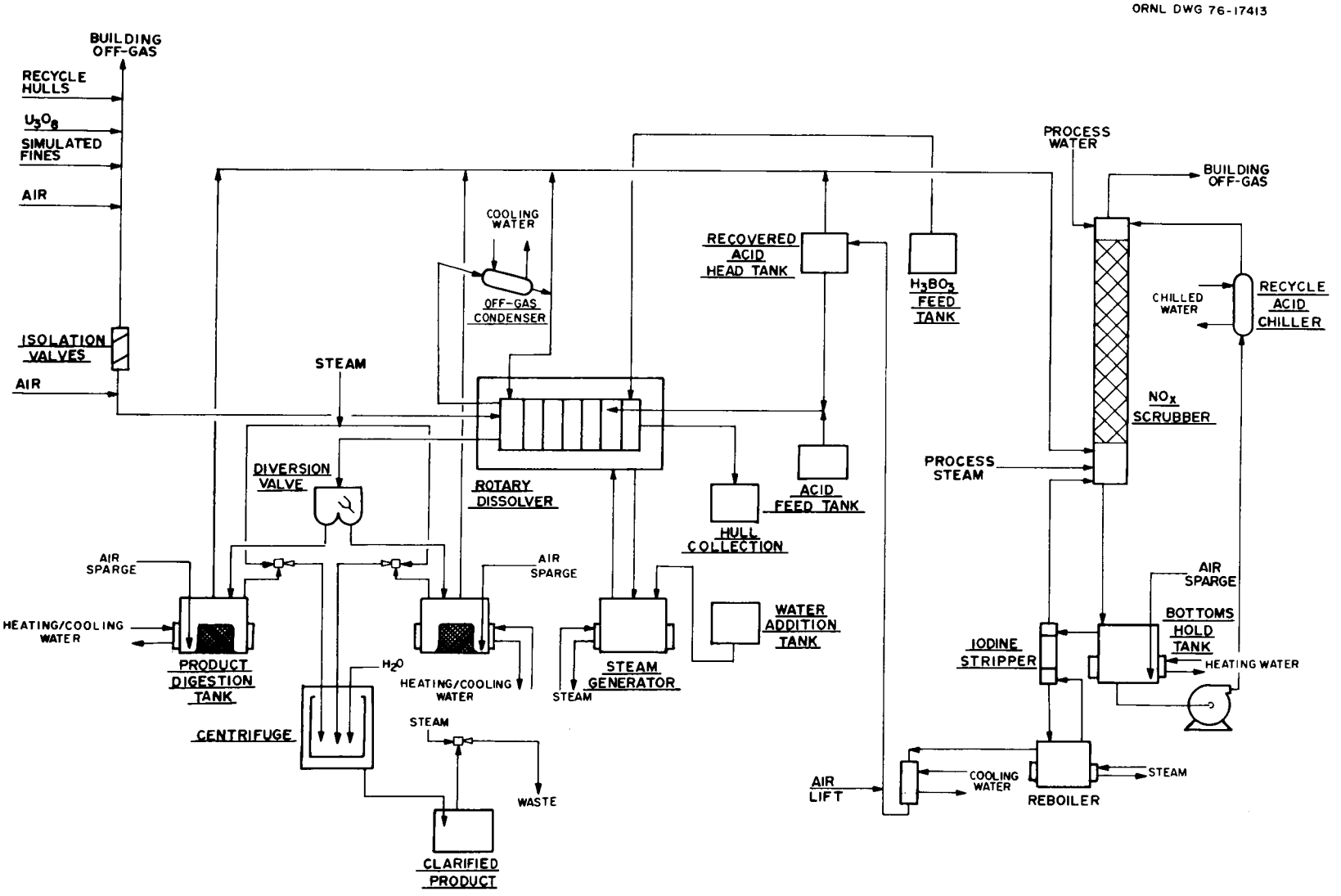

Fig. 4.12. Dissolver equipment flowsheet.

Fig. 4.13. NO_x scrubber bottoms hold tank.

4.3 SYSTEMS DEVELOPMENT

N. R. Grant

This functional area has been added to consolidate the effort in tasks that involve a series of major components that are not directly process related and have little involvement in the research and development or engineering research areas. However, Systems Development tasks are closely associated with the HEF, and a constant interface with the HEF conceptual design group is maintained. The goals in Systems Development are the same as in Component Development, namely, the design, fabrication, and operation of full-scale, remotely operable equipment.

The tasks assigned to this area are the IET facility, the receiving and storage systems, the remote maintenance systems, the waste handling systems, and the decontamination systems. One additional task has been added to Systems Development, that is, the procurement of depleted uranium fuel to be used for tests in Component Development and Systems Development equipment. All tasks except decontamination have reportable progress.

4.3.1 Integrated Equipment Test (IET) Facility
J. M. Chandler

The IET task consists of the design and construction of modifications and additions to the AFRP complex (7600 area) to provide an experimental engineering laboratory wherein systems testing can be performed or process equipment streams can be established, and where remote handling and maintenance procedures can be developed for reprocessing equipment. The task is comprised of three basic phases. The first of these establishes an area where specific process equipment pieces that have evolved from development efforts can be joined together and operated as an integrated system. This portion of the IET facility has been designated as the Integrated Process Demonstration (IPD). The second phase of the task consists of the construction of special facilities where testing of the remote operation and maintenance capabilities of process equipment can be performed. This area has been named the Remote Operation and Maintenance Demonstration (ROMD) and consists of a process cell and transfer area equipped with simulated shielding, viewing systems, manipulators, cranes, and airlock arrangements. The third phase of the task is the General Plant Facility (GPF), comprised of structural modifications, utility system expansions, and construction of auxiliary facilities, all of which are required to support the IPD and ROMD experimental programs.

IET Title I design by UCC-ND Engineering has continued, with progress being made in all areas of effort. However, progress is somewhat behind schedule. Delays have resulted in part from (1) scope changes, (2) delay of flowsheet information input from the HEF conceptual design, and (3) underestimating the time to complete the work as defined. A revised schedule that reflects the present design status and indicates the effort required to complete Title I design by October 1977 has been prepared.

Progress was made in the preparation of process flowsheets, including material balance flowsheets. About 20% of the flowsheet work is complete. The IET Project Management Plan (X-OE-39) and the Internal Management Plan were issued and distributed to the project users and to ERDA. The Project Management Plan describes primarily the interrelations between ERDA and the UCC-ND Engineering Division concerning the IET project, and the Internal Management Plan gives the relationship between UCC-ND Engineering and the AFRP–IET project. The drawing list [Engineering Design Document Master Inventory (IA)] was completed and documented in a form suitable for computer coverage of the design progress. The draft design criteria document was completed and is being used for Title I design. The document will be rearranged to be consistent in format with the IET work breakdown structure. An environmental impact assessment was prepared and submitted with the Schedule 44 data sheet. The assessment indicated that the potential environmental impact from IET task activities will be minimal and that the impact presents no known potential conflicts with state, regional, or local programs or regulations. Preparation of the quality assurance plan for IET is in progress.

Work was continued on the design of the IET facility. Information regarding configuration and requirements for transfer locks supplied by the HEF designers is being used as criteria to design IET equipment. Title I design of the ROMD facility was started using criteria provided on transfer devices. The transfer system under consideration provides for the simultaneous transfer and decontamination of equipment. The size of these cleaner–transfer devices will accommodate a cylindrical object 6 ft in diameter and 10 ft in length.

The ROMD handling and viewing requirements are being studied and evaluated preparatory to the design of the IET-funded portion of this system.

The IET Title I reference flowsheet was modified slightly (in comparison with that used in the conceptual design) to simulate more accurately the reference HEF flowsheet. For example, two, not three, solvent extraction contactors will be received from the component development task. Also, the new flowsheets will have nitrogen oxide and Iodox gas treatment equipment as part of the dissolver circuit.

The reference product conversion flowsheet selected this month is a chemical coprecipitation method using hydrogen peroxide to precipitate uranium and plutonium from a nitrate solution that contains a mixture of 75% uranium and 25% plutonium.

Emergency power requirement for essential IET safety equipment was determined to be 150 kVA. This is about half that specified in the conceptual design report. The decrease in emergency power resulted when the size of the largest essential electrical motor decreased in size from 75 to 20 hp.

4.3.2 Receiving and storage

S. A. Meacham [Westinghouse Advanced Reactors Division (WARD), Madison, Pennsylvania, on loan to ORNL]

The receiving and storage work plan has been divided into nine subtasks, including (1) system integration, (2) sodium removal equipment, (3) fuel transporter, (4) subassembly handling, (5) subassembly identification, (6) sodium removal process, (7) corrosion studies, (8) nondestructive assay, and (9) local instruments and control subsystems. The objective of each subtask, except 8 and 9, was described previously.[1] Subtask 8 has as its objective the development of a nondestructive assay device (NDA) to measure the fissile content of spent LMFBR fuel within an accuracy of 1 to 5%. The NDA device will be constructed, tested, and evaluated for use in the fuel receiving cell to confirm burnup estimates and to inventory fissile material. The data obtained will be fed into the fuel identification system and fuel handling system computer for overall inventory control.

Subtask 9 is responsible for developing a Local Instruments and Control Subsystem for the Fuel Receiving and Storage System (LICS-FRSS). The LICS will provide (1) an integrated control and information management capability required for the independent operation of the FRSS and (2) a suitable control and information management interface between the FRSS and the plant-wide supervisory management interface. This subtask will also provide engineering interfacing and design support for subtasks 4 (subassembly handling) and 5 (subassembly identification) to ensure compatibility between all FRSS instrumentation and control systems.

Systems integration

(A) *Cask receiving.* Several meetings were held with Sandia Laboratories to discuss and identify the areas of common interest and the potential interface requirements in the shipment of spent LMFBR fuel. Sandia has been designated by ERDA to provide the shipping cask(s) for the LMFBR program. The major impact on the receiving and storage task is the proposal to use sodium-filled canisters containing the spent fuel.

A functional diagram was prepared (Fig. 4.14), and the interfaces were discussed with the HEF and process groups. The following steps are being investigated to ensure system integration:

Cask receiving and inspection—preparation of the cask transport vehicle, including external radiation readings, heat shield removal, cleaning of cask exterior, and removal of cask tiedown.

ORNL DWG 77-5984

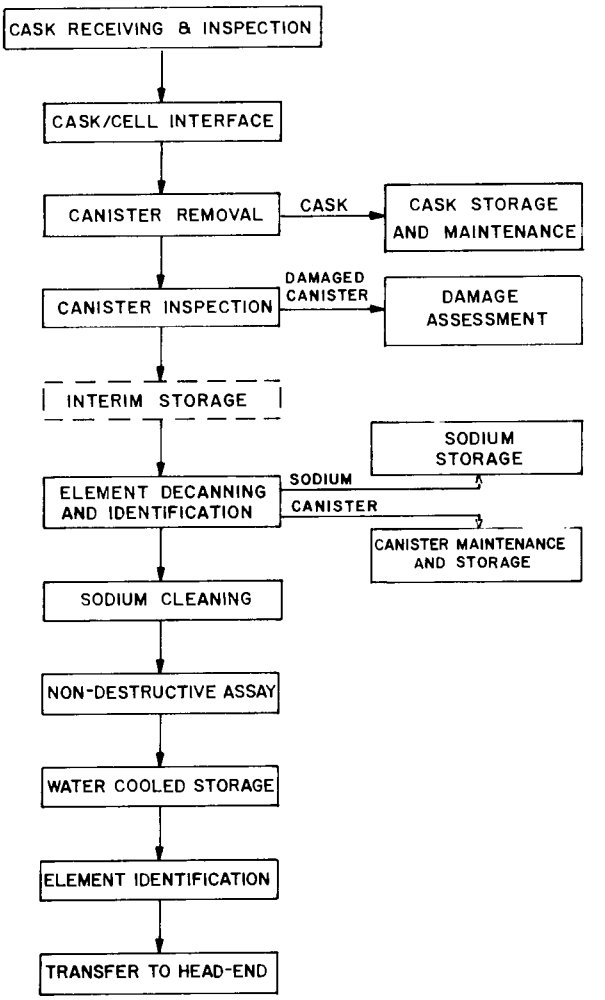

Fig. 4.14. Functional block diagram; impact of sodium-filled canisters.

Cask/cell interface—preparation of the cask for removal of its contents, including attaching the cask-lifting device, lifting of cask and loading on transfer device, atttaching cask/hot-cell interface adapter, transfer to unloading port, positioning cask to unloading port, sealing cask to unloading port, and verification of the seal.

Canister removal—removal of the canister from the cask, including opening cell port, removal of cask plug, attaching canister handling mechanism, removal of canister, replacing cask plug, closing cell port, transfer cask to cask storage and maintenance.

Canister inspection—determination of the physical integrity of the canister, including positioning of canister at inspection, visual inspection, and transfer of damaged canisters to damage assessment area.

Interim storage (tentative)—holdup area (short term) with inert gas cooling for 18 to 24 canisters prior to removal of fuel assemblies.

Element decanning and identification—removal of the fuel assembly from the canister and verification of identity, including placing canister in heating unit, opening canister, removal of fuel assembly, identification of fuel assembly, removal of sodium from canister, transfer of sodium to sodium storage, and transfer of canister to canister maintenance and storage.

Sodium cleaning—removal of residual sodium from fuel elements, including placing assembly in cleaning unit, application of cleaning procedure, and removal of assembly from cleaning unit.

Nondestructive assay—determination of the fissile content of a fuel assembly, including preparation of assay station, positioning of assembly, assay test, and removal of assembly.

Water-cooled storage—long-term storage of approximately 1000 spent fuel assemblies in a water-filled pool, including pool preparation and location assignment, assembly placement, location verification, and assembly removal.

Assembly identification—verification that the proper assembly has been removed from pool.

Transfer to head-end—delivery of the fuel assembly to the shear feeder.

(B) *Water feasibility study*. The deadline for the decision on the use of a water storage pool in the HEF conceptual design was July 1, 1977. A recommendation based on the corrosion study (subtask 7) was prepared stating that the data obtained to date indicate that water pool storage is a viable concept, providing the water chemistry is controlled within certain limits. The second phase of the water feasibility study will establish these limits.

(C) *Alternate media study*. A parallel study considering an alternate cooling medium for the storage of spent LMFBR fuel has been performed. Nitrogen was considered as the cooling medium for Clinch River Breeder Reactor (CRBR) and Prototype Large Breeder Reactor (PLBR) fuel assemblies; the thermal analysis was provided by R. A. Just of the UCC-ND Engineering Analysis group. Analyses were performed on:

1. the assembly exposed directly to a 40°C (105°F) nitrogen environment at steady state (steady state assumes loss of forced cooling but continued convection flow);
2. the assembly enclosed by a nitrogen-filled cask at steady state;
3. the assembly exposed directly to the ambient nitrogen environment on the outside of the shroud with (a) internal forced-convection cooling and (b) at steady state.

The steady-state shroud and center pin temperatures for the first two conditions are presented in Table 4.1.

For condition 3, heat transfer coefficients of 28 $Wm^{-2}\ K^{-1}$ (5 $Btu/hr^{-1}\ ft^{-2}\ °F^{-1}$) for CRBR and 45 $Wm^{-2}\ K^{-1}$ (8 $Btu\ hr^{-1}\ ft^{-2}\ °F^{-1}$) for PLBR were assumed. Calculations determined flow rates that would maintain the center-pin clad temperature below 650°C (1200°F) while using exit coolant temperatures ranging from 93 to 316°C (200 to 600°F). The results are presented in Fig. 4.15.

An analysis of the fuel assemblies was performed to predict the time–temperature history for condition 3 following a postulated loss-of-coolant accident. Initial conditions were established from the results of steady-state calculations for condition 3. The initial shroud temperature was assumed to be equal to the coolant temperature. The results of this analysis are presented in Table 4.2, with the variant of gas exit temperatures of 93, 204, and 316°C (200, 400, and 600°F) at the start of loss-of-flow.

Table 4.1. Steady-state results

Power level[a] (kW)	Days cooled	Center pin temperature				Shroud temperature			
		Configuration 1[b]		Configuration 2[c]		Configuration 1[b]		Configuration 2[c]	
		(°C)	(°F)	(°C)	(°F)	(°C)	(°F)	(°C)	(°F)
6.8	60	1058	(1937)	1085	(1985)	511	(952)	621	(1149)
5.8	90	1006	(1842)	1031	(1888)	477	(890)	583	(1081)
3.3	180	835	(1535)	857	(1575)	366	(691)	461	(862)
15	60	1223	(2234)	1257	(2295)	582	(1079)	727	(1340)

[a]For the CRBR assemblies, power levels of 3.3, 5.8, and 6.8 kW were considered. The PLBR assembly was analyzed for 15 kW only.

[b]For configuration 1, the fuel rod assembly is directly exposed to the ambient temperature.

[c]For configuration 2, the fuel rod assembly is surrounded by a transporter cask.

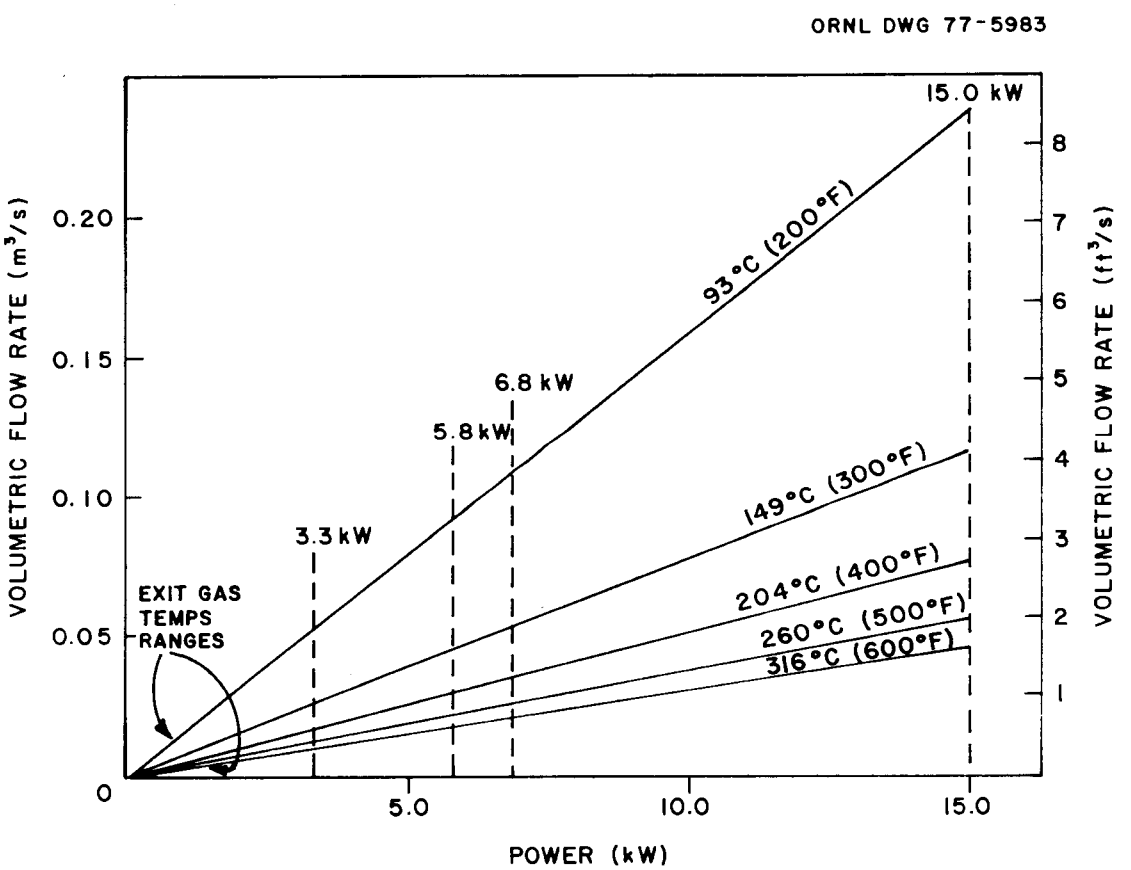

Fig. 4.15. Nitrogen flow rate vs assembly power level.

Table 4.2. Results for loss-of-cooling

Coolant temperature (°C)	Coolant temperature (°F)	650°C (1200°F) (min)[a]	980°C (1800°F) (min)[b]	Steady state (min)[c]
		CRBR Assemblies		
		Power level of 6.8 kW at 60 days		
93	(200)	26	59	
204	(400)	20	53	
316	(600)	14	46	
		Power level of 5.8 kW at 90 days		
93	(200)	31	86	
204	(400)	25	79	
316	(600)	17	71	
		Power level of 3.3 kW at 180 days		
93	(200)	61		145
204	(400)	49		133
316	(600)	36		118
		PLBR Assembly		
		Power level of 15 kW at 60 days		
93	(200)	31	56	
204	(400)	24	49	
316	(600)	18	42	

[a]Time required for center pin to reach 650°C.
[b]Time required for center pin to reach 980°C.
[c]Time required for center pin to reach 99% of steady-state temperature; applicable when the steady-state center-pin temperature is less than 180°C.

The conclusion reached in this study was that spent LMFBR fuel, up to 15 kW, can be maintained below 650°C (1200°F) with forced convection cooling with nitrogen at flow rates of 47 to 235 liters/sec (100 to 500 cfm).

Sodium removal equipment and fuel transporter. An order was initiated with Aerojet Manufacturing Company (AMCO) of Fullerton, California, to prepare a scoping study document for the sodium-removal system and the fuel transporter. The study, which has been completed, describes different methods to transport subassemblies, either one at a time or in a group, from the shipping cask to the sodium-removal station and then to the storage pool. Discussions have been held with AMCO personnel on the impact of sodium-filled canisters on the receipt and handling of spent fuel and on the fuel transporter. A follow-up CPFF contract is being placed to have AMCO prepare the conceptual design phases for the sodium-removal station and the fuel transporters.

Subassembly handling. A request for proposal for the fuel handling system has been written and has been circulated for comments prior to submittal to UCC-ND Contracts. Comments received are being incorporated into the final draft at this time.

Subassembly identification. A request for proposal for the fuel identification system has been written; comments have been incorporated and the request has been submitted to UCC-ND Contracts for issuance. Responses to the request for proposal are expected in late July, and initial work on the engineering study should begin in September 1977.

Corrosion program. The Westinghouse Advanced Reactor Division (WARD)–ORNL program ("The WARD–ORNL Fuel Reprocessing Work Program on Sodium Cleaning and Subsequent Corrosion of Sodium-Exposed Stainless Steel Underwater Pit Storage Conditions," ORNL Subcontract 7168, Westinghouse Electric Corporation) has as its objective the determination of the corrosion behavior of sodium-exposed stainless steels, with sodium-removal procedures and storage-water conditions as major variables.

Current program. All experimental work involved in the current corrosion program has been completed, and a topical report summarizing the results is being prepared. A draft of the report has been completed and is being reviewed.

Routine operation of the water baths containing sodium-exposed stainless steel specimens continued to the point where all specimens completed their exposure time as originally specified in the test matrix. No failures were observed on the corroded type 316 stainless steel specimens for water exposure periods of up to five months. However, seven failures were observed on type 304 stainless steel specimens. Six of the failures occurred in the high-chloride neutral bath, and one failure occurred in the high-chloride high-pH bath. Tables 4.3 and 4.4 are summaries of the water exposure histories of the specimens.

Table 4.3. Corroded type 316 stainless steel specimens exposed in water baths

Sodium removal methods	Test period (month)	Water bath[a]			
		1	2	3	4
Alcohol	1				
	2				
	3	1	9	8	23
Water vapor-argon (WVA)	1		13	11	10
	2		15	12	14
	3	24,26	25,29	28,30	27
Steam-argon (KNK)	1		2	4	6
	2		3	5	7
	3	21,22	16,17	19,20	18

[a]The number shown in each water bath is a specimen number. All specimens have completed their intended exposure without incident.

Table 4.4. Deposit-bearing type 304 stainless steel specimens exposed in water baths

Sodium removal methods	Test period (month)	Water bath[a]			
		1	2	3	4
Alcohol	1				
	2				
	3	11	9	12[f]	10
Water vapor-argon (WVA)	1		8	2[f]	5
	2	3,15	7	1[f]	6
	3	3,15	4,16	14[f],17[f]	13
Steam-argon (KNK)	1		23	20	18[f]
	2		24	22	19
	3	21,26	25,29	28,30[f]	27

[a]The number shown in each water bath is a specimen number. The superscript *f* indicates that the specimen had failed before reaching its intended exposure.

Massive intragranular carbide precipitation due to severe cold work prevented the type 316 stainless steel specimens from being sensitized during high-temperature sodium exposure, which, in turn, reduced the susceptibility of this material to intergranular attack during water exposure.

The chemical composition of the deposits resulting from sodium mass transfer on the type 304 stainless steel specimens was analyzed by x-ray fluorescent analysis. The results showed that chromium and its compounds preferentially deposited at the high-temperature [above 510°C (950°F)] region, whereas iron and its compounds deposited mainly at the low-temperature region. Similar temperature dependance of nickel and manganese was also observed. The effect of compositional variations of the sodium mass transfer deposits on the subsequent corrosion behavior of the type 304 stainless steel specimens has been analyzed.

Extension program. As part of an extension to the WARD–ORNL–AFR corrosion program, a total of one hundred twenty 20% cold-worked, type 316 stainless steel specimens are being sodium exposed for subsequent water corrosion studies. These specimens will provide additional data to enhance the statistical confidence of the results obtained in the recently completed investigation.

The scope of the extension program includes both corroded hot-leg specimens and deposit-bearing cold-leg specimens. The experimental plan involves the exposure of 60 cladding specimens to hot-leg conditions [370°C (700°F)] in the MTL-3 facility.

The test section assembly being used for both the hot- and cold-leg exposures consists of four parallel exposure legs containing 15 specimens each. Figure 4.16 is a configuration of the test section

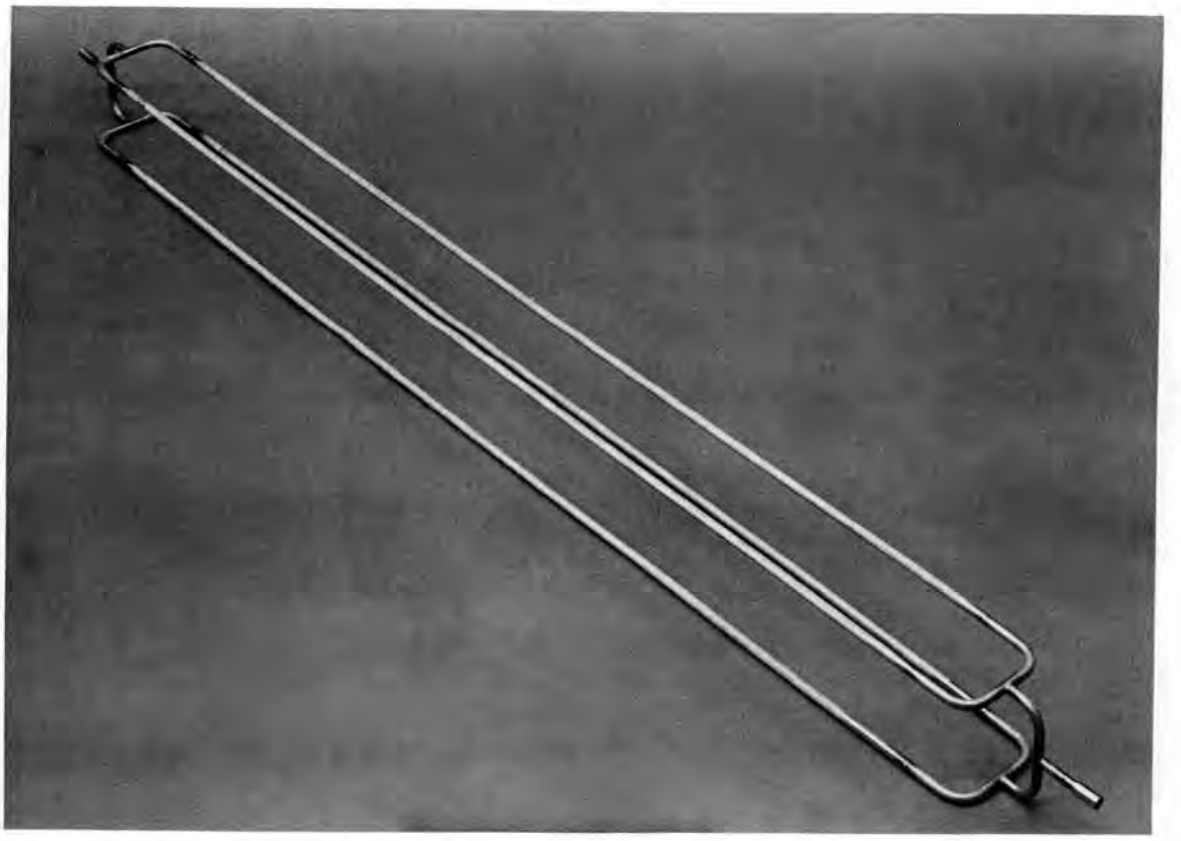

Fig. 4.16. Completed cladding exposure test assembly.

assembly. The 15 test specimens in each exposure leg are threaded together end-to-end to form a specimen stack (Fig. 4.17). Spacers are used to center the specimen stack within the exposure tubes. A total of six control specimens are also included in each exposure leg. The control specimens are located so that two each are at the inlet, at the mid-region, and at the outlet of each test leg. A typical test assembly (specimen, control specimen, and stack spacer) is shown in Fig. 4.18.

The hot-leg cladding specimens currently being sodium exposed [720° C (1325° F)] have a total accumulated exposure time of 1700 hr (as of June 10, 1977).

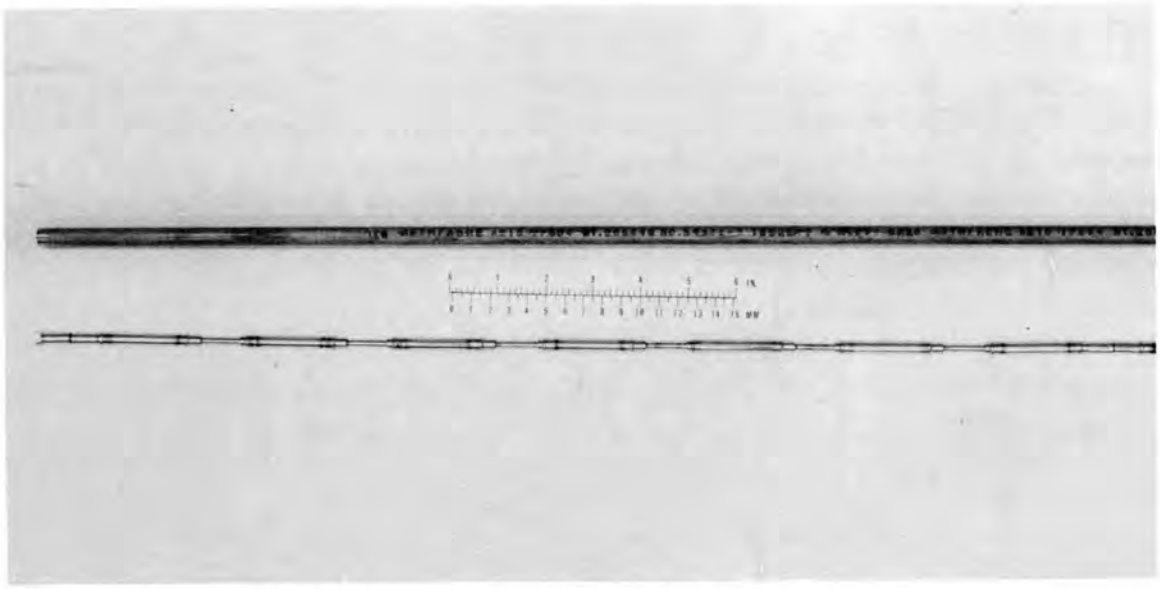

Fig. 4.17. Cladding exposure specimen stack and exposure tube.

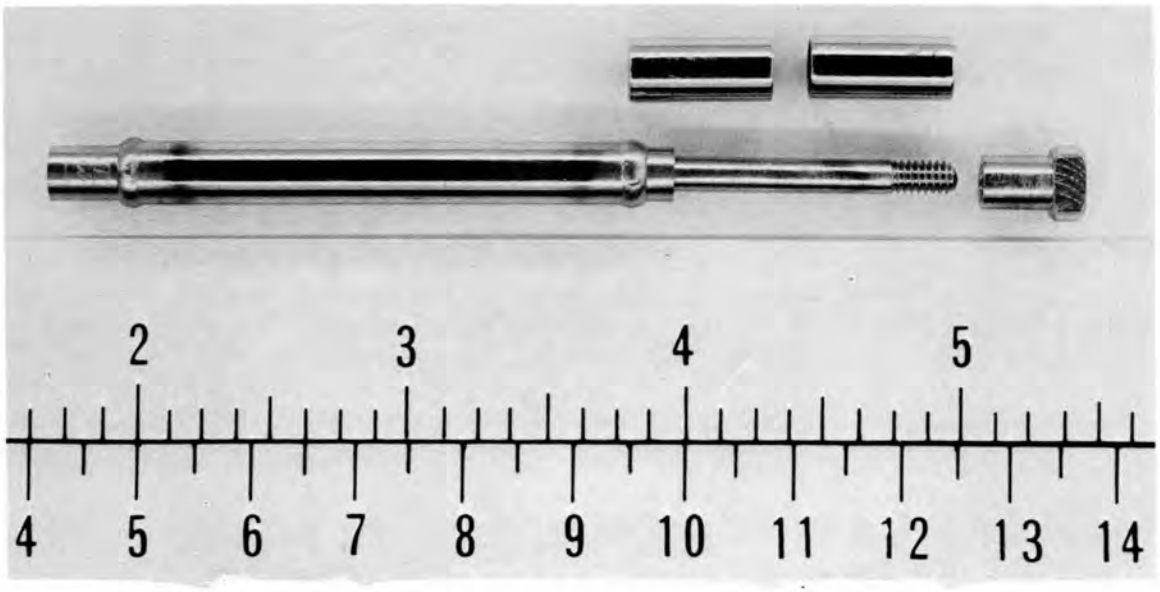

Fig. 4.18. Typical cladding exposure specimen, control specimens, and stack spacer.

4.3.3 Remote maintenance task

W. R. Hamel and W. F. Schaffer, Jr.

High on-stream efficiency in a remotely operated and maintained plant is highly dependent on a well-designed and reliable maintenance system. The component development efforts of the remote maintenance task are addressed to the development of systems and components essential in achieving this goal. The task work closely follows the activities outlined by the experimental plan and network diagrams. The progress of the several subtasks now being actively pursued are reported in the following sections.

Electromechanical system (J. O. Hylton, R. C. Muller).

Thorium-Uranium Recycle Facility (TURF) overhead system. The PaR Corporation, original supplier of the TURF overhead cranes and manipulators, is being contracted to study and recommend methods of modernizing the system. An initial meeting with PaR representatives was held to discuss plans and objectives. Concurrently with the PaR study, ORNL is investigating related problems such as remote transmission of sensor and control data, power transmission, position measurement, viewing systems, and remote maintenance of bridge-mounted equipment. The results of these studies will be incorporated into the TURF modification wherever possible.

Signal transmission. This subtask addresses the problem of transmitting the sensor and control signals required for the remote operation of a bridge-mounted crane or manipulator. A previous report[1] described a wireless telemetry system that uses a laser beam to carry the information. A commercially available laser transmitter has been selected for evaluation and will be incorporated into a prototype telemetry system presently being built.

The data that must be transmitted to and from a typical crane or manipulator system consists of position signals from synchro- or resolver-type transducers along with dc voltage signals from load sensors, tachometers, or controllers. The heart of the telemetry system is a commercially available multiplexer that samples all signals to be transmitted at a rate of 6400 channels per second and then converts them to a digital format for transmission over the laser link. The remainder of the system consists of timing and decoding circuitry that will be built from standard components.

Except for packaging the equipment for remote maintainability and for withstanding a high radiation environment, there are no unique engineering or developmental problems associated with this sytem. Off-the-shelf hardware and standard telemetry techniques can be used in the prototype system. Our goal is to construct and test a complete telemetry system in a configuration adaptable to the special remote maintenance requirements of the HEF. The system will contain a general purpose control interface for computers or manual controllers and can be used for wireless control of any type of in-cell crane or manipulator system.

Once a final working configuration is achieved, an in-cell packaged system can be produced. Most of the hardware for the prototype has been ordered and received. Fabrication and assembly of the system will begin soon.

Power transmission. Activity in this subtask has been limited thus far to a literature search for possible alternatives to the use of festooned cables and buss bars. Previous reports have mentioned the possibility of using wireless systems powered by batteries or by microwave transmissions. Power transmission by microwaves at the required levels is within today's state of the art. Hardware required to do the job is commercially available and is relatively reliable and easy to maintain, especially the receiving equipment, which would be located inside the cell. The use of lead acid batteries in conjunction with a recharging system is also a possibility and appears to offer the most

practical alternative. It is tentatively planned to install and evaluate a battery power pack on one of the TURF manipulators.

Position indication. Previous reports have discussed the possible use of laser interferometers and radar range finders for measuring the position of moving equipment inside a hot cell. The search for suitable devices and methods has been narrowed to two candidates that will be evaluated.

The first candidate is a commercially available laser interferometer that will be used to measure the position of the crane or manipulator bridge along the long axis of the cell. Tests conducted by Y-12 personnel have demonstrated reliable operation at distances up to 60 m (200 ft); however, the manufacturer reports that the devices have been used successfully at 210 m (700 ft).

The other type of device will track and measure some point on the manipulator arm as it moves relative to the bridge. The system basically will consist of a small transmitter (probably a light-emitting diode) attached to the spot on the arm (or crane hook) to be tracked. The spot is tracked by two servo-operated tracking devices mounted on the bridge. The position of the spot is determined by measuring the tracking angles. This system will be built and tested by ORNL at the TURF.

Position control. This subtask involves the application of position control to a bridge-mounted crane or boom-mounted manipulator with only four or five degrees of freedom.

Design has been started on a servo control system and operator's panel that will interface to the prototype telemetry system described earlier. The goal is to demonstrate the advantages of position control over the open-loop-rate control boxes now being used on the TURF systems.

Remote viewing. Specifications are being prepared for the purchase of a three-dimensional television system for evaluation. The system will use a high-resolution camera (approximately 1100 scan lines) and will have a projection console which permits viewing the 3-D image through standard polarized 3-D glasses or hood on a 19-in. screen. The objection to 3-D systems expressed in earlier reports (lack of resolution) has been eliminated by the use of the high-resolution camera.

Connectors and jumpers. Reliability, leaktightness, and durability are essential criteria that must be evaluated in selecting connectors for remote processing. Conceptual process cell layouts for the HEF have shown that the physical size of a remote fluid connector, together with the required access space for the remote manipulation of removing and reinstalling connectors and jumper lines, has a significant influence on pipe layout, equipment placement, and cell size, and, therefore, plant cost.

Parallel paths are being followed to obtain remotely operated connectors for test and evaluation to permit judicious selection of the types best suited for use in the pilot plant. The first approach is to reevaluate modified Hanford-Purex connectors with metal seals; the second approach is to obtain an alternate remotely operated connector, also with metal seals but lighter, smaller, and operable by the use of advanced technology in remote manipulation.

Hanford-Purex connectors. These connectors, designed in the late 1950s, have proven reliable in existing processing plants. The connectors have two major drawbacks: (1) the use of Teflon as a seal and (2) the physical size of the connector and operating mechanism. Teflon, like other plastics or elastomers, will be severely degraded by the high level of radiation expected in many regions of the pilot plant during the processing of advanced fuels. The heavy construction of the connector was necessary only because the crane and impact wrench were the tools available for remote manipulation. Later developments in remote manipulation make this requirement less stringent. We

intend to upgrade this connector by modifying the hubs to accept metal seals, and we have designated this connector as the reference connector for the HEF. Hanford-Purex connectors have been procured from Nuclear Fuel Services surplus for modification work. Industrial concerns specializing in the fabrication of metal seals or connectors employing metal seals have been asked for quotes on the modification of the connectors to accept metal seals. Drawings and specifications have been furnished to prospective bidders.

Alternate connectors. A specification for an alternate connector was prepared and reviewed in a meeting with interested program, engineering, and inspection engineering personnel. Revisions were made based on comments at that meeting, and the specification is ready for program management approval. Union Carbide Purchasing has issued an "expression of interest" letter, along with the tentative specification and work scope, to prospective vendors to determine their interest in participating in the development program. Replies to this document are expected early in July.

Sampling. The requirements of the sampling system are being defined by the HEF conceptual design study. This portion of the work is scheduled for review in about two months. Development work will begin after the conceptual design group has adopted a firm approach.

Seals for large openings. A preliminary study of the intracell transfer systems was presented during the last HEF conceptual design meeting. Additional work by program and engineering personnel is necessary to define the requirements for each transfer opening. Development work will be defined following the conceptual design phase.

Welding and joining (J. W. McEnerney). We are considering the use of a unique joining system for pipe and tubing (invented in the early 1970s) that depends upon a "shape memory" alloy known as Nitinol. Couplings are in commercial production for U.S. Air Force and U.S. Navy applications by the Raychem Corporation under the trade name Cryofit. Nitinol alloy is known as a "shape memory" metal because it remembers its original shape after being deformed. When a coupling is cooled below its phase transformation temperature (−120°F for the standard alloy) and hydraulically expanded (approx 8%), the device will return to its original manufactured size while warming up through its phase transformation temperature. The force of recovery is extremely high (80,000 to 100,000 psi), producing significant amounts of work as it returns to its original size. The standard alloy has a recovery time of about 45 sec; an alternate alloy with 5- to 8-min recovery is being obtained for evaluation under remote maintenance conditions. The Cryofit coupling is similar to a weld socket or braze sleeve. Once positioned over the pipe or tubing ends, ambient air temperature supplies the heat necessary to cause the Nitinol coupling to shrink. The shrinking occurs with such force that it forms a compression-type connection with the performance characteristics of a welded connection. Installation requires about 25% of the fabrication time as compared with welding or brazing, and inspection procedures are much simpler. Cryofit couplings are estimated to provide up to 80% reduction in pipe-joining costs over welding or brazing.

Sizes up to $1^1/_2$ in. International Pipe Standard (ips) are stock items; 2-in. ips couplings have been made, and larger sizes up to 4 in. ips are possible with current production equipment at Raychem, although the costs may be prohibitive with the largest sizes.

There is some concern over possible stress or crevice corrosion in nitric acid piping. Samples are being procured for a corrosion investigation.

Electrical and instrument connectors. A literature survey of electrical and instrument connectors indicates that many commercial connectors offer features required for remote manipulation, that is,

corrosion resistant, water resistant, hermetic sealing, locking devices, polarization, and others. One company is currently offering a connector specifically designed for remote handling with a manipulator. Criteria are being developed for a specification for remotely operated connectors. We plan initially to purchase standard connectors for evaluation in early test programs. Later, we plan to modify acceptable standard connectors for remote work and qualify them during an evaluation program.

4.3.4 Waste handling

J. E. Van Cleve, Jr.

The work plan for the waste handling task has been completed, and the system has been divided into seven subtasks.

1. interfacing activities both within and without the system,
2. preparation and packaging of stainless steel waste from subassembly hardware and scrap equipment,
3. conversion of in-cell organic waste streams (liquid and solid) to a stable solid material and packaging for storage,
4. conversion of high-level waste to a stable solid material and packaging for storage,
5. reduction of low-level solid waste (primarily from out-of-cell activities) to small volumes and packaging for storage,
6. resolution of disposal methods for other radioactive waste such as tritium, iodine, krypton, and low-level liquid waste,
7. nondestructive assay of waste streams.

A meeting was held with representatives of General Electric to discuss their participation in scoping studies on at least subtasks 2, 3, and 4. This subcontract should be approved shortly.

At Retech, Inc., we had the opportunity to observe an "Inducto Slag" furnace that Retech had built for Battelle Northwest Laboratory. This furnace will be used in their developmental program for processing light-water reactor fuel hulls. Battelle has melted Zircaloy-4 hulls and produced an ingot of sufficient quality to be fabricated into rod and tubing. The technique should be applicable to stainless steel fuel hulls volume reduction and possibly to failed equipment. Communication with Battelle personnel involved in this work will be established.

An interface was established with the Office of Waste Isolation, and the first meeting was held to discuss areas of mutual interest. The acceptance criteria for all types of waste were discussed. A report prepared by Livermore National Laboratory for the Nuclear Regulatory Commission will be available about October 1, 1977, that will propose acceptance criteria for high-level waste. The study was performed for defense-related wastes but will serve as a guideline for the preparation of additional criteria. In general, if the waste form is acceptable from a transportion standpoint, it will be accepted at the repository.

The Office of Waste Isolation indicated that they would like to stay with the 10-ft-long cylindrical canister for all wastes other than low level. The diameter of the canister could be increased to about 2 ft if required. This will simplify the handling and excavation requirements at the repository. Low-level waste would be accepted in 55-gal drums. No pressurized gas cylinders

will be accepted for underground storage. Problems associated with carbon-14, tritium, and iodine have not been considered.

4.3.5 Uranium for tests

N. R. Grant and R. W. Knight

This task is divided into three areas: (1) the procurement of depleted uranium dioxide as feed material for the voloxidizer and/or the dissolver; (2) the procurement of dummy subassemblies as feed material for the disassembly–shear; and (3) the disposal and/or recycle of uranyl nitrate. Ideally, one would always feed dummy subassemblies containing depleted uranium to the shear and then use the sheared product to feed the voloxidizer and dissolver. However, dummy subassemblies are very expensive. Therefore, a large part of the feed for the shear is made from short sections of subassemblies; ceramic aluminum oxide pellets replace depleted uranium. Subsequently, some of the feed for the voloxidizer and dissolver must be mixtures of depleted uranium oxide powder, empty fuel element tubes, pieces of spacer wire, and pieces of hex shroud. Since the dissolver will need some feed material early in 1978, an order has been placed with the Y-12 plant for 10,000 kg of U_3O_8. It is planned to ship the resulting uranyl nitrate to a vendor to have this material converted back to the oxide form. Eventually, when product conversion equipment is operational, at least a portion of the uranyl nitrate will be converted on site.

Preparations are under way to obtain bids for the procurement of dummy subassemblies. A package containing specifications and drawings is being assembled, and a summary of fuel requirements over the next ten years is being prepared. The following options will be available in the dummy subassemblies: (1) Type of assembly—FFTF core, CRBR core, or CRBR blanket; (2) Pellet loading—UO_2, ThO_2, or Al_2O_3; (3) Clad/spacer wire/shroud—type 316 stainless steel or type 446 stainless steel (can be embrittled to simulate post-reactor material conditions); (4) Shroud—with hard face on pad or without hard face on pad.

4.4 HOT EXPERIMENTAL FACILITY (HEF) CONCEPTUAL DESIGN

O. O. Yarbro

The conceptual design of the HEF has continued throughout the past quarter with no change in direction, scope, or schedule. A study has been initiated in the past two months to evaluate the effects and modifications in HEF direction and scope that will be required by the recent changes in U.S. policy relative to reprocessing. The results of this study will be factored into the detailed plans for the HEF conceptual design toward the end of the fiscal year. Capital funding for Title I design, originally planned for FY 1979, will be delayed for one year to FY 1980, and conceptual design will be extended from the previously scheduled two years to three years.

An interim report on the sutdy by Westinghouse Electric on the corrosion behavior of sodium-exposed stainless steel in waste storage indicated that water is an acceptable storage media for type 316 stainless steel fuel elements after sodium cleaning. The recommendation has been made to proceed with a water medium for the HEF fuel element storage pool.

4.4.1 HEF process design

E. D. North

The basic design chosen for the HEF is the chop-leach Purex process, including voloxidation and continuous dissolution. Material balance process flow diagrams are 95% complete. Process flow diagrams have been completed for co-processing a 75:25 blend of uranyl nitrate and plutonium nitrate to a UO_2–PuO_2 solid product using hydrogen peroxide as a precipitant.

A process equipment layout has been completed using two main process cells and smaller auxiliary cells for UO_3 conversion, for co-processing UO_2–PuO_2, and for krypton recovery.

Sampling and analytical requirements have been developed and are being reviewed.

4.4.2 HEF design

J. R. White

Siting and support building. Preliminary core drilling and a topographic survey of the recommended HEF site on the west end of Bethel Valley Road near ORNL has been completed, and a report describing the results has been issued. A recommendation to locate the HEF on the ORNL site (Fig. 4.19) has officially been made to ERDA. Bechtel is continuing preparation of the site-utility and support-building criteria. About half of these criteria have been submitted to UCC-ND for review.

Process building. Design and basic concept criteria for the building and cell ventilation and heat-removal systems have been prepared by UCC-ND and transmitted to Bechtel for conceptual design. Design criteria for the remaining process building service systems have been started.

The arrangement of the cell complex has been established. The concept selected consists of two process cells and an interconnecting remote decontamination and maintenance cell located beneath the process cells, as in Fig. 4.20.

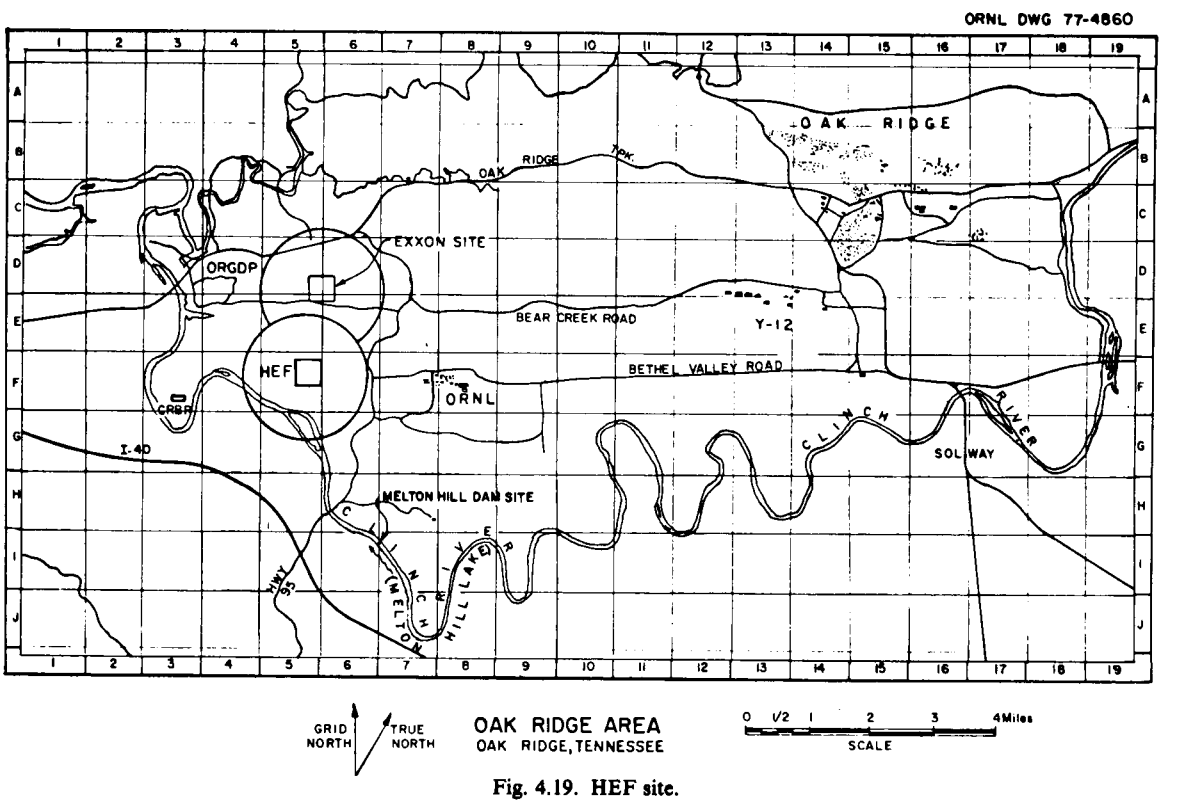

Fig. 4.19. HEF site.

ORNL DWG 77-4874

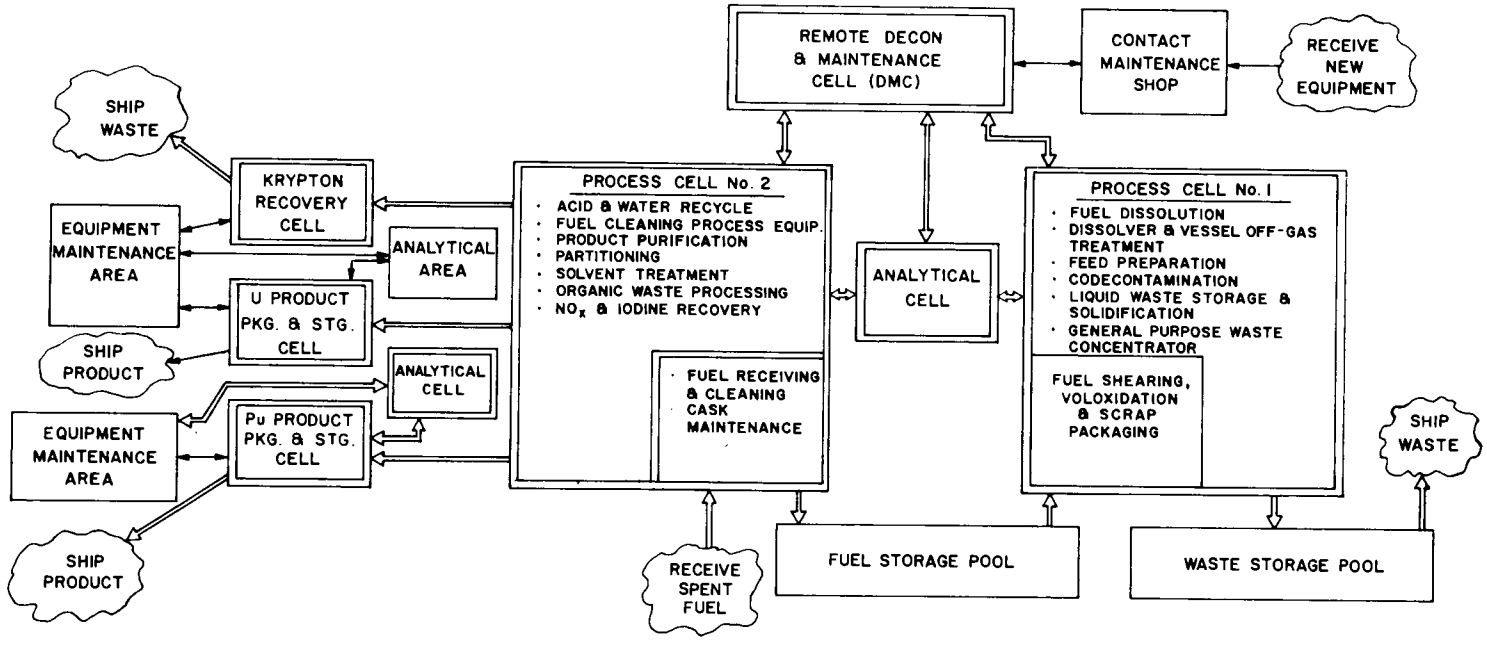

Fig. 4.20. HEF cell complex.

Fuel receiving and cleaning is performed within an enclosed area in process cell 2. Fuel shearing, voloxidation, and scrap packaging are performed within an enclosure in process cell 1. Product purification, packaging, and storage operations are performed in a separate set of cells. This cell complex arrangement was selected over others primarily because of improved seismic characteristics, in-cell process pipe routing, in-cell material–equipment transfer paths, out-cell pipe routing, and out-of-cell personnel traffic patterns. The revised schematic of the cell complex (Fig. 4.21) supercedes that shown in the last quarterly report.

Effort is now being directed toward the product cells and the contaminated equipment maintenance facilities. This effort includes the establishment of the type and location of cell equipment and the optimization of cell shapes.

Design criteria for the in-cell material handling system have been approved. A contract is being processed to obtain the service of a specialty contractor to perform the conceptual design study of this system. Design criteria for the utility service plugs through the cell walls has been issued, and Bechtel is evaluating alternate designs.

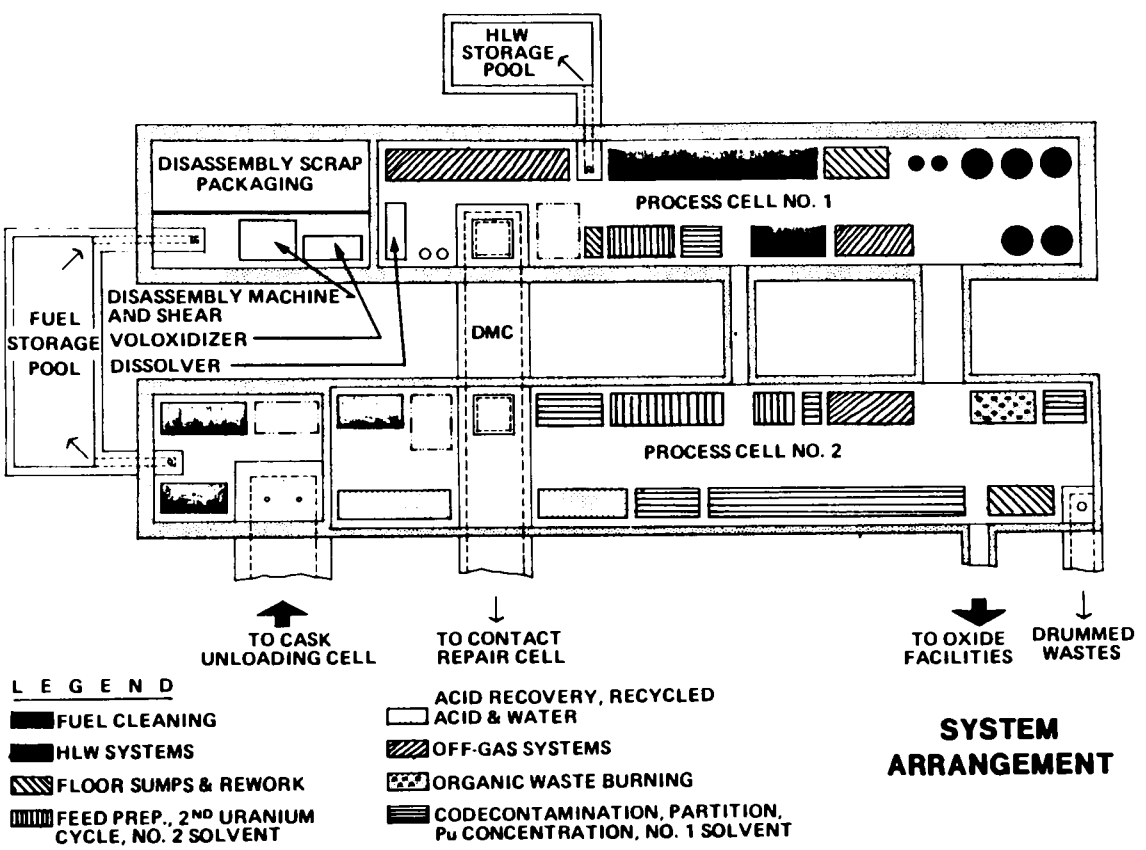

Fig. 4.21. Schematic of HEF cell complex.

REFERENCE FOR SECTION 4

1. W. D. Burch et al., *LMFBR Fuel Reprocessing Program Progress Report for Period January 1 to March 31, 1977,* ORNL/TM-5879 (May 1977).

5. NUCLEAR SAFETY

H. T. Kerr and J. D. Jenkins

A program has been initiated to address questions about nuclear safety in reprocessing facilities. Although the nuclear safety program encompasses a broad range of responsibilities, initial efforts have focused exclusively on accurate determinations of nuclear subcriticality, which are essential to the efficient design and safe operation of reprocessing facilities. Direct determination of subcriticality for each fuel configuration in each facility component would be physically impractical and prohibitively expensive. Therefore, extensive dependence on calculated subcriticality is required. The reliability of the calculations depends on the availability of validated computational methods (i.e., methods that have been tested by comparison with experiment to establish the reliability of results when the methods are applied to conditions of interest). Therefore, complete data from appropriate criticality experiments must be available to develop validated computational methods.

Only limited experimental data are available for fissile materials characteristic of mixed oxides in the LMFBR fuel cycle. The reprocessing facility will be concerned with fissile oxides that range from the fuel pellet density to loose powders and may entail various amounts of hydrogeneous materials. The aqueous solutions will range from very dilute to high concentrations of product levels as supplied to fuel fabricators. Information on the influence of isotopic composition is not complete in the midconcentration range and particularly in the dilute region.

Furthermore, information is needed for special geometries such as annular cylinders and for the nuclear work of various absorber materials. Data are needed to fully assess variations in the plutonium content of Pu-U mixtures and also ^{240}Pu content of the plutonium.

Most of the criticality data needed for validation purposes is presently nonexistent, and existing data is generally inadequate as a validation base. A program of criticality experiments has been initiated at Battelle Northwest Laboratory, and the data generated will be used to validate computational codes and cross sections. The validated computational models will then be extended to evaluate criticality conditions in specific components of the recycle facilities. This approach is consistent with the specifications of the American National Standard – ANSI N-16.1-1969.

Although validated computational models are not available, preliminary criticality calculations for some equipment components have been performed with existing computational models.

Survey calculations have been completed to provide perspective on the question of nuclear criticality in the 30-in.-diam rotary dissolver. The specific considerations addressed were: (1) dependence of the system K_{eff} on heavy metal concentration in the fuel solution over the concentration range $0 \leqslant \text{HM} \leqslant 350$ g/liter, (2) concentration of natural gadolinium required to achieve $k = 1.0$ for each supercritical configuration, (3) effect of an infinite water reflector.

For these survey calculations, the dissolver was modeled as a 30-in.-diam (ID) cylinder of infinite height and 3/8-in. wall thickness. The cylinder was filled with fuel solution consisting of specified amounts of unirradiated FFTF fuel, 3.5 *M* nitric acid, and water. The stainless steel hulls *were not* included in these calculations. The calculations were done with the S_N transport theory code, ANISN,[1] and used HANSEN-ROACH[2] cross sections.

The results of these calculations are summarized in Fig. 5.1. Some important points are:

1. If completely filled with fuel solution in the absence of stainless-steel hulls, the dissolver will be supercritical for all heavy metal concentrations above 30 g HM/liter.
2. Natural gadolinium at a maximum concentration of 2.1 (g GD/liter) in the fuel solution will make all the calculated configurations (i.e., $\leqslant$ 350 g HM/liter) subcritical.
3. There is little difference between the reflected and unreflected conditions for the 30-in.-diam system. However, reflectors are much more important for smaller diameter systems.
4. If stainless-steel hulls were admixed with the fuel solution, the system K_{eff} would certainly be lower, and less gadolinium would be needed to assure subcriticality.

A three dimensional MONTE CARLO model of the rotary dissolver has been completed, and calculations can now be made for realistic postulated conditions in the dissolver. Results from these calculations will be reported as available.

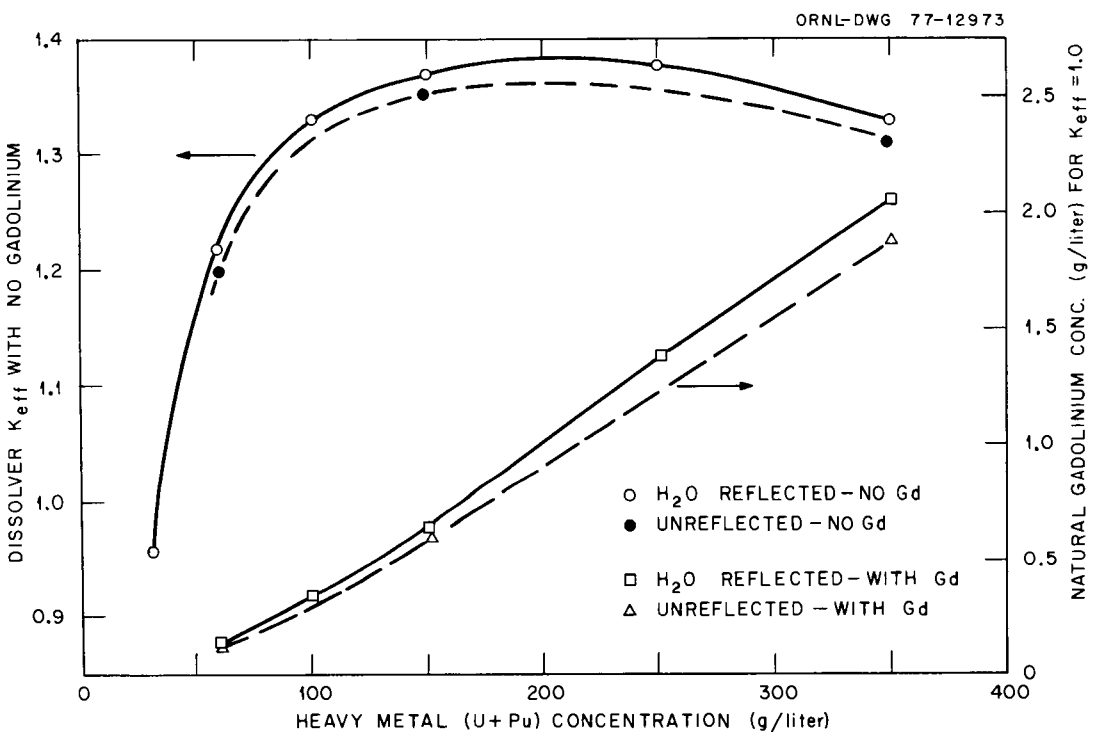

Fig. 5.1. Calculated K_{eff} and critical gadolinium concentrations as a function of heavy metal concentration in a 30-inch-diam infinite cylinder.

REFERENCES FOR SECTION 5

1. W. W. Engle, Jr., *A Users Manual for ANISN – A One-Dimensional Discrete Ordinates Code with Anisotropic Scattering,* K-1693 (March 1967).

2. J. R. Knight and L. M. Petric, *16 and 123 Group Weighting Functions for KENO,* ORNL-TM-4660 (1975).

ORNL/TM-5993
Dist. Category UC-79c

INTERNAL DISTRIBUTION

1. J. T. Bell
2. M. Bender
3. M. R. Bennett
4. R. E. Blanco
5. J. O. Blomeke
6. W. D. Bond
7. B. F. Bottenfield
8. E. C. Bradley
9. N. C. Bradley
10. R. E. Brooksbank
11. K. B. Brown
12–21. W. D. Burch
22. D. D. Cannon
23. J. M. Chandler
24. W. E. Clark
25. L. T. Corbin
26. D. A. Costanzo
27. R. M. Counce
28. D. J. Crouse
29. B. F. Crump
30. F. L. Culler
31. B. C. Duggins
32. D. E. Dunning
33. J. H. Evans
34. M. J. Feldman
35. D. E. Ferguson
36. L. M. Ferris
37. S. D. Floyd
38. J. H. Goode
39. N. R. Grant
40. W. S. Groenier
41. W. R. Hamel
42. D. C. Hampson
43. B. A. Hannaford
44. W. O. Harms
45. J. N. Herndon
46. R. M. Hill
47. W. D. Holland
48. D. E. Horner
49. A. R. Irvine
50. J. D. Jenkins
51. R. T. Jubin
52. P. R. Kasten
53. A. D. Kelmers
54. L. J. King
55. J. Q. Kirkman
56. J. A. Klein
57. C. E. Lamb
58. B. E. Lewis
59. M. H. Lloyd
60. A. L. Lotts
61. J. C. Mailen
62. A. P. Malinauskas
63. D. L. Manning
64. L. Maya
65. J. D. McGaugh
66. L. E. McNeese
67. R. P. Milford
68. A. D. Mitchell
69. J. G. Morgan
70. J. M. Morrison
71. E. L. Nicholson
72. E. D. North
73. J. H. Pashley
74. F. L. Peishel
75. H. Postma
76. R. H. Rainey
77. G. W. Renfro
78. J. E. Rushton
79. W. F. Schaffer, Jr.
80. C. D. Scott
81. T. Shapiro
82. B. B. Spencer
83. R. G. Stacy
84. M. J. Stephenson
85. W. G. Stockdale
86. J. G. Stradley
87. O. K. Tallent
88. D. B. Trauger
89. W. E. Unger
90. V. C. A. Vaughen
91. B. L. Vondra
92. C. D. Watson
93. B. S. Weil
94. T. D. Welch
95. M. E. Whatley

96. J. R. White
97. R. G. Wymer
98. O. O. Yarbro
99. J. Zasler
100. S. Beard (consultant)
101. L. Burris, Jr. (consultant)
102. A. B. Carson (consultant)
103. E. L. Gaden, Jr. (consultant)
104. C. H. Ice (consultant)
105. W. H. Lewis (consultant)
106. R. B. Richards (consultant)
107. A. Schneider (consultant)
108. M. J. Szulinski (consultant)
109. J. S. Theilacker (consultant)
110. A. K. Williams (consultant)
111–112. Central Research Library
113. ORNL–Y-12 Technical Library, Document Reference Section
114–115. Laboratory Records
116. Laboratory Records, ORNL RC
117. ORNL Patent Office
118. Nuclear Safety Information Center

EXTERNAL DISTRIBUTION

119. Director, Reactor Division, ERDA-ORO
120–121. Director, Division of Nuclear Fuel Cycle and Production, ERDA, Washington, D.C. 20545
122–123. Director, Division of Reactor Research and Development, ERDA, Washington, D.C. 20545
124. M. L. Bleiberg, Westinghouse Electric Corporation, Advanced Reactors Division, Waltz Mill Site, P. O. Box 158, Madison, PA 15663
125. R. B. Chitwood, Chief, Industrial Programs Branch, Division of Waste Management, Production, and Reprocessing, ERDA, Washington, D.C. 20545
126. Duane E. Clayton, Battelle Pacific Northwest Laboratory, P. O. Box 999, Richland, WA 99352
127. Martin Friedland, Gulf + Western Advanced Development and Engineering Center, 101 Chester Road, Swarthmore, PA 19081
128. Jerry M. Friedman, Sandia Laboratories, P. O. Box 5800, Albuquerque, NM 87115
129. Frank J. Jones, Bechtel Corporation, P. O. Box 3965, San Francisco, CA 94119
130. Burt Judson, General Electric Company, Nuclear Energy Programs Division, 175 Curtner Avenue, San Jose, CA 95125
131. R. S. Karinen, Programmed and Remote Systems Corporation, 3460 Lexington Avenue, St. Paul, MN 55112
132. Robert H. Karlsson, Rockwell International, Atomics International Division, Rocky Flats Plant, P. O. Box 464, Golden, CO 80401
133. W. H. McVey, Chief, Technology Branch, Division of Waste Management, Production, and Reprocessing, ERDA, Washington, D.C. 20545
134. R. E. Mullen, Aerojet Manufacturing Company, 601 South Placentia Avenue, P. O. Box 4210, Fullerton, CA 92634
135. W. S. Scheib, Jr., Chief Projects Branch, Division of Waste Management, Production, and Reprocessing, ERDA, Washington, D.C. 20545
136. D. R. Spurgeon, Acting Assistant Director for Reprocessing, Division of Waste Management, Production, and Reprocessing, ERDA, Washington, D.C. 20545
137. D. E. Wood, Kaman Sciences Corporation, 1500 Garden of the Gods Road, P. O. Box 7463, Colorado Springs, CO 80933
138. Research and Technical Support Division, ERDA–ORO
139–383. Given distribution as shown in TID-4500 under UC-79c, Fuel Recycle category (Applied)

☆ U.S. GOVERNMENT PRINTING OFFICE: 1977-748-189/192